JOURNAL OF THE AERONAUTICAL SCIENCES

VOLUME 14 NOVEMBER, 1947 NUMBER 11

CONTENTS

Use of Vectors in Vibration Measurement and Analysis ..... CHARLES C. KENNEDY AND C. D. P. PANCU 603

The Linearized Subsonic and Supersonic Flow About Inclined Slender Bodies of Revolution ..... E. V. LAITONE 631

The Dynamics of a Swept Wing ..... H. R. LAWRENCE 643

Fluid Dynamic Aspects of Axial-Flow Compressors and Turbines ..... JOHN R. WESKE 651

Letters to the Editor 625

Published by the
INSTITUTE OF THE AERONAUTICAL SCIENCES, INC.

JOURNAL OF THE AERONAUTICAL SCIENCES

Editor: HUGH L. DRYDEN, *Director of Aeronautical Research, N.A.C.A.*

Associate Editor: ROBERT R. DEXTER *Associate Editor:* BERNEICE H. JARCK

The Institute of the Aeronautical Sciences publishes monthly the JOURNAL OF THE AERONAUTICAL SCIENCES and the AERONAUTICAL ENGINEERING REVIEW.

The JOURNAL OF THE AERONAUTICAL SCIENCES prints papers of scientific and technical interest to Institute members and subscribers. In general, it provides an opportunity for specialists to publish articles disclosing new knowledge and new applications in the field of the aeronautical sciences. The JOURNAL restricts itself to the aeronautical aspects of advances in science and engineering, and papers printed have either been submitted directly to the JOURNAL or have been previously presented at a meeting of the Institute.

The AERONAUTICAL ENGINEERING REVIEW keeps members and subscribers informed regarding the contents of new books and current periodicals in the field of aeronautics. It reviews new developments in the aircraft industry and reports on progress from house organs and catalogs published by aircraft and engine manufacturers and other companies engaged in aeronautical activities. It publishes papers on applied engineering and aircraft production. News of Institute activities is published in the REVIEW.

Statements and opinions expressed in the JOURNAL are to be understood as individual expressions of the authors and not those of the Institute.

SUBSCRIPTION RATES

Journal of the Aeronautical Sciences
Published Monthly

United States and Possessions		Foreign Countries Including Canada (American Currency Rates)	
1 Year	$7.00	1 Year	$9.00
Single Copies	0.70	Single Copies	1.00

Aeronautical Engineering Review
Published Monthly

United States and Possessions		Foreign Countries Including Canada (American Currency Rates)	
1 Year	$3.00	1 Year	$3.50
Single Copies	0.30	Single Copies	0.35

Notices of change of address should be sent to the Institute at least 30 days prior to actual change of address.

Manuscripts for publication, proofs, and all correspondence should be addressed to the Editorial Office of the JOURNAL.

Correspondence regarding subscriptions may be addressed to Publication Office, 20th and Northampton Sts., Easton, Pa., or to the Editorial Office of the JOURNAL OF THE AERONAUTICAL SCIENCES, 2 East 64th Street, New York 21, New York.

Copyright, 1947, by the Institute of the Aeronautical Sciences, Inc.

Entered as Second Class Matter at the Post Office, Easton, Pa., May 1, 1937. Acceptance for mailing at a special rate of Postage provided for in the Act of August 24, 1912. Authorized April 29, 1937.

INSTITUTE of the AERONAUTICAL SCIENCES

President

P. R. BASSETT

Vice-Presidents

WELLWOOD E. BEALL
REX B. BEISEL
LUIS DE FLOREZ
JOHN K. NORTHROP

Director

S. PAUL JOHNSTON

Executive Vice-President

BENNETT H. HORCHLER

Past-Presidents

J. C. HUNSAKER
CHARLES L. LAWRANCE
DONALD W. DOUGLAS
GLENN L. MARTIN
CLARK B. MILLIKAN
T. P. WRIGHT
GEORGE W. LEWIS
JAMES H. DOOLITTLE
FRANK W. CALDWELL
HALL L. HIBBARD
HUGH L. DRYDEN
R. H. FLEET
CHARLES H. COLVIN
ARTHUR E. RAYMOND

Secretary

ROBERT R. DEXTER

Treasurer

BURDETTE S. WRIGHT

Controller

JOSEPH J. MAITAN

Counsel

ALLAN D. EMIL

COUNCIL

E. E. ALDRIN
LAWRENCE D. BELL
GEORGE W. BRADY
W. A. M. BURDEN
VICTOR E. CARBONARA
CARL DE GANAHL
JAMES H. DOOLITTLE
WILLIAM K. EBEL
SHERMAN M. FAIRCHILD
C. C. FURNAS
J. A. HERLIHY
WILLSON H. HUNTER
JEROME LEDERER
JOHN C. LESLIE
A. ELLIOTT MERRILL
EARL D. OSBORN
EARL A. SPERRY, JR.
JOHN C. SQUIRES
M. F. STOUGHTON
ERNEST G. STOUT
C. FAYETTE TAYLOR

ADVISORY COMMITTEE

Chairman: CHARLES H. COLVIN

WALTER BEECH
FRANK W. CALDWELL
RALPH S. DAMON
KENNETH S. M. DAVIDSON
R. H. FLEET
R. PAUL HARRINGTON
R. M. HAZEN
HALL L. HIBBARD
J. C. HUNSAKER
TH. VON KÁRMÁN
THOMAS A. KNOWLES
I. M. LADDON
GROVER LOENING
GLENN L. MARTIN
CLARK B. MILLIKAN
THOMAS A. MORGAN
R. C. MUIR
ARTHUR E. RAYMOND
F. W. REICHELDERFER
L. B. RICHARDSON
RUSSELL G. ROBINSON
LAURANCE S. ROCKEFELLER
T. CLAUDE RYAN
EDWARD P. WARNER

HONORARY MEMBERS

JOHN C. ADAMS
GRIFFITH BREWER
JOHN N. BROWN
W. A. M. BURDEN
E. U. CONDON
L. C. CRAIGIE
IRA C. EAKER
HARRY F. GUGGENHEIM
HENRY G. HOUGHTON
GEORGE C. KENNEY
CURTIS E. LE MAY
GEORGE B. PEGRAM
E. M. POWERS
J. LAURENCE PRITCHARD
ARTHUR W. RADFORD
F. W. REICHELDERFER
H. B. SALLADA
CARL SPAATZ
L. C. STEVENS
NATHAN F. TWINING

HONORARY FELLOWS

H. H. ARNOLD
FRANK W. CALDWELL
SIR GEOFFREY DE HAVILLAND
DONALD W. DOUGLAS
HUGH L. DRYDEN
W. F. DURAND
SIR RICHARD FAIREY
SIR ROY FEDDEN
J. C. HUNSAKER
SIR MELVILL JONES
GEORGE W. LEWIS
GLENN L. MARTIN
GEORGE J. MEAD
SIR FREDERICK HANDLEY PAGE
D. R. PYE
IGOR I. SIKORSKY
SIR GEOFFREY TAYLOR
TH. VON KÁRMÁN
EDWARD P. WARNER
ORVILLE WRIGHT
T. P. WRIGHT

BENEFACTORS

E. E. ALDRIN
HART O. BERG (Deceased)
W. A. M. BURDEN
E. L. CORD
DONALD W. DOUGLAS
SHERMAN M. FAIRCHILD
SIR RICHARD FAIREY
R. H. FLEET
FLORENCE GUGGENHEIM (Deceased)
C. D. HANSCOM
JOHN P. V. HEINMULLER
ALEXANDER KLEMIN
PAUL KOLLSMAN
BELLA C. LANDAUER
WILLIAM LANDAUER
GROVER LOENING
EDMUND C. LYNCH (Deceased)
F. W. MAGIN
GLENN L. MARTIN
GEORGE J. MEAD
S. A. REED (Deceased)
LAURANCE S. ROCKEFELLER
EDWARD P. WARNER

AMERICAN FELLOWS

JOHN D. AKERMAN
E. E. ALDRIN
HARRY G. ARMSTRONG
KARL ARNSTEIN
J. L. ATWOOD
PAUL S. BAKER
RALPH S. BARNABY
P. R. BASSETT
WELLWOOD E. BEALL
REX B. BEISEL
G. M. BELLANCA
DON R. BERLIN
HENRY A. BERLINER
WILLIAM BOLLAY
B. C. BOULTON
GEORGE W. BRADY
LYMAN J. BRIGGS
W. G. BROMBACHER
WILLIAM G. BROWN
CHARLES P. BURGESS
KENNETH CAMPBELL
CHARLES H. CHATFIELD
ALLAN CHILTON
V. E. CLARK
FRANKLIN R. COLLBOHM
CHARLES H. COLVIN
KARL T. COMPTON
EMERSON W. CONLON
JOHN W. CROWLEY, JR.
RALPH S. DAMON
LUIS DE FLOREZ
SMITH J. DE FRANCE
J. P. DEN HARTOG
WALTER S. DIEHL
JAMES H. DOOLITTLE
C. S. DRAPER
IVAN H. DRIGGS
WILLIAM K. EBEL
C. L. EGTVEDT
FREDERIC FLADER
CHARLES FROESCH
JACK FRYE
GARLAND FULTON
LESTER D. GARDNER
RICHARD C. GAZLEY
MICHAEL E. GLUHAREFF
MELVIN N. GOUGH
LEROY R. GRUMMAN
HAROLD R. HARRIS
R. M. HAZEN
ALBERT F. HEGENBERGER
EDWARD H. HEINEMANN
S. D. HERON
HALL L. HIBBARD
L. S. HOBBS
PAUL E. HOVGAARD
WILLIAM HOVGAARD
ROBERT INSLEY
EASTMAN N. JACOBS
CLARENCE L. JOHNSON
S. PAUL JOHNSTON
ALEXANDER KARTVELI
PAUL H. KEMMER
J. H. KINDELBERGER
OTTO E. KIRCHNER
ARTHUR L. KLEIN
ALEXANDER KLEMIN
W. B. KLEMPERER
PAUL KOLLSMAN
OTTO C. KOPPEN
B. V. KORVIN-KROUKOVSKY
S. M. KRAUS
I. M. LADDON
E. S. LAND
CHARLES L. LAWRANCE
JEROME LEDERER
JOHN G. LEE
JOHN C. LESLIE
CHARLES A. LINDBERGH
WILLIAM LITTLEWOOD
GROVER LOENING
ALBERT E. LOMBARD
W. RANDOLPH LOVELACE, II
EUGENE E. LUNDQUIST
R. D. MACCART
JOHN R. MARKHAM
ERLE MARTIN
WM. H. MCAVOY
C. J. MCCARTHY
CLARK B. MILLIKAN
ROBERT J. MINSHALL
JOSEPH S. NEWELL
ALFRED S. NILES
JOHN K. NORTHROP
ARTHUR NUTT
SHATSWELL OBER
ROBERT R. OSBORN
W. BAILEY OSWALD
GEORGE A. PAGE, JR.
F. W. PAWLOWSKI
F. W. PENNOYER, JR.
A. A. PRIESTER
ARTHUR E. RAYMOND
F. W. REICHELDERFER
ELLIOTT G. REID
H. J. E. REID
H. C. RICHARDSON
RUSSELL G. ROBINSON
LEONARD E. ROOT
C. E. ROSENDAHL
ADDISON M. ROTHROCK
WILLIAM T. SCHWENDLER
FRANCIS R. SHANLEY
JAMES M. SHOEMAKER
MAC SHORT
IGOR ALEXIS SIKORSKY
ABE SILVERSTEIN
SELDEN B. SPANGLER
ELMER A. SPERRY, JR.
JOHN STACK
WILLIAM B. STOUT
HARRY A. SUTTON
C. FAYETTE TAYLOR
EDWARD S. TAYLOR
PHILIP B. TAYLOR
TH. THEODORSEN
T. E. TILLINGHAST
S. TIMOSHENKO
L. B. TUCKERMAN
RALPH H. UPSON
J. PARKER VAN ZANDT
J. G. VINCENT
RICHARD VON MISES
FRANK L. WATTENDORF
P. V. H. WEEMS
FRED E. WEICK
R. D. WEYERBACHER
JOHN B. WHEATLEY
ANDREW V. WILLGOOS
DONALD H. WOOD
ROBERT J. WOODS
JOHN E. YOUNGER
ALBERT F. ZAHM
STEPHEN J. ZAND

An Appreciation

TO CORPORATE MEMBERS OF THE INSTITUTE OF THE AERONAUTICAL SCIENCES

Listed below are the leading aeronautical and industrial companies that make possible the publication of the *Journal of the Aeronautical Sciences*.

They enable the Institute to publish scientific and technical papers in the *Journal* and so devote its pages exclusively to editorial material.

Dues from individual members which would normally be used to publish this scientific and engineering monthly are thus released for additional services to the profession and industry.

The *Aeronautical Engineering Review* and the *Aeronautical Engineering Catalog*, together with the *Journal*, provide a comprehensive technical information service for the benefit of the aircraft and related industries.

ACADEMY OF AERONAUTICS, INC.
CASEY JONES SCHOOL OF AERONAUTICS
AERO INSURANCE UNDERWRITERS
AEROJET ENGINEERING CORPORATION
AERONCA AIRCRAFT CORPORATION
AEROPRODUCTS DIVISION, GENERAL MOTORS CORPORATION
AEROQUIP CORPORATION
AGAWAM AIRCRAFT PRODUCTS, INC.
AIRBORNE INSTRUMENTS LABORATORY, INC.
AIRCHOX COMPANY DIVISION, JOYCE AVIATION, INC.
AIRCRAFT RADIO CORPORATION
AIRESEARCH MANUFACTURING COMPANY
AIRESEARCH MANUFACTURING COMPANY OF ARIZONA, INC.
ALLIS-CHALMERS MANUFACTURING COMPANY
ALLISON DIVISION, GENERAL MOTORS CORPORATION
ALUMINUM COMPANY OF AMERICA
AMERICAN AIRLINES SYSTEM
AMERICAN OVERSEAS AIRLINES, INC.
AMERICAN BOSCH CORPORATION
AMERICAN PHENOLIC CORPORATION
ASSOCIATED AVIATION UNDERWRITERS
ASSOCIATED FOUNDRIES & MANUFACTURERS, INC.
ATLAS SUPPLY COMPANY
BAKER STEEL & TUBE COMPANY
BEECH AIRCRAFT CORPORATION
BELL AIRCRAFT CORPORATION
BENDIX AVIATION CORPORATION
BENDIX PRODUCTS DIVISION
BENDIX RADIO CORPORATION
ECLIPSE-PIONEER DIVISION
EXPORT DIVISION
FRIEZ INSTRUMENT DIVISION
PACIFIC DIVISION
SCINTILLA MAGNETO COMPANY
THE BG CORPORATION
BOEING AIRCRAFT COMPANY
BREEZE CORPORATIONS, INC.
ESSEX TOOL & DIE COMPANY
FEDERAL LABORATORIES, INC
CAL-AERO TECHNICAL INSTITUTE, A DIVISION OF GRAND CENTRAL AIRPORT COMPANY
CARRIER CORPORATION
CESSNA AIRCRAFT COMPANY
CHANDLER-EVANS DIVISION, NILES-BEMENT-POND COMPANY
CHASE NATIONAL BANK OF THE CITY OF NEW YORK
THE CLEVELAND GRAPHITE BRONZE COMPANY
THE CLEVELAND PNEUMATIC TOOL COMPANY
AUTOMOTIVE-AIRCRAFT DIVISION
CLIFFORD MANUFACTURING COMPANY
CONSOLIDATED VULTEE AIRCRAFT CORPORATION
NASHVILLE DIVISION
STINSON AIRCRAFT DIVISION
CONTINENTAL MOTORS CORPORATION
COX AND STEVENS AIRCRAFT CORPORATION
CURTISS-WRIGHT CORPORATION
AIRPLANE DIVISION
DEVELOPMENT DIVISION
PROPELLER DIVISION
WRIGHT AERONAUTICAL CORPORATION
DOAK AIRCRAFT COMPANY, INC.
DOUGLAS AIRCRAFT COMPANY, INC.
EL SEGUNDO PLANT
LONG BEACH PLANT
THE DOW CHEMICAL COMPANY
DZUS FASTENER COMPANY, INC.
EASTERN AIR LINES, INC.
EATON MANUFACTURING COMPANY
THOMAS A. EDISON, INCORPORATED, INSTRUMENT DIVISION
EDO AIRCRAFT CORPORATION
ELECTROL INCORPORATED
ENGINEERING AND RESEARCH CORPORATION
ETHYL CORPORATION
FAIRCHILD CAMERA & INSTRUMENT CORPORATION
FAIRCHILD AERIAL SURVEYS, INC.
FAIRCHILD ENGINE AND AIRPLANE CORPORATION
DURAMOLD DIVISION
FAIRCHILD AIRCRAFT DIVISION
RANGER AIRCRAFT ENGINES DIVISION
FEDERAL TELEPHONE AND RADIO CORPORATION
FIRESTONE AIRCRAFT COMPANY
GENERAL AVIATION EQUIPMENT COMPANY, INC.
GENERAL ELECTRIC COMPANY
THE B. F. GOODRICH COMPANY
THE GOODYEAR TIRE & RUBBER COMPANY
GRUMMAN AIRCRAFT ENGINEERING CORPORATION
W. & L. E. GURLEY
THE INTERNATIONAL NICKEL COMPANY
IRVING AIR CHUTE COMPANY, INC.
JACK & HEINTZ PRECISION INDUSTRIES, INC.
JOHNS-MANVILLE SALES CORPORATION
KAISER FLEETWINGS, INC.
WALTER KIDDE & COMPANY, INC.
KOLLSMAN INSTRUMENT DIVISION, SQUARE D COMPANY
LAVELLE AIRCRAFT CORPORATION
LEAR INCORPORATED
LINK AVIATION DEVICES, INC.
THE LIQUIDOMETER CORPORATION
LOCKHEED AIRCRAFT CORPORATION
LONGINES-WITTNAUER WATCH COMPANY, INC.
THE GLENN L. MARTIN COMPANY
WARREN McARTHUR CORPORATION
McDONNELL AIRCRAFT CORPORATION
MENASCO MANUFACTURING COMPANY
MINNEAPOLIS-HONEYWELL REGULATOR COMPANY
MOORE DROP FORGING COMPANY
NATIONAL CITY BANK OF NEW YORK
NATIONAL CREDIT OFFICE, INC.
NORTH AMERICAN AVIATION, INC.
NORTH AMERICAN AVIATION, INC., OF TEXAS
NORTHROP AIRCRAFT, INC.
NORTHWEST AIRLINES, INC.
OWENS-CORNING FIBERGLAS CORPORATION
PAN AMERICAN WORLD AIRWAYS SYSTEM
THE PARKER APPLIANCE COMPANY
PESCO PRODUCTS COMPANY DIVISION, BORG-WARNER CORPORATION
PHILLIPS PETROLEUM COMPANY
PIONEER PARACHUTE COMPANY, INC.
PURE OIL COMPANY
RADIOPLANE COMPANY
REPUBLIC AVIATION CORPORATION
A. V. ROE CANADA LIMITED
JOHN A. ROEBLING'S SONS COMPANY
ROHR AIRCRAFT CORPORATION
THE RYAN AERONAUTICAL COMPANY
SCOTT AVIATION CORPORATION
SHELL OIL COMPANY, INC.
SIMMONDS AEROCESSORIES, INC.
SKYDYNE, INC.
SOCONY-VACUUM OIL COMPANY
SOLAR AIRCRAFT COMPANY
SPERRY GYROSCOPE COMPANY, INC.
SQUARE D COMPANY
STANDARD OIL COMPANY OF CALIFORNIA
STANDARD OIL COMPANY (INDIANA)
STANDARD OIL COMPANY OF NEW JERSEY
THE TEXAS COMPANY
THOMPSON PRODUCTS, INC.
TINNERMAN PRODUCTS, INC.
TRANS WORLD AIRLINE
UNION CARBIDE AND CARBON CORPORATION
BAKELITE CORPORATION
HAYNES STELLITE COMPANY
LINDE AIR PRODUCTS COMPANY
NATIONAL CARBON COMPANY
UNITED AIRCRAFT CORPORATION
CHANCE VOUGHT AIRCRAFT DIVISION
HAMILTON STANDARD PROPELLERS DIVISION
PRATT & WHITNEY AIRCRAFT DIVISION
PRATT & WHITNEY AIRCRAFT CORPORATION OF MISSOURI
SIKORSKY AIRCRAFT DIVISION
UNITED AIR LINES, INC.
UNITED STATES AVIATION UNDERWRITERS, INC.
UNITED STATES RUBBER COMPANY
DOMINION RUBBER COMPANY, LTD.
VICKERS, INC.
WARNER AIRCRAFT CORPORATION
THE WEATHERHEAD COMPANY
WESTERN AIR LINES, INC.
WESTINGHOUSE ELECTRIC CORPORATION
WESTON ELECTRICAL INSTRUMENT CORPORATION
WILLYS-OVERLAND MOTORS, INC., AIRCRAFT RESEARCH AND DEVELOPMENT DIVISION
WYMAN-GORDON COMPANY
YOUNG RADIATOR COMPANY

JOURNAL OF THE AERONAUTICAL SCIENCES

VOLUME 14 NOVEMBER, 1947 NUMBER 11

Use of Vectors in Vibration Measurement and Analysis*

CHARLES C. KENNEDY AND C. D. P. PANCU†

Consolidated Vultee Aircraft Corporation

SUMMARY

The authors' main concern with vibration measurement and analysis is the identification and description of the normal modes of vibration of an airplane for the purpose of checking calculated modes to be used in flutter analyses or in the computation of dynamic loads. A technique for using four vibrators to separate normal modes directly while testing is presented. The basis of the technique lies in the fact that a single normal mode can be immediately recognized as such by its property of having the same phase response relative to the force at all points on the airplane. The relation between responses is either 0° or 180° and remains such if the vibrator frequency is changed. The procedure consists of systematically sweeping the point of application and frequency of the applied force until the responses are found to be exactly in or out of phase. The method is absolutely valid for separating two symmetrical and two antisymmetrical modes having resonant frequencies close together.

For more complex systems, a technique is given for the identification of normal modes on polar plots representing the variation of the response vector with forcing frequency. The basic element is that such a plot for a single mode is a circle; as the vibrator goes through a certain resonance, the tip of the total response vector describes an arc approaching that of the pure mode response. Identification of these arcs gives the normal modes, which might otherwise be confusingly located or completely hidden in the current practice of considering just the amplitude of the forced response.

Miscellaneous new points include treatments of the specific disadvantages of rotary vibrators, and the possibility of increasing the resonance sensitivity of the response measurements by differentiation with respect to the forcing frequency. Many other details of vibration analysis and record interpretation are given.

INTRODUCTION

THE BASIC OBJECT of the paper is to make apparent the benefits of thinking in terms of time and space vectors and to awaken a phase consciousness on the part of those who desire to bring about correlation between measured and calculated modes. The theory presented is a major step in the direction of such correlation; the main obstacle at present is the need for suitable vibration exciting and measuring equipment to apply the theory. The designers can meet this need as soon as there is a demand, for elements satisfying the requirements have already been developed in other fields.

Received November 21, 1946.

* The research on which this paper is based was done while both authors were Flutter Engineers at the Cornell Aeronautical Laboratory (formerly Curtiss-Wright Research Laboratory).

† Now, Dynamics Group, San Diego Division.

DESCRIPTION OF MOTION

Normal Modes and Coordinates

Since the main object of this paper will be that of determining and identifying the normal modes of vibration of mechanical systems, one must first consider what are normal modes and normal coordinates.

It is a well-known theoretical conclusion that in the case of the forced oscillation of an undamped structure (or electrical network) the total motion is a sum of responses in its characteristic modes of vibration; the latter are variously referred to as the normal, principal, natural, or coupled modes of the system. The general problem of conservative systems has been studied by a number of authors in various texts and papers. (For example, see treatment by von Kármán and Biot.[1]) Rather than to attempt a complete and rigorous mathematical definition, only the pertinent properties of normal modes will be given here; they may serve as a definition for the nonmathematical reader.

(1) Each normal mode responds to an applied force as a single-degree-of-freedom system—i.e., there is no coupling between normal modes.

(2) In a normal mode, each point of the system oscillates about its equilibrium position along a certain line in space, fixed relative to the equilibrium position

and straight when the oscillations are small enough so that all angles are equal to their sines.

(3) In the case of simple harmonic vibration in a normal mode, all points move either exactly in or exactly out of phase with each other. That is, all points reach maximum departures from their equilibrium positions at the same instants.

(4) The shape of each normal mode is fixed for a given system and is independent of the magnitude, frequency, or location and direction in space of the applied external forces or of the deflections in other normal modes present. That is, in any given normal mode, the ratios of the deflections at all the points of a structure to the deflection at an arbitrary reference point are always constant, and the directions of these deflections are fixed in space. These relative magnitudes and directions in space are characteristic of the normal mode, and their specification for every point in the structure will be referred to as the description of the "shape" of that mode.

Actual measured airplane vibrations may rarely seem to have the properties of normal modes, but that is usually because of inability to separate normal modes when several are present simultaneously and not necessarily because the normal mode theory is inapplicable. The properties of normal modes hold rigorously only for zero damping, which is, in general, closely enough approximated by aircraft structures. Damping is always present in actual systems and, as such, constitutes a controlling factor on the response of a normal mode as a whole; because the damping is small, however, the mode shapes, phase relations between motions at various points, and couplings between the various degrees of freedom will be assumed to be unaffected.

Turning now to coordinate systems, the following is quoted from von Kármán and Biot:[1] "Let us consider a system of r degrees of freedom; for example, let us assume that the configuration of n mass points is given by r independent parameters. We call them the r generalized coordinates $q_1, q_2, \ldots, q_r$ and assume that we are able to express the Cartesian coordinate of the n points in terms of the r quantities $q_1, q_2, \ldots, q_r$ by $3n$ relations of the form:

$$\begin{aligned} x_i &= x_i(q_1, q_2, \ldots, q_r) \\ y_i &= y_i(q_1, q_2, \ldots, q_r) \\ z_i &= z_i(q_1, q_2, \ldots, q_r) \end{aligned} \tag{1}$$

where $i = 1, 2, \ldots, n$. Then we are also able to express the displacements $\delta x_1, \delta y_1, \delta z_1$; $\delta x_2, \delta y_2, \delta z_2$; $\ldots\ldots$; $\delta x_n, \delta y_n, \delta z_n$ in terms of the variations $\delta q_1, \delta q_2, \ldots\ldots, \delta q_r$ of the generalized coordinates by differentiation of Eqs. (1). For instance, we have:

$$\delta x_i = \sum_{k=1}^{r} (\partial x_i/\partial q_k)\, \delta q_k = \sum_{k=1}^{r} \delta x_{ik} \tag{2}$$

where δx_{ik} is the displacement at the point i in the coordinate q_k or due to the mode k. We obtain analogous formulas for δy_i and δz_i.

A particular kind of generalized coordinate p_k can be associated with every normal mode k; the more significant properties of this type of coordinate are as follows:

(1) A normal coordinate deflection δp_k in the kth normal mode determines the deflection (in Cartesian coordinates x, y, z or in terms of any generalized coordinates $q_1, q_2, \ldots, q_r$) corresponding to that mode for every point i in the system, the deflection relations being given by the mode "shape." (Since the generalized coordinates, and particularly the normal coordinates, are not commonly used to describe the location of the points but only their displacements from equilibrium positions, the symbol δ is often omitted below.)

(2) When using normal coordinates the total kinetic and potential energies of a conservative system can be expressed as sums of the energies in the various normal modes, where the kinetic and the potential energies of each normal mode can be calculated as the kinetic and the potential energies of a single mass.[1] There is no coupling between normal modes and, consequently, the equations of motion are greatly simplified, each equation involving only one coordinate and its time derivatives. They are simply:

$$M_k\ddot{p}_k + K_k p_k = F_k \tag{3}$$

where $k = 1, 2, \ldots, r$, $\ddot{p}_k$ is the second time derivative of p_k, and M_k, K_k, and F_k are defined under (3) and (4) below.

(3) In connection with every normal mode, a generalized mass M_k is determined so that $M_k\dot{p}_k^2$ will equal the total kinetic energy of the structure in that mode—i.e.,

$$M_k\dot{p}_k^2 = \sum_{i=1}^{n} m_i(\dot{x}_{ik}^2 + \dot{y}_{ik}^2 + \dot{z}_{ik}^2) \tag{4}$$

where

$$\dot{x}_{ik} = \frac{d}{dt}\left(\frac{\partial x_i}{\partial p_k}\, p_k\right) = \dot{p}_k \frac{\partial x_i}{\partial p_k}$$

$$\dot{y}_{ik} = \frac{d}{dt}\left(\frac{\partial y_i}{\partial p_k}\, p_k\right) = \dot{p}_k \frac{\partial y_i}{\partial p_k}$$

and

$$\dot{z}_{ik} = \frac{d}{dt}\left(\frac{\partial z_i}{\partial p_k}\, p_k\right) = \dot{p}_k \frac{\partial z_i}{\partial p_k}$$

are the x, y, z components of the velocity of point i in mode k. A generalized spring stiffness K_k is also determined by the relation $\omega_k = \sqrt{K_k/M_k}$. ($\omega_k$ is the natural frequency in rad. per sec. of mode k.)

(4) Corresponding to an actual force f that may be applied by a vibrator in a certain direction in space at a point i of the structure, a generalized force F_k in the kth mode can be defined by the coordinate system in such a way that the work done by the force over a displacement at i in that mode, δp_{ik}, equals the product of the generalized force times the generalized normal displacement δp_k. Thus,

$$f(\partial q_i/\partial p_k)\delta p_k = f_x\delta x_{ik} + f_y\delta y_{ik} + f_z\delta z_{ik} = F_k\delta p_k \quad (5)$$

where q_i is a linear coordinate measuring the displacement of point i along the line of action of f; f_x, f_y, f_z are the components of the force in the x, y, z directions; and

$$\delta x_{ik} = \frac{\partial x_i}{\partial p_k}\delta p_k, \qquad \delta y_{ik} = \frac{\partial y_i}{\partial p_k}\delta p_k, \qquad \delta z_{ik} = \frac{\partial z_i}{\partial p_k}\delta p_k$$

When forces are applied at different points,

$$F_k = \sum^{i}\left(\frac{\partial x_i}{\partial p_k}f_{xi} + \frac{\partial y_i}{\partial p_k}f_{yi} + \frac{\partial z_i}{\partial p_k}f_{zi}\right) \quad (6)$$

the summation being taken over all the points and directions in space i at which vibrators are applied to the structure.

A generalized force may be made 0, thus eliminating the response in the corresponding mode by: (1) locating a vibrator at a point of the structure which is an "absolute node" in that mode—i.e., $\partial x_i/\partial p_k = \partial y_i/\partial p_k = \partial z_i/\partial p_k = 0$; (2) orienting a vibrator in space so that the force applied is normal to the response in that mode at the point where the vibrator is located—i.e., if θ is the angle in space between the direction of the force applied f and the response in that mode δp_{ik} at the point i where the vibrator is located

$$\cos\theta = (f_x\delta x_{ik} + f_y\delta y_{ik} + f_z\delta z_{ik})/f\delta p_{ik} = 0$$

(3) locating multiple vibrators so that their effects cancel (e.g., use symmetrical locations to eliminate unsymmetrical modes); (4) varying the ratio of forces applied by the vibrators until the resultant is either located at an "absolute node" as in (1) or at a node in the corresponding direction in space as in (2). (It should be pointed out that the preceding also applies without any essential modifications to the case when a vibrator is used which applies a torque and thus tends to produce angular rather than linear deflections.)

Since the generalized forces depend on responses, which are not the same for different modes, a single vibrator will apply different generalized forces in various modes. If two or more vibrators are not all in phase, the total generalized force F_k can be found by vectorial addition of the component generalized forces from each vibrator with their respective phases, thus obtaining a new phase ψ_k for each F_k relative to a reference vibrator. A rotary vibrator can be considered the equivalent of two linear-type vibrators contained in its plane of rotation, applying forces that are 90° out of phase along directions in space perpendicular to each other. Hence, a rotary vibrator will apply a generalized force of a certain phase ψ_k in the kth normal mode, but that phase will be different for different modes. At the instant when the vibrator mass is in line with the projection of the normal mode deflection on the plane of rotation, the generalized force is a maximum, whence the phase between any generalized force and the vibrator rotation can be determined (Fig. 1).

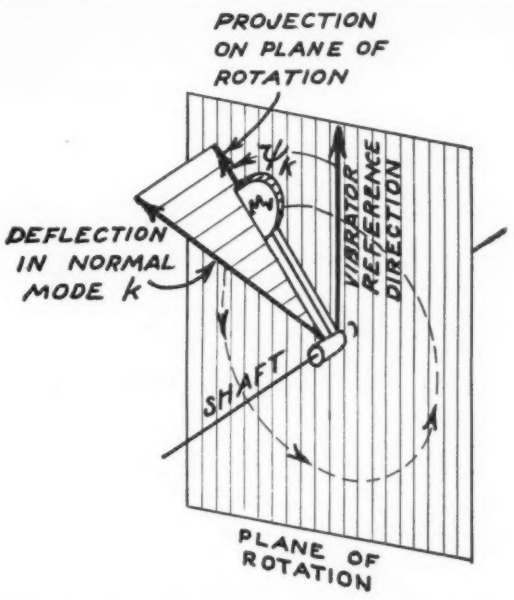

FIG. 1. Phase ψ_k of generalized force from rotary vibrator.

Motion of a Point

A displacement δq_k in a generalized coordinate k determines the displacement δq_{ik} at the point i with components δx_{ik}, δy_{ik}, δz_{ik} along the x, y, z axes (Fig. 2). δq_{ik} is a vector quantity since it has magnitude and direction. It will be referred to as being a *space* vector since its direction is given in a space coordinate system.

If δq_{ik} varies along the fixed direction sinusoidally with time, it may be represented as a different type of vector in a polar coordinate system, where the length of the vector is the amplitude of the motion and its direction is given by the phase angle $(\omega t + \phi)$. This type of vector will be called a *time* vector. The motion could be expressed analytically as

$$\delta q_{ik} = (\delta q_{ik})_A \sin(\omega t + \phi)$$

or

$$\delta q_{ik} = (\delta q_{ik})_A e^{i(\omega t + \phi)}$$

and the latter terminology will be used subsequently for convenience in mathematical operations, vectors being plotted in the complex plane.

The x, y, z components of a sinusoidal motion along a straight line are also sinusoidal functions of time and have the same frequency and phase angle; the direction cosines of the space vector will obviously remain constant throughout the cycle. It can now be seen that the condition of motion of a certain point along a straight line in space can only exist: (1) if there is but one normal mode present; (2) if the deflection at that point corresponding to each mode present has the same

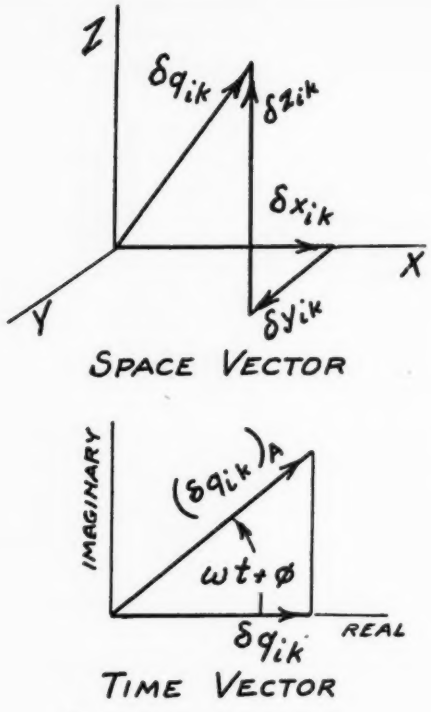

FIG. 2. Space and time vectors.

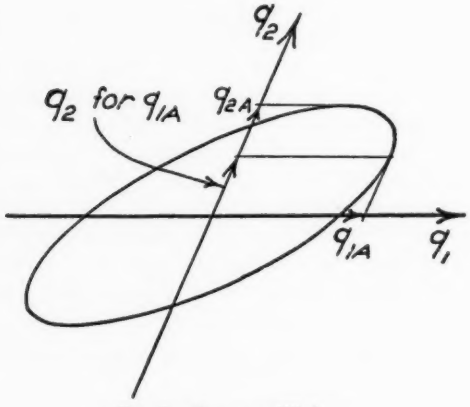

FIG. 3. Force equilibrium.

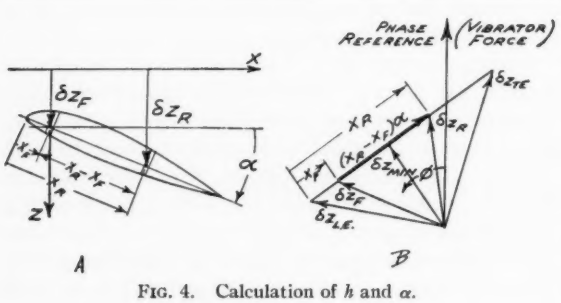

FIG. 4. Calculation of h and α.

direction in space; or (3) if the responses in all the modes are in phase.

When responses in two or more modes that do not have the same space and time vector directions are present at the same point of a structure, the motion along each normal coordinate direction can be resolved into its x, y, and z components of the form

$$\delta x_k = \delta x_{kA} e^{i(\omega t + \phi_k)}$$

for each mode k. On any of the axes these components could be represented as time vectors and thus could be added together; the resultant time vector has a new phase angle, which will be different for the resultant on each axis. E.g.:

$$\delta x = \sum_{k=1}^{r} \delta x_{k_A} e^{i(\omega t + \phi_k)} = \delta x_A e^{i(\omega t + \phi_x)} \qquad (7)$$

When the x, y, and z components of the resultant have different phases, the motion cannot be a straight line in space because the direction cosines $\partial x/\partial q$, $\partial y/\partial q$, and $\partial z/\partial q$ will vary with time. The motion is instead an ellipse, which is the most general type of motion for a point as long as the vibration in all the modes present is at the same frequency, as in the case of forced vibration without harmonics.

The phase relation between the components of motion along any two directions q_1 and q_2 can be determined if the shape and orientation of the ellipse are known—a well-known technique with Lissajous figures. Consider the projection of the ellipse on the plane containing directions q_1, q_2 as in Fig. 3. The components of motion are:

$$\begin{aligned} q_1 &= q_{1A} \cos(\omega t + \phi_1) \\ q_2 &= q_{2A} \cos(\omega t + \phi_2) \end{aligned} \qquad (8)$$

The amplitudes of the two coordinates are q_{1A} and q_{2A} the distances along the axis in question to the tangent parallel to the other axis. From Eqs. (8) it follows that q_1 equals q_{1A} when $\omega t = -\phi_1$. At that instant:

$$(q_2)_{\text{for } q_1 = q_{1A}} = q_{2A} \cos(-\phi_1 + \phi_2) \qquad (9)$$

Hence, the phase relation between the two motions is:

$$(\phi_2 - \phi_1) = \pm \cos^{-1}[(q_2)_{\text{for } q_1 = q_{1A}}/q_{2A}] \qquad (10)$$

(Note the ambiguity of sign.)

A linear vibration pickup measures the component of deflection along a certain direction in space which shall be called the pickup axis. When the point i to which it is attached oscillates sinusoidally along a straight line, this motion is obviously in phase with its projection on the pickup axis. Corresponding to a deflection p_k in a normal mode k, the pickup measures $q_{ik} = (\partial q_i/\partial p_k)p_k$, where q_i is a linear coordinate measuring the displacement of point i in the direction of the pickup axis and $\partial q_i/\partial p_k$ may be called the sensitivity of the pickup *location* to mode k. The sensitivity of the pickup itself, S (= output reading/input), must include

phase as well as amplitude response; therefore, it is a time vector quantity. The overall mode sensitivity of the pickup, $S(\partial q_i/\partial p_k)$, must be considered to be a vector quantity both in space and time. When the point of attachment moves in an ellipse, the projection of the motion on the pickup axis is sinusoidal, but it will have any phase angle depending on the relative orientation in space of q_i—i.e., of the pickup axis—and the ellipse.

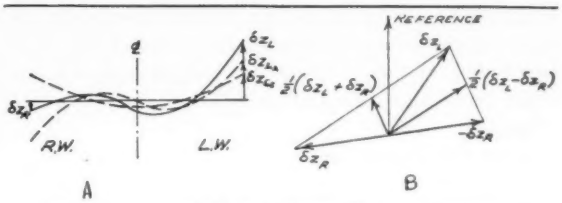

FIG. 5. Symmetrical and antisymmetrical components.

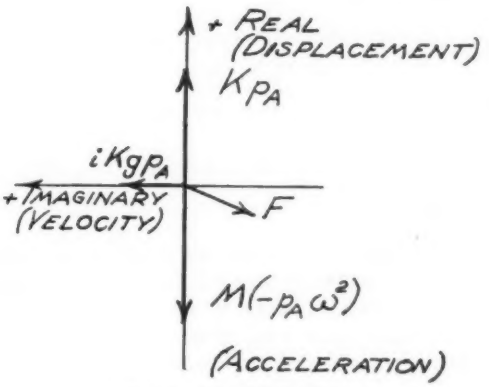

FIG. 6. Lissajous ellipse.

Relations Between Motions at Various Points

In a complicated structure such as an airplane, all parts participate in a normal mode vibration, and relations between all the parts must be considered. When only one mode is present, some points will have no motion at all; they may be called absolute nodes. For any point one may speak of node directions in which there is no motion, and for any direction one may speak of node points at which there is no motion in that direction. A linear pickup or vibrator located at a point and oriented in a direction in space in which there is no motion in a certain mode will not respond to or excite that mode.

If more than one mode is present, the components of motion along fixed directions in space at various parts of the structure will have various phases, just as the x, y, z components of motion at any one point will have different phase relations. Calculations of relative motions will thus have to be made vectorially.[2] Some special examples are now treated below.

The method for the vectorial calculation of h and α, the bending and torsional components of the wing motion, from responses measured by two pickups located at the same spanwise station, makes use of the formula:

$$\alpha = \tan \alpha = \frac{\delta z_F - \delta z_R}{x_F - x_R} \text{ (rad.)} \qquad (11)$$

which holds at any instant for small angles (Fig. 4A). If $\delta_F z$ and δz_R vary sinusoidally, α does also and all three may be represented by time vectors. The projection of the vectors on the real axis represents the magnitude of each quantity at the instant in the cycle when the vibrator force chosen for a phase reference is a maximum. If we combine the vectors according to the formula, the projections will also obey the formula—i.e., if the formula holds for the projections, it holds for the vectors.

Given the vectors for δz_F and δz_R, the deflections at two points on the chord, the vectors for δz_x and α, the deflection at any point, and the wing twist are found as in Fig. 4B where δz_F and δz_R are laid off from the same origin O. The vector from δz_F to δz_R, $(\delta z_R - \delta z_F)$ or δz_R relative to δz_F differs from α only by a scale factor. Hence, to get α in radians, the magnitude of vector $(\delta z_R - \delta z_F)$ is measured to the scale of δz_F and δz_R, and it is then divided by $(x_R - x_F)$, the distance between the front and rear pickups. The formula for α may be rewritten $\alpha = (\delta z_x - \delta z_F)/(x - x_F)$ and solved for the deflection at any point, giving:

$$\delta z_x = (x - x_F)\alpha + \delta z_F \qquad (12)$$

Hence, once the vector for α has been obtained, a linear scale of x may be laid off on it and the deflection for any other point on the chord may be found, such as the trailing edge or a point on the aileron. Note that instead of a true node there is only a point of minimum amplitude at which the deflection $\delta z_{min.}$ is always 90° out of phase with the angle of attack. When there is no fore-and-aft motion, the blur that the moving chord makes, as seen by an observer looking normal to the plane of motion (i.e., the projection of the envelope of the successive positions of the chord), is a hyperbola. Measurements made on this hyperbola may be used to obtain the phase relations between the motions at any points along the chord or between the angle of attack and the motion at any point.

The angle of attack of the aileron may be found by a similar method, setting up the equation for linear measurement which will hold at any instant and applying it to the vectors representing the sinusoidal variation of the various deflections.

It will often be useful to break down responses measured at symmetrical points into components of symmetrical and antisymmetrical motion. The normal modes of a closely symmetrical airplane are of two types. One type can be separated from the other because the following mode shape data are known or can be assumed

in advance: (1) In a given symmetrical mode, the vertical deflections at any symmetrical points R and L are equal ($\delta z_{RS} = \delta z_{LS}$); (2) in an antisymmetrical mode, these deflections are equal but opposite ($\delta z_{RA} = -\delta z_{LA}$) (Fig. 5A).

The total deflections are:

$$\begin{aligned} \delta z_L &= \delta z_{LS} + \delta z_{LA} \\ \delta z_R &= \delta z_{RS} - \delta z_{RA} \end{aligned} \tag{13}$$

These two equations may be solved for the components in the two modes:

$$\begin{aligned} \delta z_{LS} &= {}^1/_2(\delta z_L + \delta z_R) \\ \delta z_{LA} &= {}^1/_2(\delta z_L - \delta z_R) \end{aligned} \tag{14}$$

The graphical construction is given in Fig. 5B.

Vector Response to Forced Vibration

Single Mode

Eq. (3) above needs but the inclusion of damping effects to be applicable to actual systems. In airplane structural vibration work it is common practice to consider each mode k to have a structural damping coefficient g_k, representing a damping force proportional to the spring force but 90° out of phase with it.[3] The equation of motion in one mode is (dropping mode subscripts):

$$M\ddot{p} + K(1 + ig)p = Fe^{i\omega t} \tag{15}$$

for a simple harmonic force.[4] (F, the amplitude of the force, may be complex.) Assuming that $p = p_A e^{i\omega t}$ is a solution and substituting,

$$-M\omega^2 p_A + K(1 + ig)p_A = F \tag{16}$$

Fig. 6 is a graphical representation of the relation in Eq. (16) [or in Eq. (15) if the vectors are considered to rotate with a circular frequency ω].

From Eq. (16) the force required per unit displacement is obtained:

$$F/p_A = (K - M\omega^2) + iKg \tag{17}$$

and the variation with forcing frequency is represented vectorially in Fig. 7b for $g = 0.25$. The locus of the tip of F/p_A is obviously a straight line parallel to the real axis, because the imaginary component of the force required for unit displacement is always equal to Kg.

The plot of displacement per unit force amplitude (Fig. 7c) is a circle, with its "resonance diameter" (diameter through the resonant frequency point) perpendicular to the generalized force. (This circle is the inverse conformal transformation of the straight line of Fig. 7b[5].) Analytically, substituting the frequency ratio $\beta = \omega/\omega_n$, where $\omega_n = \sqrt{K/M}$ is the natural frequency, one gets:

$$\frac{p_A}{F} = \frac{1}{(K - M\omega^2) + iKg} = \frac{1}{K[(1 - \beta^2) + ig]} \tag{18}$$

Nondimensionalizing the displacement in terms of the static deflection F/K, the following expressions result:

$$Kp_A/F = 1/[(1 - \beta^2) + ig] \tag{19a}$$

or

$$\frac{p_A}{F/K} = \frac{1}{\sqrt{(1 - \beta^2)^2 + g^2}} e^{i \tan^{-1}[-g/(1 - \beta^2)]} \tag{19b}$$

$$Kp_A/F = \mu e^{i\phi} \tag{19c}$$

in polar form, and

$$\frac{p_A}{F/K} = \left[\frac{1 - \beta^2}{(1 - \beta^2)^2 + g^2}\right] + i\left[\frac{-g}{(1 - \beta^2)^2 + g^2}\right] \tag{19d}$$

$$Kp_A/F = \mu_R + i\mu_I \tag{19e}$$

in rectangular coordinates. (The symbols introduced are defined by comparison of terms.)

The response at a point i and along a direction in space or coordinate q_i, induced by an exciting force of the form $F \cos \omega t$ is:

$$\delta q_i = \frac{\partial q_i}{\partial p}\frac{F}{K}\mu \cos(\omega t + \phi) \tag{20a}$$

where the phase angle ϕ is the lead of the motion relative to the generalized force. The complex vector is represented in a coordinate system rotating at a frequency ω as:

$$\delta q_i = \frac{\partial q_i}{\partial p}\frac{F}{K}\mu e^{i\phi} \tag{20b}$$

The generalized force corresponding to a single linear vibrator applying a force f at a point j in a direction q_j is $F = (\partial q_j/\partial p)f$ by Eq. (5). The response induced by this force along direction q_i at a point i is obtained by replacing in Eq. (20b):

$$\delta q_i = \frac{\partial q_i}{\partial p} \times \frac{\partial q_j}{\partial p} \times \frac{f}{K}\mu e^{i\phi} \tag{21}$$

It can be seen that the response at i due to the vibrator force at j is equal in magnitude and phase to the response that would be induced at j if the same vibrator were located at i, because the same partial derivatives would be involved (Maxwell's reciprocity theorem). (In the preceding statement i and j should be understood to represent points as well as directions in space.)

The polar form of Eq. (19c) is familiar, but the rectangular form with the new symbols for the real and imaginary compoents μ_R and μ_I of the nondimensional response is unusual.[5] The usefulness of these terms will be seen later. Figs. 7d and 7e give plots of μ, ϕ, μ_R, and μ_I vs. β^2 for a damping coefficient $g = 0.03$. It should be noted that resonance is indicated by maxima in μ and μ_I (their derivatives with respect to β^2 are 0), and by points of inflection in ϕ and μ_R (maximum slope or maximum derivative with respect to β^2). Also $\mu_R = 0$ and $\phi = 90°$ at resonance.

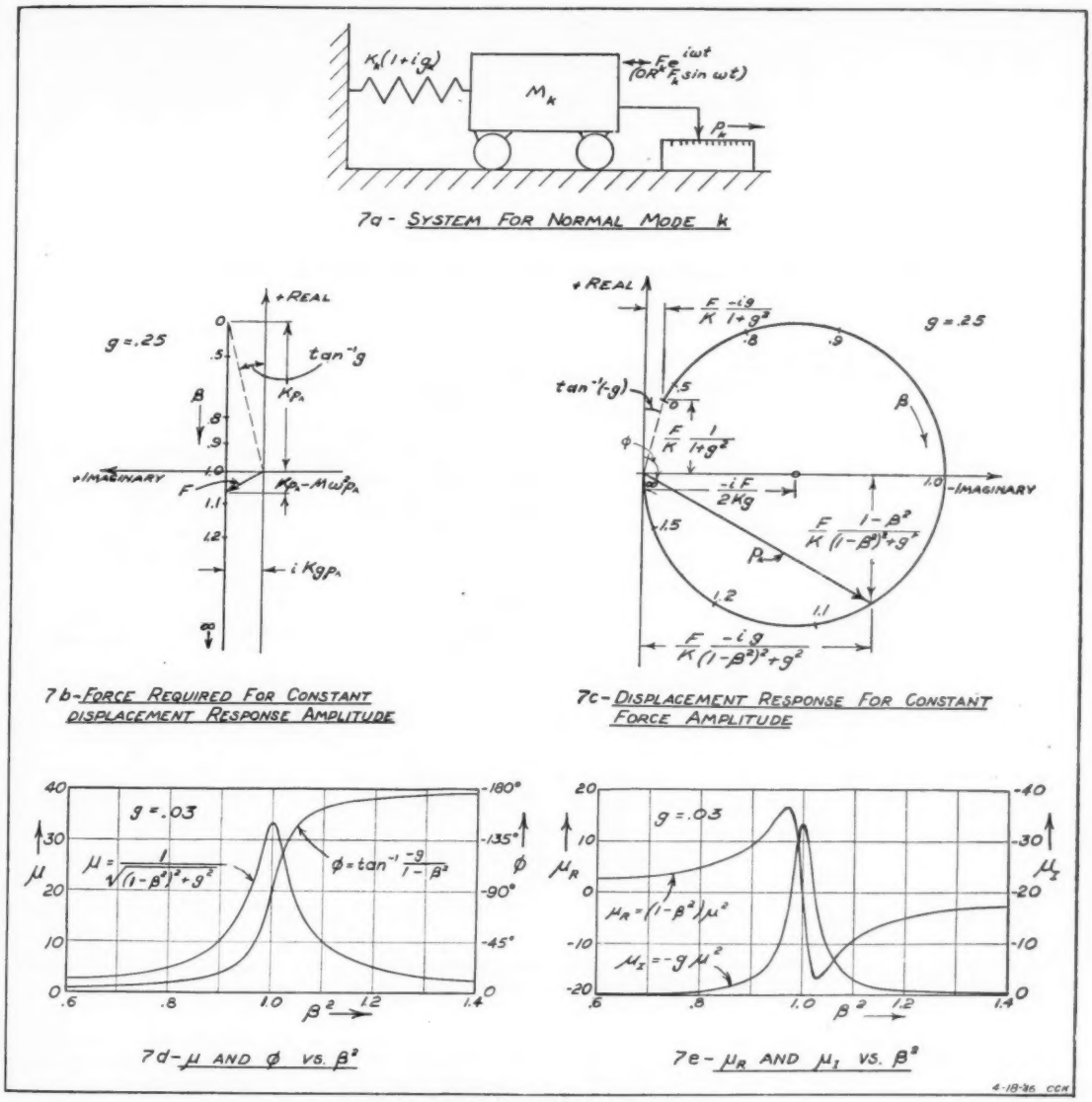
7a - SYSTEM FOR NORMAL MODE k
7b - FORCE REQUIRED FOR CONSTANT DISPLACEMENT RESPONSE AMPLITUDE
7c - DISPLACEMENT RESPONSE FOR CONSTANT FORCE AMPLITUDE
7d - μ AND φ VS. β²
7e - μR AND μI VS. β²
g = .25
g = .03
+REAL
+IMAGINARY
4-18-36 CCH

FIG. 7. Single degree of freedom response.

For a rotary or inertia vibrator with a constant unbalance, the force does not have a constant amplitude since the forcing frequency is varied; it is equal to the unbalance mass m_v, multiplied by the absolute acceleration of its center of gravity—i.e.:

$$\text{Actual force} = -m_v(\ddot{q}_R + \ddot{q}_v) = m_v(R\omega^2 e^{i\omega t} - \ddot{q}_v)$$

where $\ddot{q}_R$ = acceleration of m_v relative to v, the point of attachment to the structure; $\ddot{q}_v$ = absolute acceleration of the point of attachment; R = arm of rotation; and ω = angular frequency. The equation of motion in any normal mode is of the form:

$$M\ddot{p} + K(1 + ig)p = (\partial q_v/\partial p)m_v(R\omega^2 e^{i\omega t} - \ddot{q}_v) \quad (22a)$$

which, after rearranging and substituting $\ddot{q}_v = (\partial q_v/\partial p)\ddot{p}$, becomes:

$$\frac{M + m_v(\partial q_v/\partial p)^2}{\partial q_v/\partial p}\ddot{p} + \frac{K(1 + ig)}{\partial q_v/\partial p}p = m_v R\omega^2 e^{i\omega t} \quad (22b)$$

This represents the new system shown in Fig. 8a for which: the generalized mass is increased by the contribution of the vibrator mass; the generalized mass and spring are changed in proportion to the normal mode deflection at the point of attachment and the driving force is directly proportional to the frequency squared.

Again assuming a solution of the form $p = p_A e^{i\omega t}$, the response is obtained as:

$$p_A = \frac{m_v(\partial q_v/\partial p)R}{M + m_v(\partial q_v/\partial p)^2}\mu\beta^2 e^{i\phi} \quad (23)$$

where

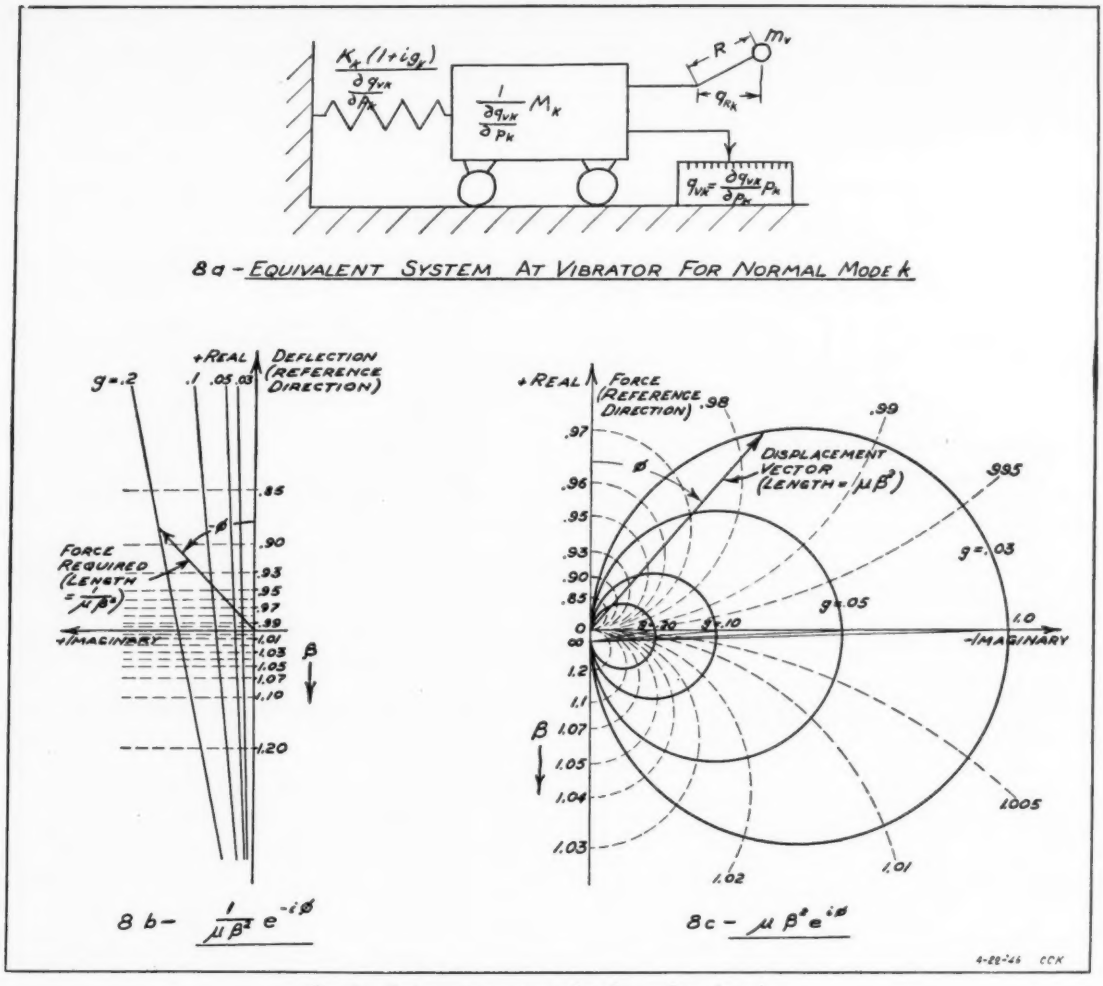

FIG. 8. Frequency response plots for various dampings.

$\mu = 1/\sqrt{(1-\beta^2)^2 + g^2}$, $\quad \phi = \tan^{-1}[-g/(1-\beta^2)]$

and

$$\beta = \omega/\sqrt{K/[M + m_v(\partial p_v/\partial p)^2]}$$

For the case of a rotary vibrator, an additional phase angle ψ will be added in each mode as explained with Fig. 1.

Figs. 8b and 8c are vector plots of $(1/\mu\beta^2)e^{-i\phi}$ and the inverse, $\mu\beta^2 e^{i\phi}$, for various values of g. These may be considered as nondimensionalized graphs of, respectively, unbalance required per unit displacement and displacement response to a unit unbalance for variable forcing frequency for the system of Fig. 8a. They may be also considered to be plots of the force required for unit acceleration and the acceleration response to a unit force for the system shown in Fig. 7a, since:

$$\frac{\ddot{p}_A}{F/M} = -\frac{p_A\omega^2}{F/M} = -\frac{p_A\omega^2}{F\omega_n^2/K} = -\mu\beta^2 e^{i\phi} \quad (24)$$

Fig. 8b is also, by coincidence, a straight line, sometimes called the "damping line" in graphical flutter analyses.[6-8] Similar curves corresponding to products of $\mu e^{i\phi}$ with any other powers of β are more complex. (For systems with viscous damping, only the plot of force required per unit velocity is a straight line;[9] the curve of force per unit displacement is a parabola.[10]) When damping is small, however, a nearly straight line is always obtained in the vicinity of the natural frequency. Note the simplicity of Figs. 8b and 8c as compared to the usual separate phase and amplitude response plots. The effect of lowering the damping, which is that of increasing the diameters of the circles and of expanding the frequency scale, can be readily observed. For any one given damping, the frequency scale is most expanded in the vicinity of resonance; as shown below, this property is the basis of a novel method of locating natural frequencies of considerable utility when the curves are complicated by the presence of many modes.

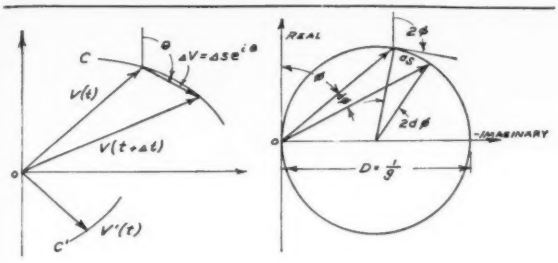

a - GENERAL CURVE V(t) b - V(t) = μe^iφ

FIG. 9. Vector derivatives.

Vector Derivatives of Response Vectors

Before considering the rate of change of the response curves with frequency ratio, a brief review of the differentiation of vector quantities in general will be made. In Fig. 9a let curve C be the path of motion of a point P constrained to move in the XOY plane. The position of the point is given by the tip of the vector $V(t)$, which is a function of a certain parameter t. The derivative with respect to t is:

$$V'(t) = \frac{dV}{dt} = \text{limit}_{\Delta t \to 0}\left[\frac{V(t+\Delta t) - V(t)}{\Delta t}\right] \quad (25)$$

(The minus sign indicates vector subtraction.) $V'(t)$ is a vector itself, having the direction of the tangent to curve C and a magnitude equal to the "speed" of the tip of $V(t)$, ds/dt, along the path C. The curve C' is the hodograph of C.

Applying this to differentiating $\mu e^{i\phi}$ with respect to β^2, it may be shown that

$$(\mu e^{i\phi})' = (\mu e^{i\phi})^2 = \mu^2 e^{i(2\phi)} \quad (26)$$

i.e., that the square of $\mu e^{i\phi}$ equals its first derivative with respect to β^2. This can be proved by using the properties of the circular vector plot, Fig. 9b. The angle of the tangent is 2ϕ, which is the angle of the derivative. The length s of the arc on the curve is the radius times the angle subtended; hence

$$ds = R \times 2d\phi = d\phi/g$$

The argument of the derivative is:

$$\frac{ds}{d(\beta^2)} = \frac{1}{g}\frac{d\phi}{d(\beta^2)} = \frac{1}{g}\frac{d}{d(\beta^2)}\left[\tan^{-1}\left(\frac{-g}{1-\beta^2}\right)\right] = \mu^2$$

Q.E.D.

Fig. 10a gives the locus of the tip of $\mu^2 e^{i(2\phi)}$ in the complex plane. The equation for this curve in polar coordinates, obtained by eliminating β^2 between μ^2 and 2ϕ, is

$$\mu^2 = (1/2g^2)[1 - \cos(2\phi)] \quad (27)$$

On plots of the amplitude and phase (μ^2 and 2ϕ, respectively) of the derivative vs. β^2, resonance would again be indicated by a maximum or an inflection point, respectively, in the two curves. The peak in the μ^2 plot, however, is sharper than that in μ, and the maximum slope of the 2ϕ curve is greater than that of ϕ; consequently, it may be said that the derivative is more sensitive to a resonant frequency than is the original quantity.

In theory, the vector differentiation with respect to β^2 of $\mu e^{i\phi}$ can be repeated any number of times and the nth vector derivative can be shown by inductive reasoning to be:

$$\frac{d^n}{d(\beta^2)^n}(\mu e^{i\phi}) = n!\,\mu^{n+1} e^{i[(n+1)\phi]} \quad (28)$$

Each successive differentiation will sharpen the peak

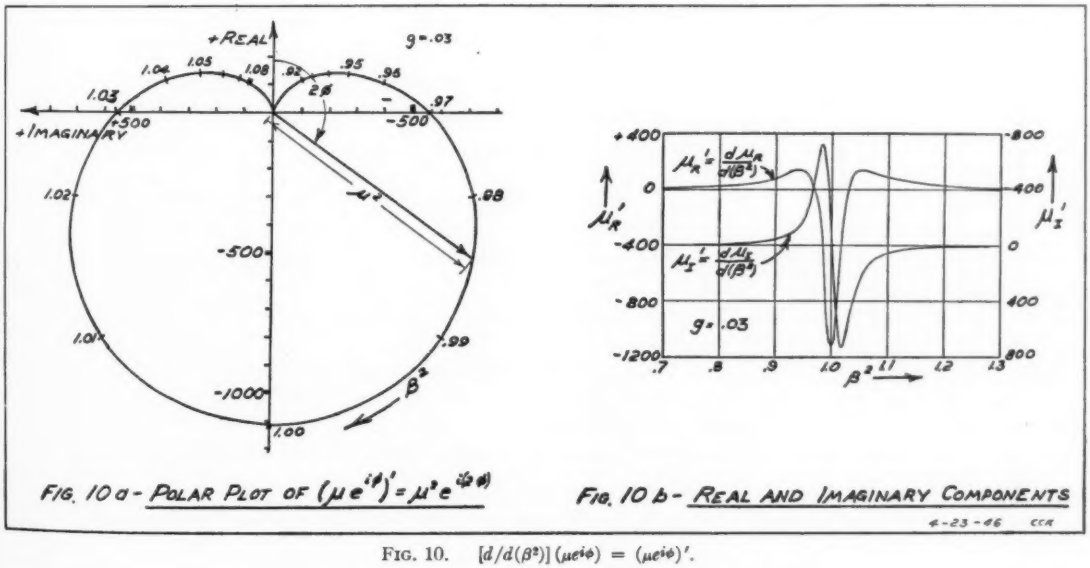

FIG. 10a - POLAR PLOT OF $(\mu e^{i\phi})' = \mu^2 e^{i(2\phi)}$

FIG. 10b - REAL AND IMAGINARY COMPONENTS

4-23-46 CCR

FIG. 10. $[d/d(\beta^2)](\mu e^{i\phi}) = (\mu e^{i\phi})'$.

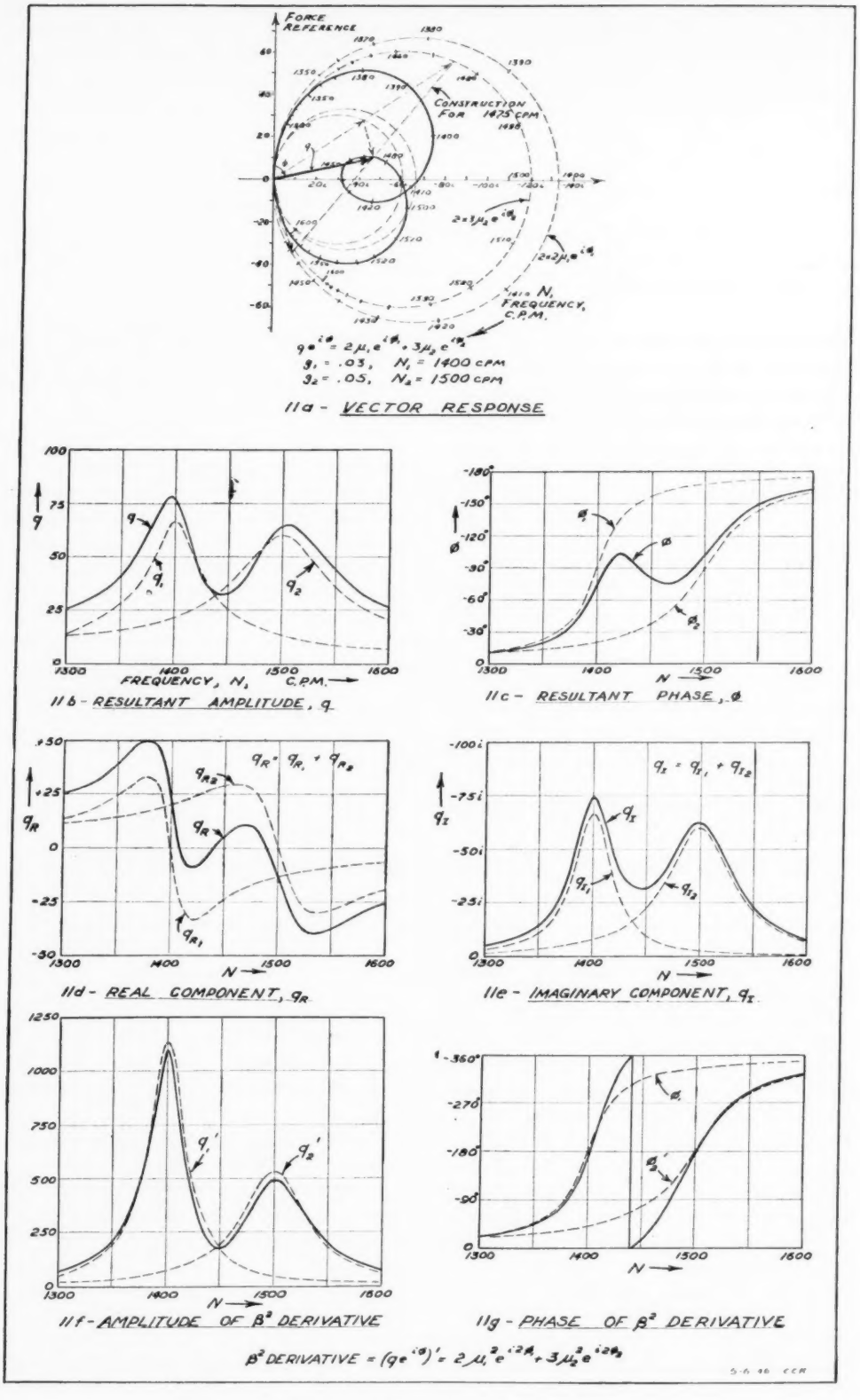
FORCE REFERENCE
CONSTRUCTION FOR 1475 CPM
N, FREQUENCY, C.P.M.
$q e^{i\phi} = 2\mu_1 e^{i\phi_1} + 3\mu_2 e^{i\phi_2}$
$\mu_1 = .03$, $N_1 = 1400$ CPM
$\mu_2 = .05$, $N_2 = 1500$ CPM
11a - VECTOR RESPONSE
FREQUENCY, N_1 C.P.M.
11b - RESULTANT AMPLITUDE, q
11c - RESULTANT PHASE, ∅
11d - REAL COMPONENT, q_R
11e - IMAGINARY COMPONENT, q_I
11f - AMPLITUDE OF β^2 DERIVATIVE
11g - PHASE OF β^2 DERIVATIVE
β^2 DERIVATIVE = $(qe^{i\phi})' = 2\mu_1^2 e^{i2\phi_1} + 3\mu_2^2 e^{i2\phi_2}$

FIG. 11. Response for the summation of two arbitrary modes.

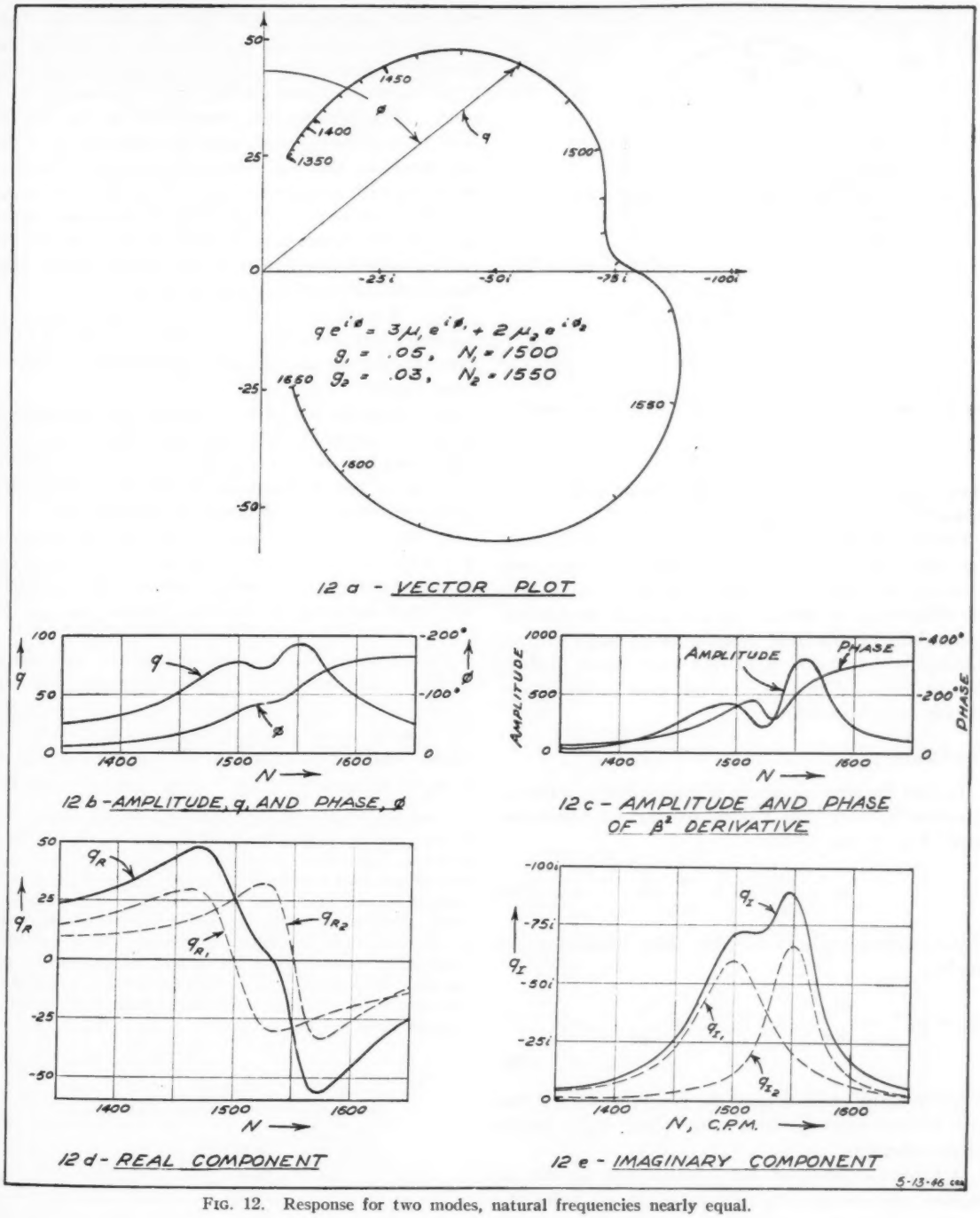

FIG. 12. Response for two modes, natural frequencies nearly equal.

in the curve of amplitude response vs. β^2 and also steepen the inflection slope of the curve of phase response vs. β^2 near the natural frequency; in other words, the sensitization to resonance is increased by differentiation.

The same effect can be seen in another manifestation. The real and imaginary components of the derivative are equal to the derivatives of, respectively, the real and imaginary components of the response vector. In Fig. 10b are given plots of μ_R' and μ_I', the rates of change with β^2 of the real and imaginary components of $\mu e^{i\phi}$:

$$\mu_R' = \frac{d}{d(\beta^2)}(\mu_R) = \frac{d}{d(\beta^2)}(\mu \cos \phi) = \mu^2 \cos(2\phi)$$

and similarly

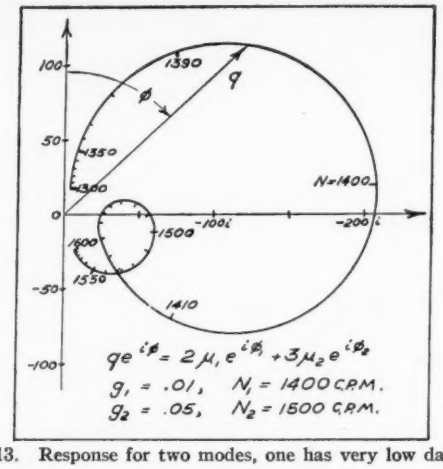

FIG. 13. Response for two modes, one has very low damping.

$$\mu_I' = \mu^2 \sin(2\phi)$$

These derivatives too have greater slopes and sharper peaks than the original quantities.

The importance of the derivatives in practical vibration work lies mainly in giving another point from which to view the vector plots. However, more than one differentiation will be impractical with the present uncertainty of vibration measurements made on mechanical systems. It might find more direct application in electrical problems where experimental inaccuracies may be smaller.

Two Modes

To find the response δq_i at a point i and in a pickup direction q_i when two modes are excited simultaneously, Eq. (2) can be used:

$$\delta q_i = \frac{\partial q_i}{\partial p_1}\delta p_1 + \frac{\partial q_i}{\partial p_2}\delta p_2 \qquad (29a)$$

If the oscillation is harmonic, Eq. (20b) applies for each mode:

$$\delta q_i = q_i e^{i\phi_i} = \frac{\partial q_i}{\partial p_1}\frac{F_1}{K_1}\mu_1 e^{i(\phi_1+\psi_1)} + \frac{\partial q_i}{\partial p_2}\frac{F_2}{K_2}\mu_2 e^{i(\phi_2+\psi_2)} \qquad (29b)$$

where ψ is the phase lead of the generalized force relative to some reference such as the phase of the motion of the vibrators.

A typical example of such a summation for two arbitrary modes is shown in Fig. 11, which is a polar plot of the locus in the complex plane of the tip of vector $q_i e^{i\phi_i}$ as given by Eq. (29b) above, when the forcing frequency is varied from 0 to ∞. As can be seen, it is a curve having two nearly circular parts corresponding to the two modes. This vector plot could be obtained in three different ways: (1) adding separately the real and imaginary components of the responses in the two modes (from Figs. 11d and 11e); (2) adding vectorially the responses in the two modes taking into account the respective magnitudes and time phases (from Figs. 11b and 11c); and (3) geometrically by finding the locus of the point midway between points corresponding to the same frequency on the two single mode vector plots. (This construction, exemplified in Fig. 11a for $N = 1475$ cycles per min., gives the vector $0.5(q_1 + q_2)$, and, therefore, the single mode response circles have to be drawn with a double radius.) Note that the peaks and inflection points corresponding to resonance on the q_R, q_1 and the differentiated curves occur more closely to the natural frequencies of the normal modes than they do on the resultant q and ϕ curves.

Figs. 12 to 16 are similar plots for other examples of responses with more than one mode present. Table 1 lists the values of the various constants in Eq. (29b) for these figures.

Fig. 12 shows the effect of having two modes with natural frequencies close together. The vector plot still shows two distinct circular parts, but the connecting loop in Fig. 11 has become merely a bulge; two points of inflection in the curve replace the loop.

In Fig. 13 one mode has an extremely low damping, $g = 0.01$, which increases its relative amplitude. The smaller damping mode tends to obscure the mode with the larger damping, but the two circular parts are still apparent.

Fig. 14 shows the variation of response with pickup location along the wing chord when two modes are present. The curves for points A and D exemplify the case when $\partial q_i/\partial p_k$ has opposite signs for the two modes which causes part of the curve to fall in the positive imaginary region.* For curve D the two

* Only when a single linear vibrator or its equivalent is employed, and then only at the point of application and in the direction in space of the exciting force, must the response vector plot be contained entirely in the negative imaginary half of the complex plane. This is due to the fact that all mode response circles are on the same side of the force phase reference test which is a corollary of the Driving Point Impedance Theorem.[5] When single mode response circles fall on both sides of the real axis, the paradoxical situation may arise where a resonant frequency is indicated by a minimum rather than a peak in the amplitude response curve (see Fig. 16).

TABLE 1
Summary of Mode Data for Figs. 11 to 16

Fig.	Mode	N_k, Cycles per Min., Natural Frequency	g_k, Damping Coefficient	$\frac{\partial q_i}{\partial p_k}\frac{F_k}{K_k}$	ψ_k
11	1	1,400	0.03	2	0
	2	1,500	0.05	3	0
12	1	1,500	0.05	3	0
	2	1,550	0.03	2	0
13	1	1,400	0.01	2	0
	2	1,500	0.05	3	0
14				Point: A O_2 B C O_1 D	
	1	1,400	0.03	5 3.5 2 0.5 0 −1	0
	2	1,500	0.05	−3 0 3 6 7 9	0
15	1	1,400	0.03	2	90°
	2	1,500	0.05	3	0
16	1	1,400	0.03	2	0
	2	1,450	0.03	−0.75	0
	3	1,500	0.05	3	0

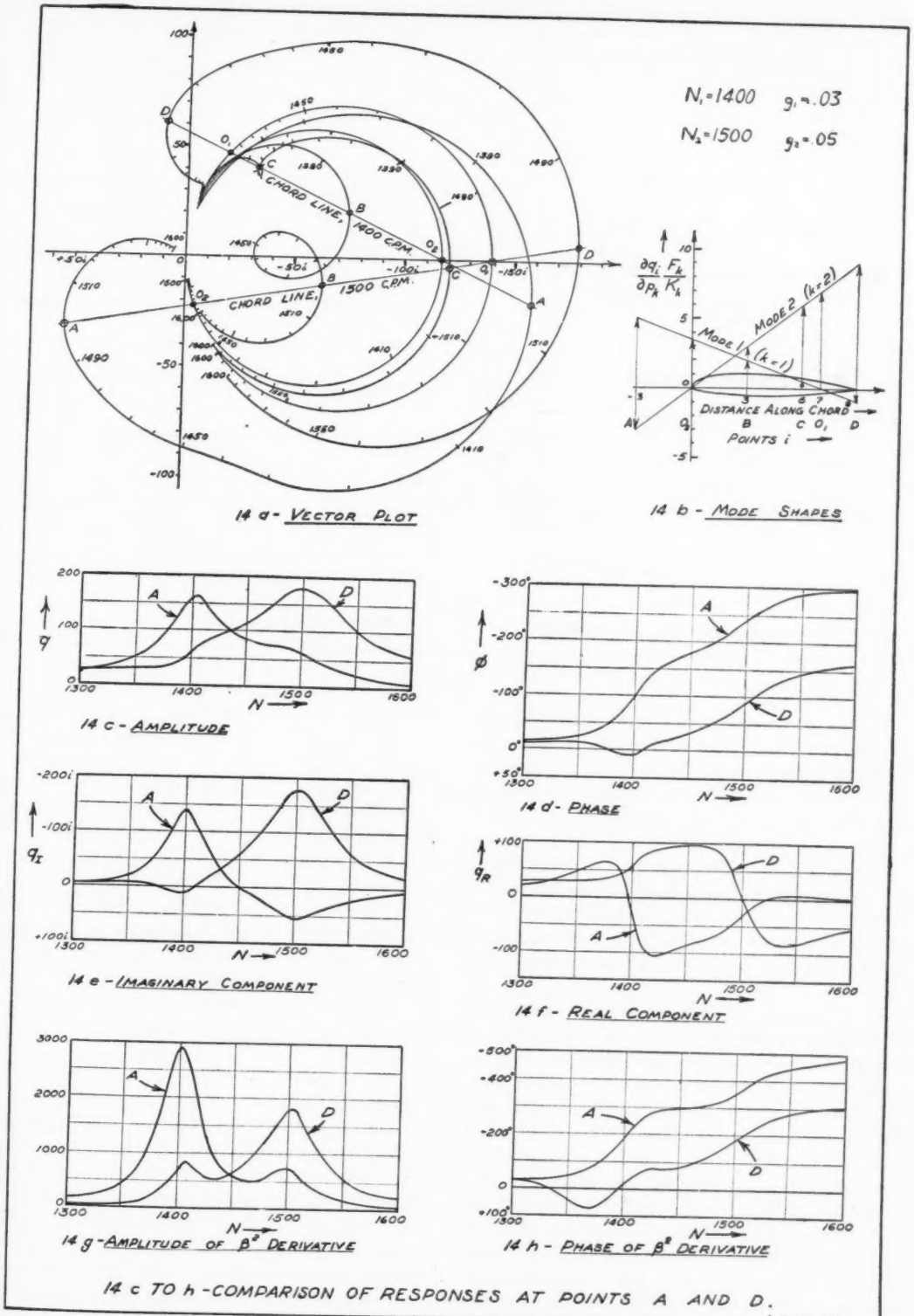
N₁=1400 g₁=.03
N₂=1500 g₂=.05
CHORD LINE, 1400 C.P.M.
CHORD LINE, 1500 C.P.M.
MODE 2 (k=2)
MODE 1 (k=1)
DISTANCE ALONG CHORD
POINTS i
14 a - VECTOR PLOT
14 b - MODE SHAPES
14 c - AMPLITUDE
14 d - PHASE
14 e - IMAGINARY COMPONENT
14 f - REAL COMPONENT
14 g - AMPLITUDE OF β² DERIVATIVE
14 h - PHASE OF β² DERIVATIVE
14 c TO h - COMPARISON OF RESPONSES AT POINTS A AND D.

FIG. 14. Response for two modes, various pickup locations on chord.

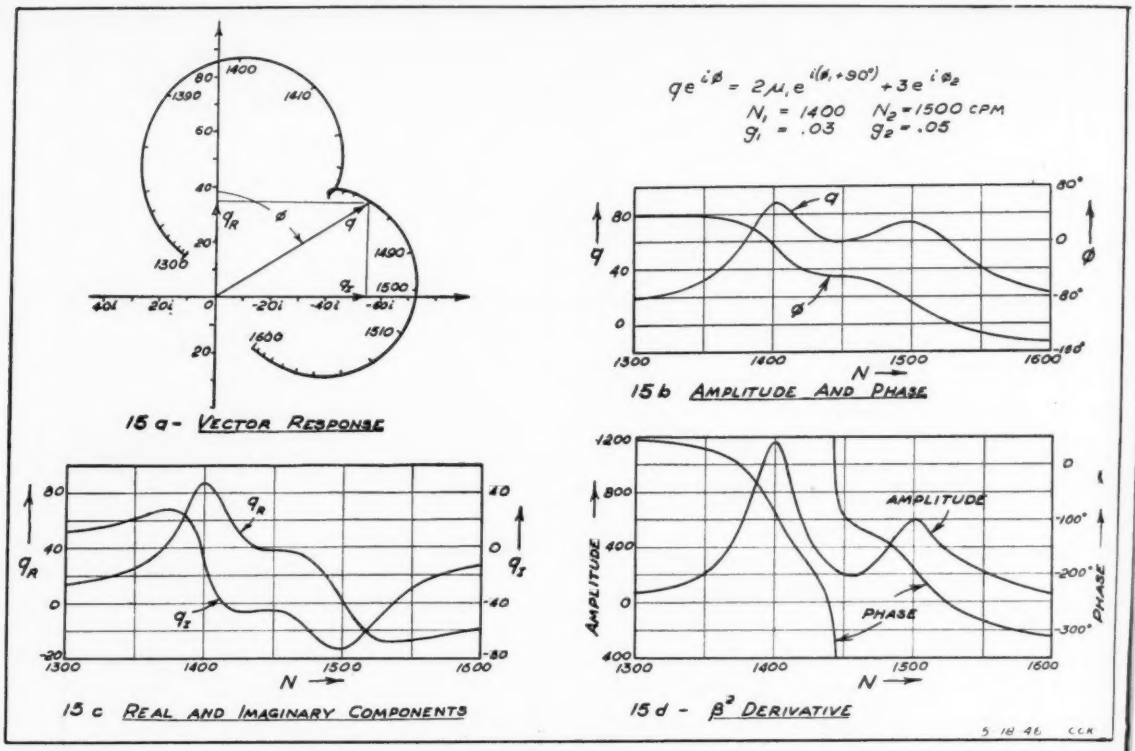
$qe^{i\phi} = 2\mu_1 e^{i(\phi_1+90°)} + 3e^{i\phi_2}$
$N_1 = 1400$ $N_2 = 1500$ CPM
$g_1 = .03$ $g_2 = .05$
15 a - VECTOR RESPONSE
15 b AMPLITUDE AND PHASE
15 c REAL AND IMAGINARY COMPONENTS
15 d - β^2 DERIVATIVE
AMPLITUDE
PHASE
5 18 47 CCK

FIG. 15. Response for two modes, generalized forces 90° out of phase.

nearly circular parts are not even separated by two inflection points; they are only distinguishable by the increased rate of change with frequency of the response vector at resonance. The frequency scale is marked in constant intervals of 10 cycles per min. (as in all the other vector plots) to make the changes in ds/dN and correspondingly in $ds/d(\beta^2)$ apparent. In Figs. 14c to 14h the various types of response for points A and D are compared. Note that only one peak in amplitude occurs in either curve (Fig. 14c), but the amplitude of the derivative shows peaks for both modes (Fig. 14g).

The vector plots of Fig. 14a are obtained as follows: If the responses in the two modes at O_1 and O_2, the nodes of the modes for motion in vertical direction, are given, the respective circles can easily be constructed by Fig. 7. Then, at any frequency, the response vectors for these two points are combined, according to Eqs. (11) and (12) and Fig. 4B, to find the response at any other points A, B, C, ... along the chord. To illustrate this, the "chord" lines (loci of the tips of the response vectors for various points along the wing chord) are drawn in for 1,400 and 1,500 cycles per min. If the construction is repeated for a number of frequencies, curves A, B, C, ... of Fig. 14a corresponding to points A, B, C, ... of Fig. 14b are obtained. (A different interpretation can be given by considering the curves O_1, O_2, A, B, C, ... to represent responses at the same point P but along different directions in space. Particularly then O_1 and O_2 are the node directions—i.e., the directions of zero response in, respectively, modes 1 and 2 at point P.) The method can be used to find the response curves at any point in the structure and for any direction in space, because the points along the chord line (extended to infinity) represent all possible combinations of proportions of responses in the two modes. That is, all the possible *shapes* of frequency response curves will be given by this construction, although the actual magnitudes might be different at other parts of the structure. Note that by the reciprocity theorem the same figure would also represent the responses at the present vibrator location if the same vibrator were placed at points A, B, C, ... of the structure.

In Fig. 15, the generalized forces are assumed to be 90° out of phase to exemplify the effect of using a rotary vibrator or, in general, linear vibrators that are out of phase with one another. As the resonance diameters of the various response circles have to be perpendicular to the generalized forces in the respective modes, the maxima in the imaginary components will indicate natural frequencies only when these generalized forces are all in phase. In a case as that of Fig. 15, resonances must be identified by the fact that they correspond to points of maximum "velocity" along the curve as N changes (i.e., points at which $ds/d(\beta^2)$ is a maximum).

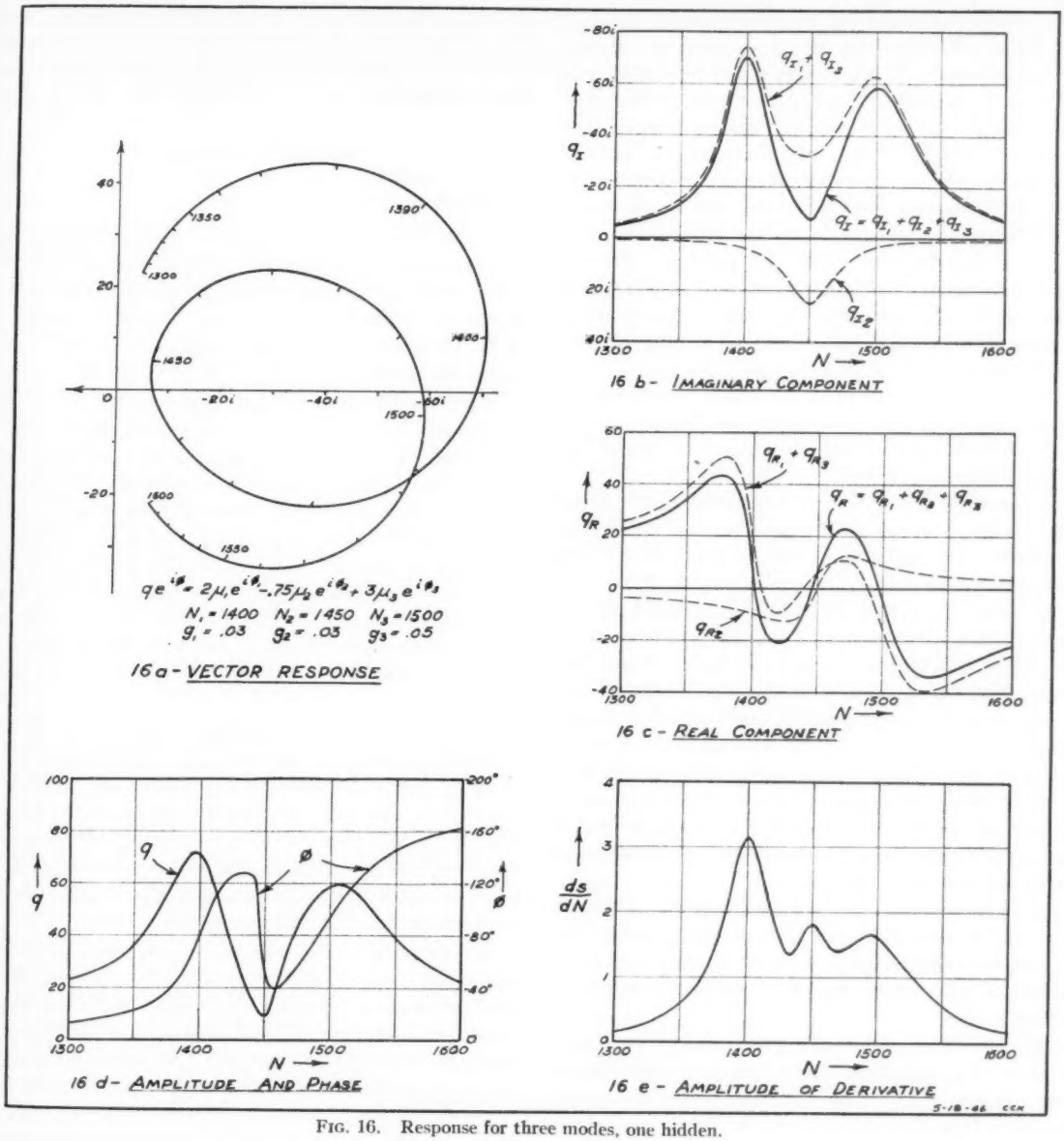
16 a - VECTOR RESPONSE
$qe^{i\phi} = 2\mu_1 e^{i\phi_1} - .75\mu_2 e^{i\phi_2} + 3\mu_3 e^{i\phi_3}$
$N_1 = 1400$ $N_2 = 1450$ $N_3 = 1500$
$g_1 = .03$ $g_2 = .03$ $g_3 = .05$
16 b - IMAGINARY COMPONENT
16 c - REAL COMPONENT
16 d - AMPLITUDE AND PHASE
16 e - AMPLITUDE OF DERIVATIVE
5-19-46 CCK

FIG. 16. Response for three modes, one hidden.

More than Two Modes

It is apparent that the vector responses at a point can be synthesized for any number of modes when given g_k and $(\partial q_l/\partial p_k)\cdot(F_k/K_k)$. The circles for response in any one mode may be displaced farther and farther from the origin, but they will usually still be evident, having distortions similar to those seen in the examples given for two modes. The phase and amplitude curves will flatten out as the circles are displaced farther, and, consequently, it becomes more and more necessary to make vector plots to identify modes.

In some cases, however, the circles may be hidden. This may happen when the resonance diameter of the circle lies on the side of the reference opposite to that shown in most of the examples. In this case the circle may only accentuate a loop or inward bulge of the curve by increasing its size, and thus, adding no new characteristic to the plot, the corresponding mode might go unnoticed. An example is given in Fig. 16. Mode Nos. 1 and 3 are the same as shown in Fig. 11. A mode No. 2 has been added at $N = 1{,}450$. Comparing these figures, the most apparent difference is the increase in the size of the loop; an unwary person might think the response represented only two modes. On closer inspection a criterion appears: comparing Δs for a constant ΔN three maxima are found in Fig. 16a as compared to only two on Fig. 11a. This is obvious in the plot of the amplitude of the derivative, Fig. 16e,

but in none of the other curves is the 1,450 mode apparent. Again, the sensitivity to resonance of the derivative is illustrated. (The previous derivatives were with respect to β^2 or, in effect, to N^2. The shape of the derivative with respect to N will be little different, since $dq/dN = 2N[dq/d(N^2)]$.) In extreme cases, one differentiation may not bring out the hidden peak in the valley between two obvious peaks, but in theory it would eventually appear in the amplitude curve as higher derivatives were taken. In practice, however, the uncertainties in measurements are magnified with differentiation; hence, with the present inaccuracy of experimental data more than one such differentiation may be impractical.

The following are the more important conclusions regarding frequency response vector plot shapes:

(1) In the vicinity of a resonance the shape approaches that of a circle.

(2) In most cases, for frequencies intermediate between two resonances the response vector tip describes a characteristic loop such as that of Figs. 11a, 13, 14a (points B, C), and 15a.

(3) When resonant frequencies are close to one another (Fig. 12a), or when dampings are large or responses are different in size and angular positions [Fig. 14a (point A)]—i.e., whenever the effect in the vicinity of one natural frequency due to another mode is substantial, no such connecting loop can be observed. However, the radius of curvature, which usually is directed toward the origin in the vicinity of resonances, will still be directed the opposite way in this transition region, the change being accompanied by two inflection points which replace the loop.

(4) At resonance $ds/d(\beta^2)$ is always a maximum. This can be seen either on plots of this quantity (the amplitude of the derivative) vs. β^2, or then directly on the vector plots when equal intervals of $\Delta\beta$ or ΔN are laid off.

All of the discussion in these sections can be applied to plots of acceleration response to constant vibrator force amplitude and closely to other forms of response and other types of damping, even in the cases when the latter is sufficiently large so that the vibration modes do not have the simple characteristics listed at the beginning of this paper. The departures of the various kinds of response plots from the circles discussed here will be negligible in actual airplane vibration practice.

A similar type of vector representation of frequency responses is used commonly in electrical problems such as the oscillatory stability of feedback amplifiers.[11, 12] More recently, the method of plotting a forced oscillation response in the complex plane has been mentioned in connection with the design of servomechanisms.[13] The problem of airplane vibration is made more complicated than these by the fact that an airplane is a distributed system with fixed and unknown stiffness, damping, and inertia constants, and the experimental technique and apparatus is less well developed. Fortunately, the damping of structures is usually low enough to enable approximations by normal modes, which is not always possible in connection with other kinds of systems.

Separating Modes

The Problem

We are now ready to discuss the main problem of exciting, measuring, and analyzing the vibration modes of a structure and of airplanes in particular. The object is first to "identify" the various normal modes in a certain frequency range and then to "describe" each mode of interest.

The *identification* of a mode will be made by giving its natural frequency and if necessary, some shape characteristic that will distinguish it from other modes with resonant frequencies in that vicinity. Rough descriptions such as bending, torsion, wing, tail, or fuselage modes may thus serve a useful purpose; however, one must be careful not to assume that the mode shape is known when such a label is attached, because several of these uncoupled degrees of freedom may participate in an actual normal mode. It is safer to use just the natural frequency as an identification whenever possible.

The *description*, to be complete, must include (1) the natural frequency, (2) the damping, (3) the generalized mass or generalized spring stiffness (one will determine the other), and (4) the complete shape of the mode. The shape will give the motion of every point corresponding to a unit displacement in that normal mode—i.e., it will determine $\partial x_i/\partial p_k$, $\partial y_i/\partial p_k$, and $\partial z_i/\partial p_k$ at all the points of the system. [See Eq. (1).]

To carry out the identification, the total forced vibration of enough points of the structure must be measured so as to be sure that all modes will show their resonance characteristics in at least one of these responses. For this purpose it is now common practice to use plots of the total amplitude response vs. forcing frequency. One of the main objects of this paper is to show that the best way—and, when the total response is especially complicated, the only way—is to plot the response vector (i.e., to take into account simultaneously both amplitude and phase response).

The first step in trying to simplify a complex total response is to eliminate as many undesired modes as possible by using vibrators that do not excite those modes. In general, with one linear vibrator it is possible to eliminate at most three modes; the point of application of the force will have to be an absolute node of the first mode, and the direction of the force must be perpendicular to the plane containing the space directions of the responses at that point in the second and third modes. In practice this is not always possible because absolute nodes may be inaccessible. On the other hand, several modes may have common node

points or directions and then more than three modes may be eliminated (e.g., a vibrator acting in the plane of symmetry of a symmetrical structure will excite none of the antisymmetrical modes). A fourth mode may also be eliminated by adding a second vibrator so that it also will not excite the first three modes and then varying its force output until its contribution to the generalized force in the fourth mode cancels that of the first vibrator, Eq. (6). Similarly, each additional vibrator allows one more mode to be eliminated.

The above paragraph applies identically to the elimination of responses in undesirable modes by properly locating and orienting linear vibration measuring pickups. Forced responses at different points of a structure may be combined mechanically, and the pickup responses may be combined electrically before recording. Finally, the recorded responses may be combined graphically by the methods discussed in connection with Figs. 4, 5, and 14. (It should be noted that responses in undesirable modes are eliminated from all the points of the structure when vibrators are properly used, while only one response at a time may be thus "purified" by combining pickups.)

For the identification of modes of a symmetrical structure such as an airplane, the most practical setup is that in which two or four linear vibrators are employed. A technique for the separation of normal modes which can be used directly during the vibration test will be presented.

Use of Four Vibrators (on Symmetrical Structures)

The equipment must consist of:

(1) Four linear vibrators that can be kept closely in phase under varying load conditions and may be connected so that two in a pair will have exactly equal or opposite forces. These forces must be variable but need not be entirely controllable (for example, they may depend to some extent on the response of the structure); an accurate indication of both their magnitudes and time phases must be available, however. An absolutely immediate force cutoff is extremely useful for taking decay records. Electrical "loudspeaker"-type vibrators with heavy field coils acting as seismic elements may be made to satisfy these requirements. The "voice" or "armature" coils of any pair of vibrators can be connected in series and the direct current fields are adjusted to equalize the forces applied. The alternating voltage across the voice coils is supplied by a beat-frequency oscillator, and the magnitude and phase of the applied force are obtained from a record of the armature current to which the former may be assumed to be directly proportional. (Such a system, originally developed by the Lockheed Aircraft Corporation, has been used by the writers with good results.)

(2) A number of linear vibration measuring pickups (no less than four) with which the phase and amplitude responses at various points can be compared simultaneously and directly with the vibrator force while testing. The phase sensitivities of the pickups must be identical, known, and preferably equal to zero. Ability to record when desired is almost essential for complicated systems and for determining the damping. At present, these requirements may be met more or less satisfactorily with electrical accelerometers and a recording oscillograph with a viewing screen. (The accurate measurement of phase responses on sinusoidal records is somewhat tedious, however.)

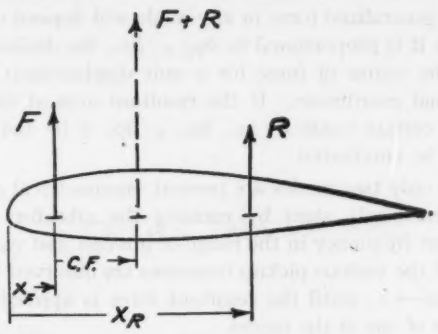

FIG. 17. Resultant force—two vibrators.

The procedure is as follows:

(1) Attach the vibrators at symmetrical locations on the airplane in such a way that when the force outputs of the right and left vibrators are either equal or exactly opposite; only symmetrical or, respectively, only antisymmetrical modes are excited. The system now reduces to the general case of two vibrators, and this will be assumed in the following discussion. To be more specific, let us also suppose that these two vibrators and two linear pickups are oriented in vertical directions and are located at the same spanwise station of a wing—e.g., at the front and rear spar on the same rib. (Possible alternative arrangements would be those in which either the two vibrators or the two pickups or both are located at two different points along the same wing spar and have parallel directions in space or then are placed at the same point of the wing but in directions in space at right angles to each other as, for example, in a chordwise and a direction normal to the plan form of the wing.) Locate the other pickups at any points and in any directions such as to best cover simultaneously all the modes of interest. At least one pickup should be used on the opposite wing to check the symmetry of the responses.

(2) When two vibrators are located on the same chord, it is possible to change the point of application of the resultant force by varying the ratio of the two forces. With symbols and sign conventions defined as shown in Fig. 17, the position of the center of force is given by

$$\text{C. F.} = (x_R - x_F)/[1 + (F/R)] \qquad (30)$$

where F/R is the ratio of the front and rear forces. The generalized force in any mode will depend on F/R since it is proportional to $\partial q_{C.F.}/\partial p_k$, the displacement at the center of force for a unit displacement in the normal coordinate. If the resultant acts at the node of a certain mode k—i.e., $\partial q_{C.F.}/\partial p_k = 0$—that mode will be eliminated.

If only two modes are present (symmetrical or antisymmetrical), start by running the vibrators at the lowest frequency in the range of interest and vary F/R until the various pickup responses are observed to be in phase—i.e., until the resultant force is applied at the node of one of the modes.

(3) Increase the forcing frequency until a peak amplitude per unit force is found. This is the first resonant frequency, and the corresponding normal mode may be identified directly and its shape measured. Damping may be obtained from a record of the response during a frequency sweep test or from a curve of free vibration decay from this forced condition.

(4) With the vibrators running at the first resonant frequency, again vary F/R until a new in-phase response is found—i.e., put the center of force on the node in the first mode. Thus, the second mode will be excited alone.

(5) Vary the forcing frequency until the peak amplitude indicating the second resonant frequency is found, and measure as before.

With the two following exceptions the procedure is absolutely valid for two modes. If the two modes have the same natural frequency and damping, all points would have the same phase response at all frequencies, and the node positions could not be found as above. Instead, the distinction must be based on the fact that the resultant mode shape would vary with the position of the resultant force. If the nodes of vertical motion in the two modes happen to coincide, it will not be possible to excite only one mode at one time. Another spanwise location could be tried. When many modes exist, the procedure is still closely valid either for separating two modes having natural frequencies close to one another but well-separated from other resonances or, in general, to eliminate from the total reponse the component corresponding to any one given mode.

Decay records serve to check the purity of the modes thus found, giving an independent means of measuring the resonant frequency, mode shape, and damping. The response in each normal mode decays exponentially with a frequency that is the natural frequency of that mode. If responses in two or more modes are measured by any pickup, that will be manifest in the number of different frequency components in the recorded wave form. If only two modes with frequencies close together are present, the record will be a beat that can be analyzed to give the two frequencies and amplitudes.[14]

Analysis of Records

As the interference of the numerous modes gets larger with increased complexity of the system, recourse must ultimately be made to vector plots of response. The procedure is to: (1) record responses during preliminary frequency sweep tests with arbitrary vibrator locations (such as on nodes of calculated, or estimated coupled, or uncoupled modes); (2) identify the modes from record analysis; (3) obtain complete mode descriptions from final forced and free vibration tests. In the last, use vibrators and pickups at locations chosen on the basis of the findings under (2), so as to best excite and measure the various modes of interest.

Frequency sweeps can be recorded for one center of force or vibrator location, and then curves for various points along the wing chord may be found graphically from any two pickups by the method of Fig. 4B (as in Fig. 14). Again the reciprocity theorem is useful: These curves give the response at the position used for the vibrator if the point of application of the force were moved along the chord, thus making it unnecessary in many cases to actually move the center of force.

The general method of identifying the modes from the frequency response vector plots consists of drawing the best circle possible through each circular arc on which maximum in $ds/d(\beta^2)$ (Fig. 9b) is distinguishable. This circle is the best approximation obtainable from the given data to the response measured by the respective pickup in the corresponding mode. The reason for this is that, when the vibrator is sweeping through a certain resonant frequency the tip of the total response vector will tend to partly describe the circle corresponding to that mode as the components due to other modes remain more or less constant. The resonance diameter is drawn perpendicularly to the generalized force in the mode (i.e., to the force phase reference when in-phase linear vibrators are used), and it should pass through the point of maximum $ds/d\beta$ on the curve; at its other end, it will determine the "displaced origin" to be used when measurements are made.

The record analysis is exemplified in Figs. 18, 19, and 20. Vector response plots from previous figures are analyzed as if they were actual record measurements. On these, the best single mode response circles are drawn through the "measured" points; subsequently, the natural frequency is found at the end of the resonance diameter, and a plot of amplitude (measured from the displaced origin) vs. frequency is made to find the peak amplitude and the damping. To obtain the latter, use was made of the relation that for a single mode with small damping:

$$g = \frac{2q/q_{max.}}{\sqrt{1 - (q/q_{max.})}} \left| \frac{N}{N_n} - 1 \right| \qquad (31)$$

which, for $q/q_{max.} = 0.707$, becomes:

$$g = 2\left|\beta_{0.707} - 1\right| \qquad (32)$$

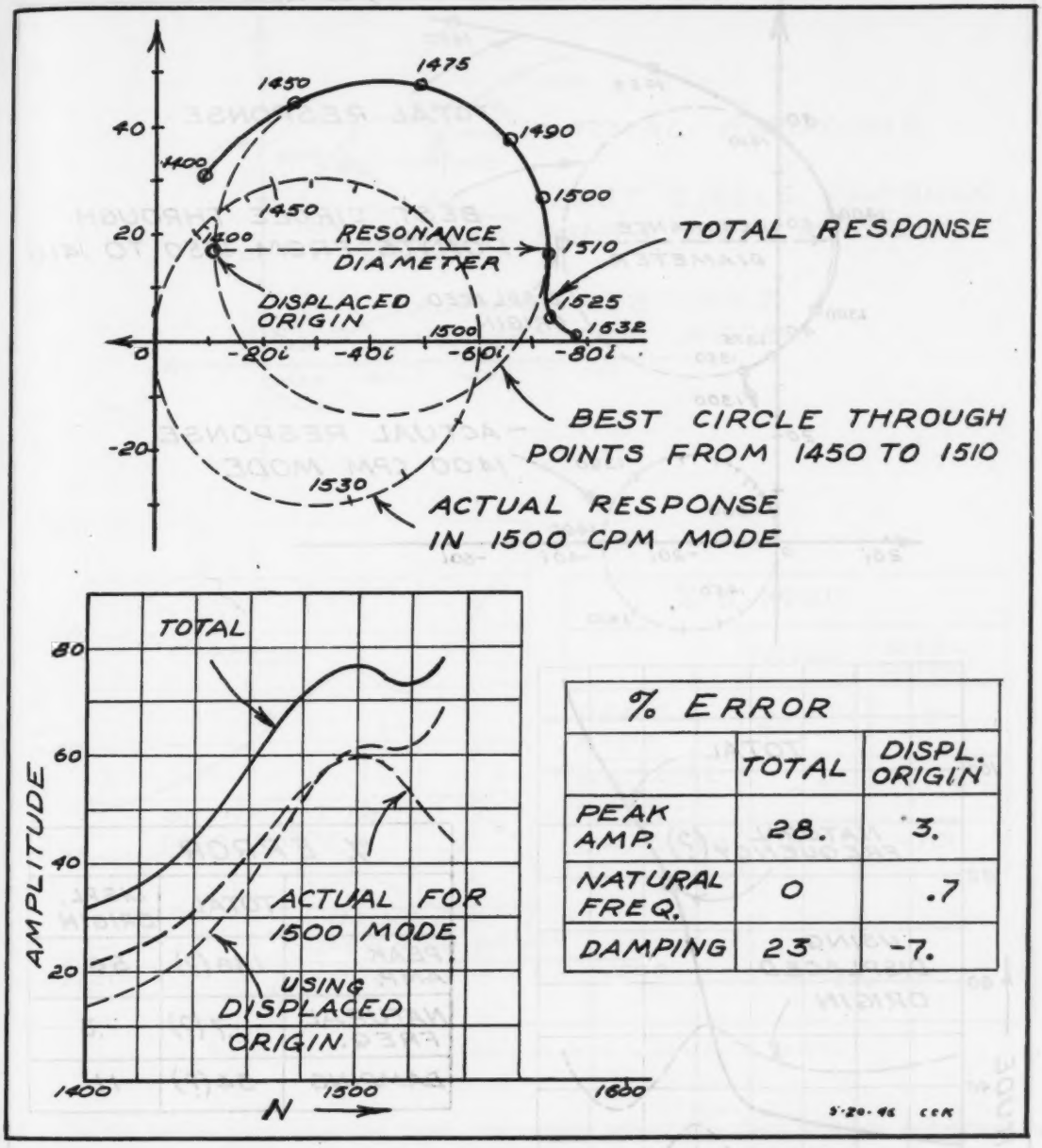

% ERROR		
	TOTAL	DISPL. ORIGIN
PEAK AMP.	28.	3.
NATURAL FREQ.	0	.7
DAMPING	23	-7.

FIG. 18. "Record" analysis—1,500 cycles per min. mode in Fig. 12.

where $\beta_{0.707}$ is the value of the frequency ratio N/N_n at the point where the amplitude q is 0.707 of the peak amplitude $q_{max.}$ or where the response vector is 45° away from the resonance diameter.

In the table given in each figure the results are compared with those obtained by the usual method of neglecting completely the effect of other modes present. The per-cent errors, based on the known true response in the pure mode, are given for the two methods; negative errors indicate that the "measured" values are too small. With regard to damping and peak amplitude, the improved accuracy of the vector analysis method is obvious. The improvement in frequency determination is not apparent from these tables; it should be noted, however, that in a case such as that in Fig. 19 in which no peak occurs, the ordinary method would give no answer at all, unless exceptional benefit of the doubt be given the analyst by assuming that he would recognize the existence of a mode near the point of maximum curvature of the amplitude response. Another such example is the 1,450 mode in Fig. 16, which would be completely hidden in the ordinary analysis.

Before drawing in the response circles, the construction indicated in Fig. 14a may first be used to find the

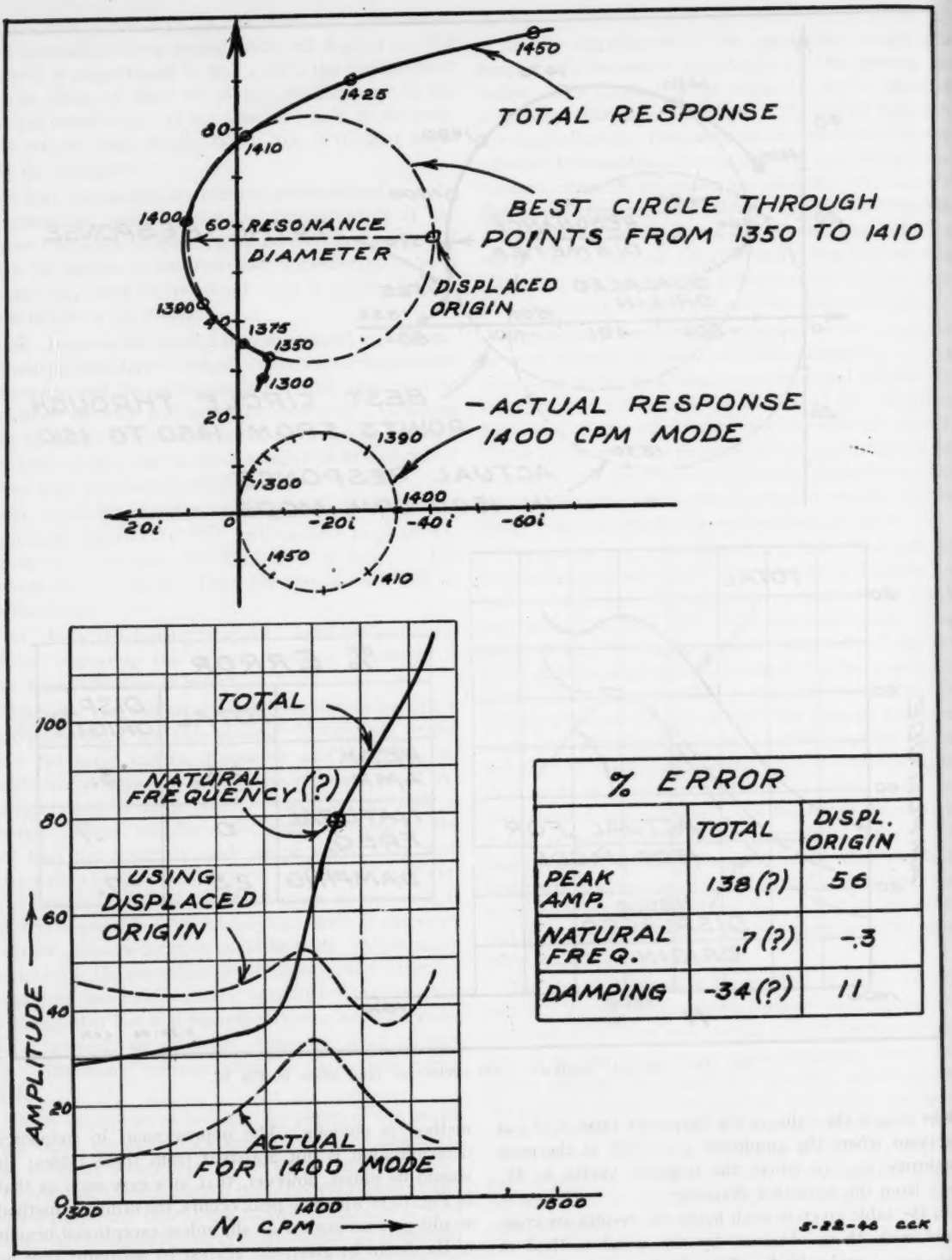

% ERROR		
	TOTAL	DISPL. ORIGIN
PEAK AMP.	138 (?)	56
NATURAL FREQ.	.7 (?)	-.3
DAMPING	-34 (?)	11

FIG. 19. "Record" analysis—1,400 cycles per min. mode in Fig. 14, curve D.

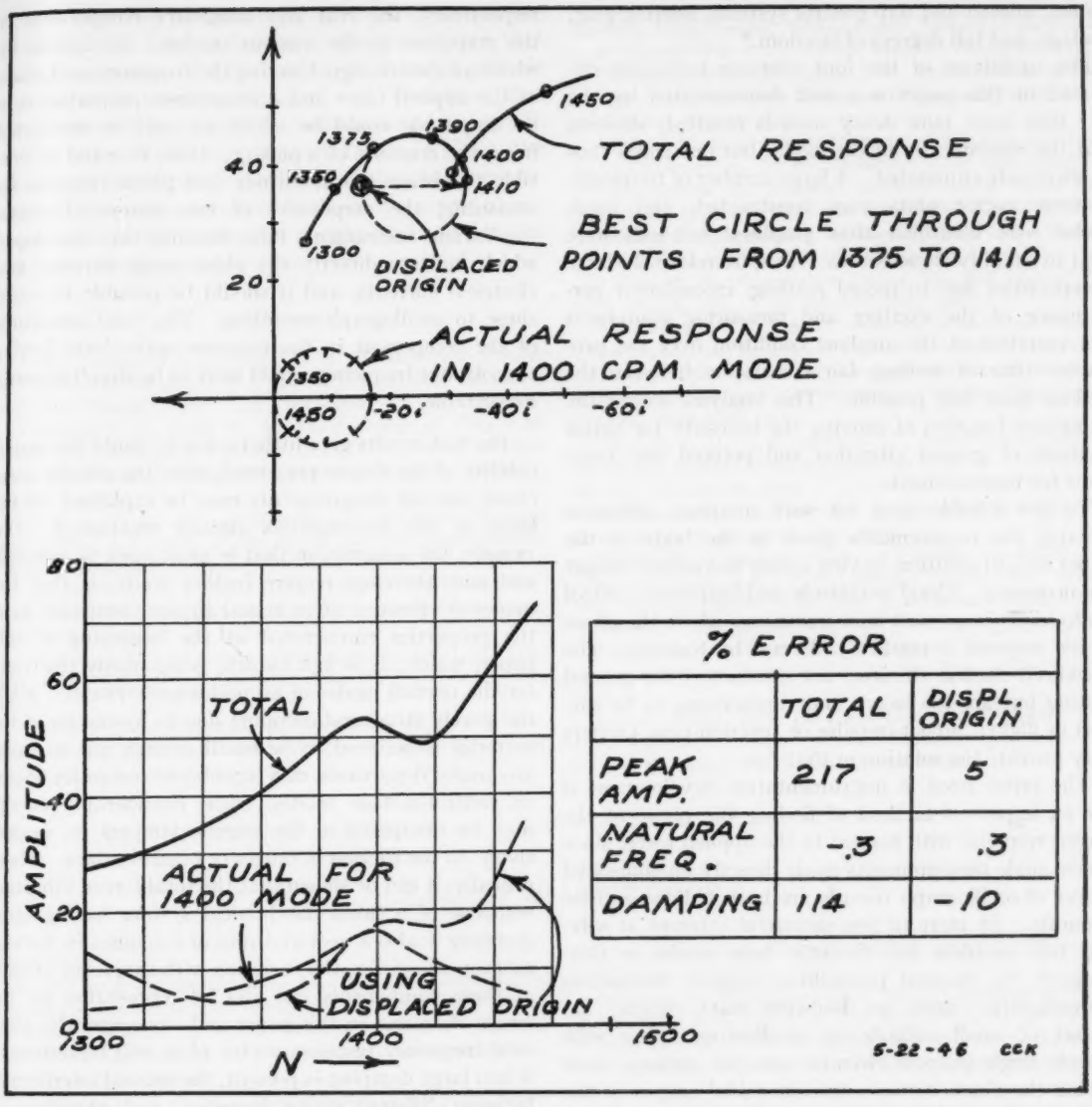

FIG. 20. "Record" analysis—1,400 cycles per min. mode in Fig. 14, curve C.

vector plots for various points along the chord; the circles then may be fitted to the simpler of these curves. On a diagram such as that of Fig. 14a, note that, since the diameter of the circle response in a given mode reduces to 0 at the node, the "chord" lines will tend to pass through a common point for a frequency range near the respective resonance. The relative position of this point and that of the tips of the various response vectors along the "chord" lines will give the actual node location of that wing station.

CONCLUSIONS AND RECOMMENDATIONS

The authors have presented a theory for the measurement and interpretation of forced vibration test data, giving several new facts, analyses, techniques, and points of view.

Since no experimental examples are given, one might well inquire as to the validity and usefulness of the theory in actual practice. The experimental work done by the authors has included a thorough survey of the vibration modes of a single-engine airplane using single mechanical linear and rotary vibrators and also multiple electric exciters. Special attention was paid to the wing vibration characteristics in the frequency range from 1,200 to 2,200 cycles per min. which presents a confusing picture on many airplanes of this type; this is due to the fact that there are between five and ten modes involved corresponding to wing torsion, second bending, and fore-and-aft

motion, aileron and flap control systems, landing gear, fuselage, and tail degrees of freedom.*

The usefulness of the four vibrator technique described in this paper was well demonstrated by the fact that some pure decay records resulted, showing that the responses in all the modes but one could thus be effectively eliminated. A large number of frequency response vector plots were constructed, and mode circles were identified after graphical methods were used to simplify these curves. Despite relatively large uncertainties due to record reading, inconsistent performance of the exciting and measuring equipment and variation of the airplane condition over the protracted time of testing, fair correlation between the various tests was possible. This analysis served the important function of proving the necessity for better methods of ground vibration and pointed out directions for improvements.

To get reliable data for such analysis, vibrators meeting the requirements given in the body of the paper and, in addition, having a pure wave-form output are necessary. Good amplitude and frequency control is especially important near resonances where the phase of the response is markedly affected by hunting. The Lockheed electric vibrators are satisfactory for ground testing but are too heavy and cumbersome to be carried in flight; air-jet-impulse or reaction-type exciters may provide the solution in that case.

The prime need in instrumentation development is for an improved method of finding the phase of the forced response with respect to the applied force, since phase angle measurements made directly on sinusoidal traces of oscillograph records are both tedious and inaccurate. (A more or less successful attempt at solving this problem has recently been made in Germany.[16, 17]) Several possibilities suggest themselves immediately; there are doubtless many others. (1) A set of small cathode-ray oscilloscope tubes with simple single purpose circuits—one per pickup—from which the phase between the sinusoidal output of the pickup and that from a vibrator reference connection can be measured on an elliptical Lissajous figure. These ellipses, together with a frequency meter, might be recorded by a photo-observer camera, and the film could be read in a microfilm projector. (2) A pickup or galvanometer system that would record directly the real and imaginary components of the response relative to the exciting force. A wattmeter-type connection between the vibrator and the measuring pickup[18] may be used for this purpose. Advantages of this type of instrument would be its filtering characteristic to eliminate undesirable harmonics and the fact pointed out previously that the real and imaginary components of the total response are simply scalar summations of, respectively, the real and imaginary components of the responses in the various modes. (3) Means by which an electric signal having the frequency and phase of the applied force and a magnitude proportional to its amplitude could be added to, and/or subtracted from, the response of a pickup; thus, it would be possible to obtain the amplitude and phase response by measuring the amplitudes of two sinusoidal traces. (4) Various instruments have recently been developed which indicate directly the phase angle between two electrical currents, and it should be possible to adapt these to oscillograph recording. The total amplitude of the component in the response wave form having the vibrator frequency would have to be simultaneously measurable.

The test results give little reason to doubt the applicability of the theory presented, since the simpler cases check and all disagreements may be explained on the basis of the uncertainties already mentioned. Obviously, the assumption that is most open to question and may therefore require further study, is that the modes of vibration of an actual airplane structure have the properties enumerated at the beginning of this paper, which, as is well known, is rigorously true only for the normal modes of an undamped system. While the purely structural damping due to hysteresis in the material is believed to be small enough not to cause any major departures, this is probably not so for engine or control-surface modes, since considerable energy may be dissipated in the engine dampers or, respectively, in the friction in hinges or control cables. Theoretically, it can be shown that the total forced vibration response of a linear mechanical system having large damping is also a vectorial sum of responses in various modes; moreover, the variation with frequency of each of these components can still be represented by the circles discussed in this paper and, consequently, identical frequency response vector plots will be obtained. When large damping is present, the mutual interference between different modes increases, and, therefore, it becomes even more important to consider the phase as well as the amplitude response—i.e., to think in terms of vectors. A more thorough theoretical study of the effect of damping will be made and several examples of experimentally obtained frequency response vector plots will be given in a later paper.

The main purpose of ground vibration testing of airplanes is to check directly the natural frequencies and shapes of the various coupled modes calculated from mass and stiffness distributions. These modes are necessary when making flutter analyses or when it is desired to treat the airplane as an elastic body in the computation of transient stresses such as those produced in landing or by air gusts in flight. The attempts made at verifying the accuracy of predicted flutter speeds or landing and gust loads through full-scale testing of airplanes have not been too successful in the past. In the

* A similar situation may arise in the vicinity of the natural frequency of the elastic suspension of an engine; in a case pointed out by Myklestad,[15] nine out of a possible 17 wing resonances were calculated to occur in the region $0.9\omega_{eng.} < \omega < 1.5\omega_{eng.}$.

future, there can be little hope of obtaining more positive results as long as it is not definitely proved that the actual modes of vibration of airplanes in still air can be satisfactorily calculated and, therefore, that proper account is taken of the internal structural forces. In the light of the work presented in this paper, the solution to the latter problem depends on the future development of more suitable vibration-measuring equipment with which to be able to identify and analyze airplane vibration modes accurately.

References

[1] von Kármán, Th., and Biot, M. A., *Mathematical Methods in Engineering*, Chapts. 3, 5, 6, pp. 70–110, 162–259; McGraw-Hill Book Company, Inc., New York, 1940.

[2] Walker, P. B., Clegg, A. W., *The Technique of Wing Resonance Tests*, Report No. A.D. 3105/M.T. 11767 of the Royal Aircraft Establishment, South Farnborough, England, February, 1939.

[3] Walker, P. B., *Note on Material and Structural Damping*, Report No. A.D. 3079 of the Royal Aircraft Establishment, South Farnborough, England, November, 1936.

[4] Rayleigh, J. W. S. Baron, *The Theory of Sound*, 2nd Ed., Vol. 1, Chapt. 5, Sec. 102, pp. 101, 102; Dover Publications, New York, 1945.

[5] Guillemin, E. A., *Communication Networks*, Vol. 1, pp. 118–120; Vol. 2, pp. 184–187, 509–518; John Wiley and Sons, 1931, 1935.

[6] Smilg, B., Wasserman, L. S., *Application of Three-Dimensional Flutter Theory to Aircraft Structures*, Army Air Forces Technical Report No. 4798, pp. 118–124, July 8, 1942.

[7] Arnold, L., *Vector Solution of the Three Degree Case of Wing Bending, Wing Torsion, Aileron Flutter*, Journal of the Aeronautical Sciences, Vol. 9, No. 13, pp. 497–500, November, 1942.

[8] Bleakney, Wm. M., Hamm, J. D., *Vector Methods of Flutter Analysis*, Journal of the Aeronautical Sciences, Vol. 9, No. 12, pp. 439–451, October, 1942.

[9] Powell, C. H., *Graphical Treatment of Vibration and Aircraft Engine Dampers*, pp. 79, 80; Bookcraft, New York, 1940.

[10] von Sanden, H., *Graphical Representation of Forced Vibrations Due to C. Runge*, Ingénieur Archiv, Vol. 1, p. 645, 1930.

[11] Black, H. S., *Stabilized Feedback Amplifiers*, The Bell System Technical Journal, Vol. 13, January, 1934.

[12] Nyquist, H., *Regeneration Theory*, The Bell System Technical Journal, Vol. 11, pp. 126–147, July, 1932.

[13] Brown, G. S., Hall, A. C., *Dynamic Behavior and Design of Servo-Mechanisms*, Preprint of Paper No. 45-A-20, Presented at the Annual Meeting of the American Society of Mechanical Engineers, Instruments and Regulators Division, November 26–29, 1945, New York City.

[14] Pancu, C. D. P., Kennedy, C. C., *Beat Analysis*, Letter to the Editor, Journal of the Aeronautical Sciences, Vol. 13, No. 3, pp. 140, 141, March, 1946.

[15] Myklestad, N. O., *Vibration Analysis*, pp. 192, 193; McGraw-Hill Book Company, Inc., 1944.

[16] Späth, W., *Theory and Practice of Vibration Testing Machines*, Chapt. 4, Sec. 12, p. 52; Julius Springer, Berlin, 1934. Translation No. 51, March, 1938, U.S. Experimental Model Basin, Navy Yard, Washington, D.C.

[17] de Vries, G., *Dornier Phase Meter for Vibration Measurements*, Technische Berichte, Vol. 11, No. 6, pp. 165–170, June, 1944.

[18] Bratt, Wight, Tilly, *The Application of a "Wattmeter" Harmonic Analyser to Measure Torsional Damping*, Report No. 5827, 0.263 of the A.R.C. Oscillation Subcommittee.

Letters to the Editor

Dear Sir:

Recent work for the American Iron and Steel Institute on light-gage steel sections has brought to my attention an article by George Gerard on "Effective Width of Elastically Supported Flat Plates" (JOURNAL OF THE AERONAUTICAL SCIENCES, Vol. 13, No. 10, October, 1946).

On page 521 it is stated: "Since changes in half-wave length cause *small variations in critical stress of plates with aspect ratios* '(a/b)' *greater than 2.5*, it is probably permissible for practical considerations to establish 2.5 as the lower limit of applicability of the results presented."

In view of the work of A. J. Miles quoted by S. Timoshenko, *Theory of Elastic Stability*, the case of a plate rigidly supported along the two edges normal to the direction of compression, elastically supported along the other two edges (torsion of the supports neglected), it can be shown that *there is an upper limit of aspect ratio beyond which the effective width falls off with extreme rapidity*. Using the notation of Timoshenko, let I_F be the moment of inertia of one elastic support (including effective plate width in the determination thereof) and I_P the moment of inertia of the whole plate section of width b. Then for our present purpose, the θ function is approximately $(1 - \mu^2)I_F/I_P$. For long plates, $m = 1$ and the ϕ function $\phi = \pi(b/a)$ and is small. Then the ψ function is approximately $\psi = V\theta\phi^2$. If ψ is set equal to 2π, then it can be shown that $(a/b)_0$, the upper limit, is $(a/b)_0 = 1.25\sqrt[4]{(I_F/I_P)}$, somewhat approximately. For lesser values of (a/b), it can be shown that ψ varies nearly 6 per cent from constancy, as first one m value then another tends to govern. Hence, in this region, allowance must be made for such wave effects in correcting data.

Above $(a/b)_0$, the effective width varies inversely as the square of the ratio $(a/b)/(a/b)_0$, so that at twice $(a/b)_0$ the effective width is only 25 per cent of that for shorter lengths. This effect has not been noted heretofore, but has been observed on column tests.

Reference to the JOURNAL, "An Investigation of Duraluminium Struts Under Compression," by Warren S. Parr and Wallace M. Beakley, Vol. 3, September, 1935, shows that the theoretical plate failure line was departed from further and further with increasing b/w ratio of flange depth to channel depth (flange constant, hence depth decreasing and, for constant strut length, (a/b) increasing) starting at a fairly definite point. A check of the point of departure agreed excellently with the above theory of reduction in effective plate width with $(a/b)_0$ ratio in three of the four cases permitting a check, and the percentage decrease was of the right order of magnitude. It is of interest to note that, in the so-called region of torsional failure, neither the torsion line nor the above plate line (reduced for length) governed; rather it seemed that the failure was a mean of the two values.

I have not made reference to E. Chwalla (Timoshenko, *Theory of Elastic Stability*, also *Ingénieur-Archiv.*, Vol. 5, p. 54, 1934) for the effect of torsion in the case of elastic support. Some slight variations have been noted.

I have found that the tests of George Winter ("Strength of Thin Steel Compression Flanges," *Proc. ASCE*, Vol. 72, No. 2, February, 1946) on light columns consisting of two channels

without stiffened flanges, fastened back to back, exhibited the same effect. So far, the data available have permitted check of four cases in which the theory permits of accounting for the observed results.

It should be remembered that, when $m = 1$ and (a/b) is greater than $(a/b)_0$, the plate and elastic supports deflect as a single plate of the stiffness of the reduced section *without supports along the sides parallel to the direction of compression.*

Investigation shows that many light columns in the so-called primary member category, so far as L/r ratio is concerned, may exhibit this effect and that some in the Euler range may be reduced as much as 70 per cent in strength. Hence, the effect can prove to be important.

The tests of Winter exhibit the effect of change from simple support at low values of (b/t) to clamped support at the higher values, much as suggested in Gerard's Fig. 1.

These remarks are purely preliminary to more adequate publication but seem demanded by the occasional importance of the effect and the apparent failure heretofore to recognize it.

EDWARD ADAMS RICHARDSON
Publications
Bethlehem Steel Company

Dear Sir:

I would like to add a few remarks to my previous letter concerning the So-Called Principle of Least Work Method. In considering the application of the Theorem of Least Work to the solution of practical problems, two main cases must be distinguished. The separation into these two cases was already being made by Pöschl (Theodor Pöschl, "Über die Minimalprinzipe der Elastizitätstheorie," *Der Bauingenieur*, Vol. 17, No. 17/18, p. 160 to 164, Mai, 1936. See also discussion of this paper by O. Domke, *Der Bauingenieur*, Vol. 17, No. 41/42, p. 459, 1936.) This distinction is also self-evident from the exposition of the definition of the So-Called Principle of Least Work Method given by me in my last letter, published in the October issue of the JOURNAL.

The first case is when, in the system considered, we deal only with the concentrated, separate forces in the members of the structure. In this case the total strain energy of the system is given by a quadratic form which is always a positive definite one; therefore, the extremum sought must be a minimum. The author cited previously various attempts (found in several textbooks) to prove the existence of a minimum by pointing out that the second partial derivatives taken separately with respect to X, Y, Z, etc., are positive. This condition is necessary but not yet sufficient. The fact that the quadratic form is a positive definite is the only proof of existence of a minimum. (See: Theodor Pöschl, *Elementare Festigkeitslehre*, p. 173; Berlin, Julius Springer, 1936.) In this case the solution is given by equating to zero the first partial derivatives of the total strain energy with respect to the redundant forces. Pöschl calls this case "Castigliano's Principle." This is a trivial case.

The second case occurs when, in the system, there are continuous distributed stresses. The total strain energy is expressed in this case by single, double, or triple integral forms, and the equating to zero of the first partial derivatives of the total strain energy with respect to the unknown coefficients may not lead to a correct solution of the problem. Pöschl recommends in this case as a constraining condition the equality of the strain energy and the work of the external forces (conservative system).

Two methods may give the solution. The first is to assume the curve or the surface representing in a first approximation the distribution of stresses as a two-dimensional curve function or a three-dimensional surface function of the system of coordinates. This choice may be made in many ways. The simplest may be to base the distribution on experimental tests. The chosen functions possess certain unknown coefficients, which may be determined by the application of the Theorem of Minimum Strain Energy to obtain the proper solution. As an example, let us mention that this way was chosen by Prof. Eric Reissner in his solutions of the shear lag problem. (See: E. Reissner, "Least Work Solutions of Shear Lag Problems," JOURNAL OF THE AERONAUTICAL SCIENCES, Vol. 8, No. 7, p. 284, May, 1941. This approach has its full justification in the proposition put forward by the author in the previous letter. Before we apply the Minimum Strain Energy Principle we are assured that among the chosen set of functions there is one that gives a lower value of the energy than do the others. This method may be considered to be approximate, but it is shorter.

The other approach is to apply the methods of the calculus of variations. It is no longer a problem of seeking an ordinary extremum of a function. This well-known method is thoroughly explained in the literature (Courant, Hilbert, Sokolnikoff, Pöschl, *loc. cit.*). Strictly speaking, the use of the principles of calculus of variations to the solution of problems of this kind was recommended as far back as 1914 (Oskar Domke, "Über Variationsprinzipen in der Elastitätslehre nebst Anwendungen auf die technische Statik," *Zeitschrift für Mathematik und Physik*, p. 174, Mai, 1914). Thus, the general theoretical way of attacking a problem does exist. Strangely enough, although Courant-Hilbert's book was published in 1931, and Pöschl's paper in 1936, in many books on the theory of elasticity, theory of structures, strength of materials, aircraft structures, etc., published later than the above-mentioned works, there is nothing said about the vital and basic importance of distinguishing between these two cases. Also few books mention the necessity of the application of calculus of variations methods (see Sokolnikoff). There are many examples cited in which the continuous distributed stresses were found by equating to zero the first partial derivatives. But the enormous and insurmountable difficulties in finding exact solutions of differential equations occurring in variational calculus methods applied to such problems as shells, etc. (particularly with cutouts), were the reason for the author's remark that the question of how to find such a function in any particular case is not yet solved in a rigorous way. Perhaps from an engineering standpoint it may be enough to apply some approximate solutions by use of fast computing machines (punch cards), although the computation difficulties seem to be enormous.

M. Z. KRZYWOBLOCKI
College of Engineering
Associate Professor
University of Illinois

Dear Sir:

I have two wind-tunnel items of interest; both concerned with blocking corrections.

(1) It was desired to test an NACA 0015 airfoil section through an angle of attack range of 180° in order to get forces and pressures for a helicopter blade, and some concern was felt about the blocking corrections when the 18-in. chord model was at an angle of attack of 90° in our $2\frac{1}{2}$ by 9 ft. two-dimensional tunnel. Consequently, two additional models of 6- and 12-in. chord were constructed and tested. All models were mounted between flush wall discs. Leakage to the outside around the discs was prevented by water seals. The speed was set by a single piezometer ring in the tunnel settling chamber, referenced to the atmosphere. Although this method of speed setting is inferior to a two-ring system, it is believed that no serious effects resulted thereby, since pressures read on the 18-in. chord model and worked up, assuming clear jet q, agreed well with the force data.

The force data as read included the tare and interference of the mounting discs. The true airfoil drag was obtained with a

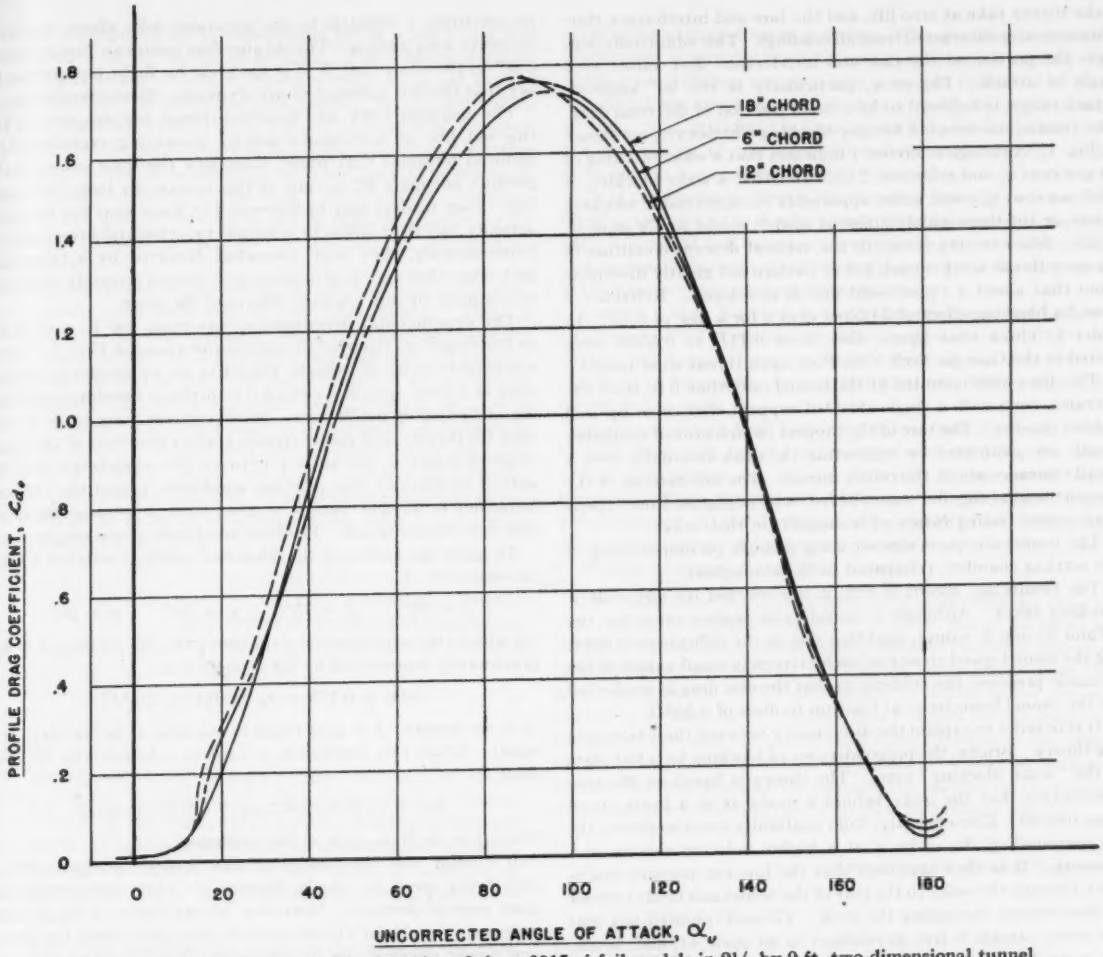

FIG. 1. Drag data uncorrected for blocking of three 0015 airfoil models in $2^1/_2$ by 9 ft. two-dimensional tunnel.

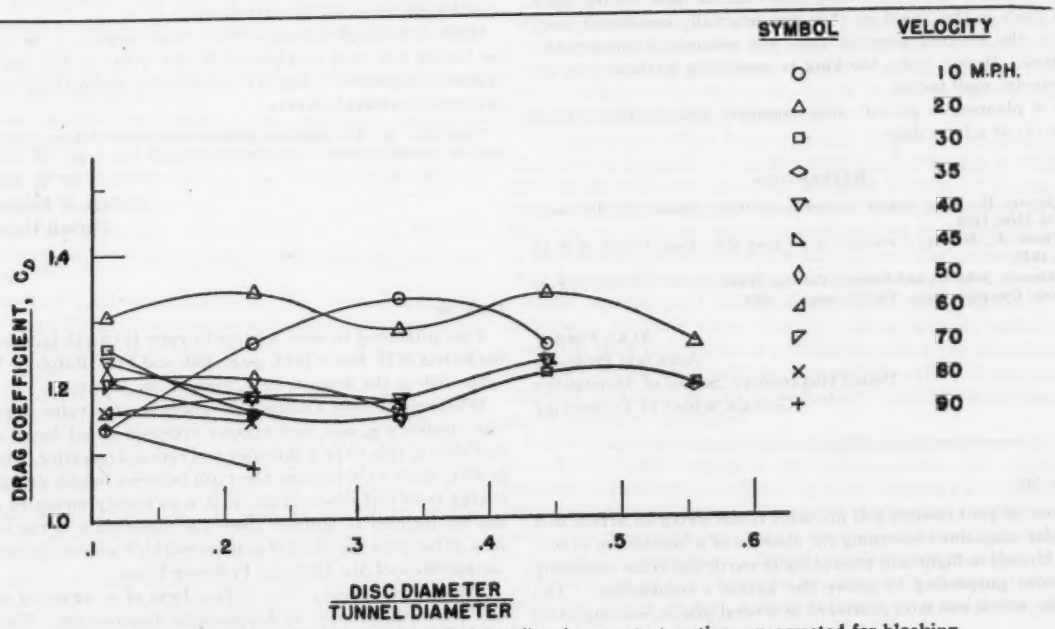

FIG. 2. Drag coefficient [= drag/$(\pi d^2/4)q$] of flat discs in open test section, uncorrected for blocking.

wake survey rake at zero lift, and the tare and interference thus obtained were subtracted from all readings. This admittedly neglects the portion of the tare and interference that varies with angle of attack. The error, particularly in the 90° angle-of-attack range, is believed to be a small fraction of the total drag. The results, uncorrected for any blocking whatsoever, are shown in Fig. 1. Although reference 1 indicates that a wake blocking of 44 per cent q, and reference 2 indicates that a wake blocking of 13.0 per cent q, could arise, apparently no appreciable blocking exists, or the three widely different models would surely show it.

(2) When testing rotors in the vertical descent condition in an open throat wind tunnel, a flow pattern not greatly dissimilar from that about a round solid disc is developed. Reference 3 found a blocking effect of 34.5 per cent q for a disc of $0.5D$. In order to check that figure, discs from $0.11D$ to $0.555D$ were tested in the Georgia Tech Nine Foot open throat wind tunnel.

The discs were mounted at the tunnel centerline 5 ft. from the entrance cone with a single shielded support that came up well behind the disc. The tare of the support (which proved negligibly small) was evaluated by supporting the discs externally with a small clearance about the center mount. The interference of the support behind the disc was believed to be negligible from experience gained testing rotors with supports in their wake.

The tunnel air speed was set using a single piezometer ring in the settling chamber, referenced to the atmosphere.

The results are shown in Fig. 2, uncorrected for any wall or blocking effect. Although a considerable scatter exists for the 10 and 20 m.p.h. values, doubtless due to the difficulties of holding the tunnel speed steady at such extremely small values of the dynamic pressure, the evidence is that the disc drag is unaffected by the tunnel boundaries at least up to discs of $0.555D$.

It is in order to explain the discrepancy between these tests and the theory. Briefly, the preponderance of blocking for a flat plate is the "wake blocking" type. The theory is based on the true assumption that the wake behind a model is at a lower speed than free air. Consequently, from continuity considerations, the air surrounding the wake is at a higher velocity and lowered pressure. It is then supposed that the lowered pressure reacts back through the wake to the rear of the model and tends to draw it downstream, increasing the drag. Glauert[3] pointed out that the entire stream is free to contract in an open jet, and, hence, no wake blocking should appear. This was substantiated in Item (2). However, the author feels that far more mixing must take place in the closed jet than was originally considered, and, hence, the lowered pressure that was assumed is not actually realized. Hence, wake blocking is, according to these data, an extremely small factor.

It is planned to present more complete data on the tests of Item (1) at a later date.

References

[1] Glauert, H., *Wind Tunnel Interference on Wings, Bodies, and Airscrews*, R & M 1566, 1933.

[2] Thom, A., *Blockage Corrections in a Closed High Speed Tunnel*, R & M 2033, 1943.

[3] Wheatly, John B., and Bioletti, Carlton, *Wind Tunnel Tests of a 10 Foot Diameter Gyroplane Rotor*, TR 536, page 7, 1935.

Alan Pope
Associate Professor
Daniel Guggenheim School of Aeronautics
Georgia School of Technology

Dear Sir:

Some of your readers will probably recall seeing an article in a popular magazine concerning the abilities of a bumblebee to sustain himself in flight and presenting in particular some confusing formulas purporting to prove the author's contentions. The article, which was later reprinted in several places, was supposed to constitute a rebuttal to the venerable joke about the bee's excessive wing loading. The old anecdote quotes an "aerodynamicist" to the effect that W/S is too great for flight but goes on to say that the bee, ignorant of aerodynamics, flies nevertheless.

The magazine story, as I have mentioned, was supposed to kill this old jibe at aerodynamicists by presenting experimentally deduced formulas that would show how the little insect might produce adequate lift in spite of this supposedly large unit loading. Your readers may be interested to know that the formulas actually had their origin in a serious experimental investigation. Unfortunately, they were somewhat distorted by a typesetter and, when they appeared in print, were almost certainly dismissed as nonsense by any engineer who read the story.

The experimental investigation was made by E. von Holst at Göttingen, as reported in *Luftfahrtforschung* of 1943.* In this remarkable series of tests, he placed in an air stream an elliptic wing of 3.2 cm. span and caused it to perform simultaneous beating and pitching oscillations. Measurements were made of lift, drag (or thrust), and power required, all as functions of the mean angle of attack α, the angle ψ between the windstream and the axis of oscillations, the pitching amplitude χ, and the reduced frequency or advance ratio $\lambda = v/u$ (where u = mean tip speed and v = stream speed). The beat amplitude φ was constant.

To assist the author of the magazine article, I selected a typical case:

$$\alpha = 45°, \quad \psi = 45°, \quad \chi = 40°, \quad \varphi = 68°$$

for which, the experimental data show, the lift coefficient is approximately represented by the straight line

$$0.06 + 0.17\lambda \backsimeq k_a \quad [\equiv \text{lift}/(\rho/2)u^2F]$$

(ρ = air density; F = area swept in one beat $= 2\pi s^2(\varphi/2\pi)$; s = span). When this expression is used to calculate the lift, one finds

$$\text{lift} = (\rho/2)F[0.06(2sn\varphi)^2 + 0.17\,(2sn\varphi)v]$$

where n is the frequency of the oscillation.

It is clear that the bumblebee can produce adequate lift at zero flying speed by simply flapping his wings fast enough (as must appear obvious). Moreover, he can reduce n as he picks up speed. von Holst's results include data from which the thrust and power required can be evaluated. For the particular case mentioned above, for example, positive thrust is obtained over a considerable range of the parameters.

With such complete data at hand, there appears to be no need for basing any rash conclusions on the value of any one aerodynamic parameter! May we consider the ancient libel on aerodynamicists refuted forever?

* von Holst, E., *Messungen an kleinen schwingenden Flächen (Grössenordnung des Insektenflugelns)*, Luftfahrtforschung 20, Lfg. 5, pp. 137–146, 1943.

W. R. Sears
College of Engineering
Cornell University

Dear Sir:

I am prompted to send a letter to your JOURNAL in answer to the letters of H. Reese Ivey (page 450) and Prof. Ralph H. Upson (page 469) in the August, 1947, issue of the JOURNAL.

Whatever quibble I might have regarding the value of propulsive efficiency η_p as a performance criterion is not based on the fact that η_p fails to be a plausible and rational quantity. It does, in fact, serve to determine the ratio between missile energy and energy from fuel expenditure, as it is obviously meant to do. I am not inclined to quibble about the plausibility of the derivation, as between the forms of η_p proposed by Professor Szczeniowoski and those of Mr. Ivey and Professor Upson.

My only comment is that neither form of η_p serves to answer any pertinent question in Aeronautical Engineering. This is to

say that economy of energy expenditure per se is not a practical consideration in the design of missiles. The primary question that is asked in our science is: How fast can a given pay load be carried how far? In answering that question the aim is to reduce the mass ratio m_e/m to as small a value as possible or, for given m_e/m, to send the net mass as fast and as far as possible. Whether in so doing the energy expended is much or little is of no more real interest than how much the fuel costs. Such mundane considerations as are used in deriving η_p are of primary importance in stationary power-plant engineering but not in Aeronautical Engineering.

I recognize that in the preceding statements I am simply voicing an opinion, and there may be some who disagree. There is no reason why the course of the energy transformations should not be traced, if anyone is interested, whether such an activity helps design rockets or not. On the other hand, no one should deceive himself: if there is a criterion like η_p that can be large or small or negative, that is decreased by an obviously advantageous change in design of rocket, that can be increased by the same change at a different missile speed, then such a performance criterion is suspect if not useless. The fact that a similarly developed criterion is useful in other engineering fields is not a good enough reason for retaining it.

DAVID T. WILLIAMS
Associate Professor
Department of Aeronautical Engineering
University of Michigan

Dear Sir:

The publication of Mr. Wang's article, "Elastic and Plastic Bending of Beams" (JOURNAL OF THE AERONAUTICAL SCIENCES, Vol. 14, No. 7, p. 422, July, 1947), raises a question of editorial policy which I believe is of interest to all scientists and engineers. This concerns the introduction of new words in scientific or engineering terminology. A few simple rules are suggested, as follows:

(1) The word should not be based on the name of the company in which the author happens to be employed.

(2) The need for a new word should be clearly shown—i.e., the possibility of using existing words, or combinations of them, should be thoroughly investigated.

(3) If introduced at all, the new word, or words, should be at least partially self-explanatory.

(4) The physical significance of the new term should be clearly explained.

Applying these suggested rules to Mr. Wang's article we find the following:

(1) The word "Norstress" is derived from Northrop Aircraft, Inc., where the author was working at the time the term was originated.

(2) The new term was introduced "for convenience." It may represent a convenience to those who originated it and use it in routine work, but it is an inconvenience to everyone else who reads the paper.

(3) Such terms as "equivalent bending stress" or "reduced bending stress" would be preferable, for reasons shown below.

(4) The only definition given by the author is a "term which represents a measurement of maximum normal stress (remote fiber stress) of cross sections of beams due to bending." The actual physical significance of the term in one of its forms (M/BH^2) can be revealed by writing this expression as $(M/H)/(BH)$. The term M/H represents in equivalent axial load, P, which is simply the bending moment divided by the maximum depth of the beam. The term BH represents the cross-sectional area, A, of a rectangular beam having the same depth and maximum width as the section in question. The so-called "Norstress," in this case, is actually the fictitious axial stress obtained by converting the bending moment into a couple composed of axial forces that are assumed to act at the top and bottom of the cross section. The axial force is then assumed to act uniformly over the entire area of the superimposed rectangle. If the actual cross section is a rectangle, the "Norstress" turns out to be one-sixth of the maximum fiber stress obtained from the conventional bending theory for the elastic range. This suggests that the term (M/BH^2) might well have been multiplied by 6, in which case the quantity could be defined as "the equivalent elastic bending stress in the superimposed rectangular cross section."

Lack of a clear physical basis for the new term has unfortunately permitted the author to introduce the term (M/R^3) for circular and tubular beams. To be consistent, the diameter, D, should have been used; in fact, the term (M/BH^2) would have served just as well.

As a result of this, the "Norstress" for sections of circular shape is eight times that for any other cross section having the same overall dimensions! (I wonder how the author would have treated an elliptical section.) The mere fact that this situation was not corrected before publication should be proof enough that the introduction of arbitrary concepts of this type is often likely to produce confusion rather than clarity.

The whole thing could be cleared up by establishing a ratio (I won't attempt to coin a word for it) between the actual stress at the outer fiber and the corresponding stress in the outer fiber of a member having a rectangular cross section which just encloses the actual cross section. This ratio would be similar to the present concept of a "form factor," except that it would include both the inelastic effects and the geometrical characteristics of the cross section. As such, it would be convenient in stress calculations, because it would eliminate the procedure of calculating the elastic stress and then correcting this to account for inelastic effects.

F. R. SHANLEY
Consulting Structural Engineer

Dear Sir:

The numerical procedure described by Marvin Stern in his article in the August, 1947, issue of the JOURNAL OF THE AERONAUTICAL SCIENCES (page 481) is a valuable contribution toward the solution of the "one-directional" shear lag problem and, with the slight extension mentioned at the end of the article, the shear lag problem involving lateral movement.

The procedure suffers from some lack of generality, however, inasmuch as it cannot be applied directly to problems in which some of the boundary conditions are given in terms of displacements rather than stresses. In many cases this lack of generality does not represent any practical limitation on the applicability of the method, since a boundary having zero displacement can often be regarded as an axis of symmetry of a hypothetical symmetrical structure and thus eliminated from consideration as a boundary. In some cases, however, particularly in problems involving skew boundaries or problems in which the prescribed boundary displacements are not zero, such an artifice is not possible and some other way has to be found of handling the displacement boundary conditions.

I should therefore like to describe a slight modification or extension of Mr. Stern's approach that makes possible the explicit handling of displacement, as well as stress boundary conditions. This modification involves the use of displacement equations rather than stress equations and the conversion of stress boundary conditions into conditions on rate of change of displacement.

The equation of equilibrium for an element dx of stringer n at lattice point (n, m) is first written in terms of u-displacements as

$$A_s E\left(\frac{\partial^2 u}{\partial x^2}\right)_{n,\,m} + tG\left(\frac{u_{n-1,\,m} - u_{n,\,m}}{\lambda} - \frac{u_{n,\,m} - u_{n+1,\,m}}{\lambda}\right) = 0 \tag{1}$$

If the u-displacements in the nth stringer are assumed to vary according to a second-degree parabola between lattice points $(n, m-1)$ and $(n, m+1)$, then

$$(\partial^2 u/\partial x^2)_{n,\,m}$$

can be expressed in terms of $u_{n,\,m-1}$, $u_{n,\,m}$, and $u_{n,\,m+1}$ as

$$(\partial^2 u/\partial x^2)_{n,\,m} = 1/l^2(u_{n,\,m-1} - 2u_{n,m} + u_{n,\,m+1}) \tag{2a}$$

or in terms of $(\partial u/\partial x)_{n,\,m-1}$, $u_{n,\,m}$, and $u_{n,\,m+1}$ as

$$\left(\frac{\partial^2 u}{\partial x^2}\right)_{n,\,m} = -\frac{2}{3l^2}\left[l\left(\frac{\partial u}{\partial x}\right)_{n,\,m-1} + u_{n,\,m} - u_{n,\,m+1}\right] \tag{2b}$$

or in terms of $u_{n,\,m-1}$, $u_{n,\,m}$, and $(\partial u/\partial x)_{n,\,m+1}$ as

$$\left(\frac{\partial^2 u}{\partial x^2}\right)_{n,\,m} = \frac{2}{3l^2}\left[u_{n,\,m-1} - u_{n,\,m} + l\left(\frac{\partial u}{\partial x}\right)_{n,\,m+1}\right] \tag{2c}$$

(The assumption of a parabolic variation is also implied in the equation above Fig. 1 in Mr. Stern's article.) Substitution of Eqs. (2a), (2b), and (2c), respectively, into Eq. (1) and solution of the latter equation in each case for $u_{n,\,m}$ give the following three equations for $u_{n,\,m}$:

$$u_{n,\,m}2(1+\beta^2) = u_{n,\,m-1} + u_{n,\,m+1} + \beta^2 u_{n-1,\,m} + \beta^2 u_{n+1,\,m} \tag{3a}$$

$$u_{n,\,m}(1+3\beta^2) = -l\left(\frac{\partial u}{\partial x}\right)_{n,\,m-1} + u_{n,\,m+1} + \frac{3}{2}\beta^2 u_{n-1,\,m} + \frac{3}{2}\beta^2 u_{n+1,\,m} \tag{3b}$$

$$u_{n,\,m}(1+3\beta^2) = u_{n,\,m-1} + l\left(\frac{\partial u}{\partial x}\right)_{n,\,m+1} + \frac{3}{2}\beta^2 u_{n-1,\,m} + \frac{3}{2}\beta^2 u_{n+1,\,m} \tag{3c}$$

(If n is an edge stringer, Eq. (1) and therefore Eqs. (3a)–(3c) must be changed somewhat to eliminate the $n-1$, m or $n+1$, m term.)

Eq. (3a), which relates the u-displacement at lattice point (n, m) to the u-displacements at four neighboring lattice points, takes the place of Eq. (3) in Mr. Stern's article. If either $(n, m-1)$ $(n, m+1)$ is a stringer-end point at which the stress σ_s rather than the u-displacement is known, the known stress can be converted into a known value of $\partial u/\partial x$ by use of Hooke's law, and Eq. (3b) or (3c), respectively, must be used instead of Eq. (3a) at lattice point (n, m).

By writing Eq. (3a), (3b), or (3c) at every lattice point, a set of equations is obtained that involves as many unknown u-displacements as there are equations. These equations can be solved for the u-displacements by means of the iteration procedure described by Mr. Stern. It is only necessary to assume values for the $u_{n,\,m}$'s and to adjust each value using Eq. (3a), (3b), or (3c), depending on what conditions are known at the neighboring lattice points. After the displacements have been determined, the stringer stresses can be calculated from the rate of change of displacement, which is the strain.

CHARLES LIBOVE
Structural Engineer
National Advisory Committee for Aeronautics

Errata

The following corrections to his article were submitted by John W. Miles, the author of the paper "The Aerodynamic Forces on an Oscillating Airfoil at Supersonic Speeds," which appeared in JOURNAL OF THE AERONAUTICAL SCIENCES, Vol. 14, No. 6, pp. 351–358, June, 1947.

On page 352, Eq. (12) should read as follows:

$$G(x, \xi) = e^{-ik^2M(x-\xi)}\, J_0[\kappa(x - \xi)]$$

On page 357 in Fig. 9, the ordinate should be: $-k^2 I_{e\alpha}$.

The real and imaginary parts of the flutter derivatives plotted in the figures are referred to the quarter chord, for $M = 0$ and $M = 0.7$; accordingly, direct comparison with the supersonic results in the figures is possible only in the case of R_{ch} and I_{ch}, the rotation α and the stalling moment being about the quarter chord.

The Linearized Subsonic and Supersonic Flow About Inclined Slender Bodies of Revolution

E. V. LAITONE*

Cornell Aeronautical Laboratory

SUMMARY

Rigorous first order linearized solutions are obtained for the subsonic and supersonic flow about bodies of revolution. The surface pressures are found by means of a Taylor's Series expansion in terms of the cross-sectional area. The resulting simple expressions are shown to be in satisfactory agreement with existing experimental data. It is proved that previous solutions of the linearized supersonic flow equations have retained terms that at high Mach Numbers are incompatible with the basic potential equation of compressible flow.

Extremely simple relations are developed for the lift and moment of bodies of revolution in inclined and curvilinear subsonic and supersonic flow. These relations are in good agreement with experimental measurements. The commonly used linearized solution for the supersonic flow about an inclined body of revolution is incorrect, since nearly all of the terms retained are of a higher order than the terms omitted in neglecting the effect of the velocity component due to the axial flow and in not considering the complete boundary conditions.

The rigorous analysis indicates that the linearized theory cannot correctly predict the variation of the surface pressure coefficient at high Mach Numbers.

SYMBOLS

a	= local velocity of sound (ft. per sec.)
M	= Mach Number = $\sqrt{u_\infty^2 + v_\infty^2}/a \backsimeq u_\infty/a$
B	= $\sqrt{M^2 - 1}$
β	= $\sqrt{1 - M^2}$
γ	= isentropic gas constant = 7/5 for dry air
u	= local velocity along x axis (ft. per sec.)
v	= local velocity along r axis (for $\omega = 0$) (ft. per sec.)
u_∞, v_∞	= free-stream velocity conditions at an infinite distance upstream of the body (ft. per sec.)
α	= free-stream angle of attack, positive nose up = $\tan^{-1}(v_\infty/u_\infty) \backsimeq v_\infty/u_\infty$ (rad.)
$\dot{\alpha}_\infty$	= pitching velocity, positive nose up (rad. per sec.)
C_p	= local pressure coefficient = $[(p - p_\infty)/q]$
p	= local static pressure (lbs. per sq. ft.)
p_∞	= free-stream static pressure (lbs. per sq.ft.)
q	= $\rho(u_\infty^2 + v_\infty^2)/2 \backsimeq \rho u_\infty^2/2$
ρ	= mass density (lb.sec.^{2} per ft.^{4})
(x, r, ω)	= cylindrical coordinates for body of revolution, Fig. 1
S	= cross-sectional area of body of revolution = $\pi r^2(x)$ (sq.ft.)
S'	= $dS(x)/dx = 2\pi r r'$ (ft.)
r'	= $dr(x)/dx$
L	= length of body of revolution (ft.)
A	= base area of body of revolution, S for $x = L$ (sq.ft.)
θ	= cone or nose semivertex angle (rad.)
F_x	= resultant transverse force per unit axial length (lbs. per ft.)
C_L	= lift coefficient = lift/qA
C_m	= pitching moment coefficient about nose ($x = 0$) = moment/qAL

Presented at Aerodynamics Session, Fifteenth Annual Meeting, I.A.S., New York, January 28–30, 1947. Revised and received April, 1947.

* Principal Aeronautical Engineer.

INTRODUCTION

THE PRESENT DEVELOPMENT was started as an attempt to justify the linearized supersonic flow solutions for a body of revolution as introduced by Kármán-Moore[1] and Tsien.[2] A mathematically rigorous development of the linearized supersonic flow solution was attempted in order to indicate its limitations and to explain some of the anomalous behavior of the Kármán-Moore and Tsien solutions.

The analysis shows that in general the effect of high Mach Numbers cannot be predicted by the linearized theory for the supersonic flow about a sharp-nose slender body of revolution. The difficulties encountered through the use of the Kármán-Moore or Tsien linearized solutions are shown to be due to the fact that they implicitly contain terms that are essentially of an order higher than those that have been already neglected in the process of linearizing the basic equation of a compressible potential flow. These terms contain the Mach Number in such a manner that the numerical value of these terms becomes larger than that of the lower order terms as the Mach Number increases. The mathematical development indicates that in general the additional work required by the Karman-Moore and Tsien methods is not justified. In fact, the additional work involved would generally lead to erroneous results, at least for Mach Numbers greater than $\sqrt{2}$.

The analysis presented here was carried out during 1946 at the Cornell Aeronautical Laboratory as a part of the investigation of the dynamic stability of missiles at subsonic and supersonic speeds. The work was done under the sponsorship of the Air Matériel Command, Wright Field.

THE SUPERSONIC AXIAL FLOW ABOUT A BODY OF REVOLUTION

The potential equation for the axially symmetric flow of a compressible fluid in cylindrical coordinates (Fig. 1) is[3]

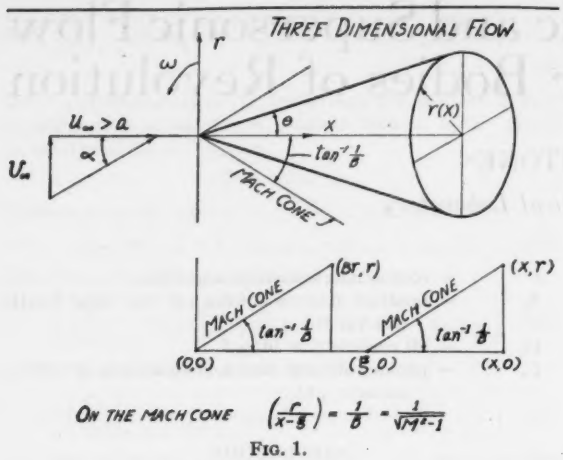

FIG. 1.

$$\left.\begin{aligned}\Phi_{xx}\left(1-\frac{\Phi_x^2}{a^2}\right)+\Phi_{rr}\left(1-\frac{\Phi_r^2}{a^2}\right)+\frac{\Phi_r}{r}-\\ 2\Phi_{xr}\frac{\Phi_x\Phi_r}{a^2}=0\\ a^2=a_\infty^2+\frac{\gamma-1}{2}\left(u_\infty^2-\Phi_x^2-\Phi_r^2-\frac{1}{r^2}\Phi_\omega^2\right)\end{aligned}\right\} \quad (1)$$

Then if Φ is taken as

$$\Phi = u_\infty x + \phi \quad (2)$$

where ϕ is a perturbation potential superimposed on a uniform constant flow field, Eq. (1) becomes

$$\left.\begin{aligned}\left[\phi_{xx}\left(1-\frac{u_\infty^2}{a^2}\right)+\phi_{rr}+\frac{\phi_r}{r}\right]=\\ \left[\phi_{xx}\left(2\frac{u_\infty}{a}\frac{\phi_x}{a}+\frac{\phi_x^2}{a^2}\right)+\phi_{rr}\frac{\phi_r^2}{a^2}+\right.\\ \left.2\phi_{xr}\left(\frac{u_\infty}{a}+\frac{\phi_x}{a}\right)\frac{\phi_r}{a}\right]\\ a^2=a_\infty^2-[(\gamma-1)/2](2u_\infty\phi_x+\phi_x^2+\phi_r^2)\end{aligned}\right\} \quad (3)$$

which is linearized to the first order as

$$\phi_{rr}+(1/r)\phi_r+(1-M^2)\phi_{xx}=0+0(\phi^2) \quad (4)$$

where for supersonic flow we define

$$B^2=(u_\infty^2/a_\infty^2)-1=M^2-1>0$$

Kármán-Moore[1] used the following as a solution of Eq. (4):

$$\phi=-(1/4\pi)\int_0^{\cosh^{-1}x/Br} f(x-Br\cosh z)dz \quad (5)$$

or with

$$\left.\begin{aligned}\xi&=x-Br\cosh z\\ \phi&=-(1/4\pi)\int_0^{x-Br}f(\xi)d\xi/\sqrt{(x-\xi)^2-B^2r^2}\end{aligned}\right\} \quad (6)$$

Eq. (6) is an improper integral, since the denominator vanishes for the upper limit, and, consequently, all previous differentiation of the perturbation potential has been accomplished by operating on the form given in Eq. (5). However, some new useful relations can be obtained by differentiating Eq. (6) in the following manner:

$$-4\pi\phi_x=\lim_{\xi_1\to x-Br}\left\{\int_0^{\xi_1}\frac{f(\xi)(\xi-x)d\xi}{[(x-\xi)^2-B^2r^2]^{3/2}}+\frac{f(\xi_1)(d\xi_1/dx)}{\sqrt{(x-\xi_1)^2-B^2r^2}}\right\}=$$

$$\lim_{\xi_1\to x-Br}\left\{\int_0^{\xi_1}\frac{[f(\xi)-f(\xi_1)]}{[(x-\xi)^2-B^2r^2]^{3/2}}(\xi-x)d\xi+\frac{f(\xi_1)}{\sqrt{x^2-B^2r^2}}-\frac{f(\xi_1)}{\sqrt{(x-\xi_1)^2-B^2r^2}}+\frac{f(\xi_1)(d\xi_1/dx)}{\sqrt{(x-\xi_1)^2-B^2r^2}}\right\}=$$

$$\int_0^{x-Br}\frac{[f(\xi)-f(x-Br)]}{[(x-\xi)^2-B^2r^2]^{3/2}}(\xi-x)d\xi+\frac{f(x-Br)}{\sqrt{x^2-B^2r^2}} \quad (7)$$

$$-4\pi\phi_r=\lim_{\xi_1\to x-Br}\left\{B^2r\int^{\xi_1}\frac{f(\xi)d\xi}{[(x-\xi)^2-B^2r^2]^{3/2}}+\frac{f(\xi_1)(d\xi_1/dr)}{\sqrt{(x-\xi_1)^2-B^2r^2}}\right\}=$$

$$\lim_{\xi_1\to x-Br}\left\{B^2r\int^{\xi_1}\frac{[f(\xi)-f(\xi_1)]d\xi}{[(x-\xi)^2-B^2r^2]^{3/2}}-\frac{(x/r)f(\xi_1)}{\sqrt{x^2-B^2r^2}}-\frac{[(\xi_1-x)/r]f(\xi_1)}{\sqrt{(x-\xi_1)^2-B^2r^2}}+\frac{f(\xi_1)\,d\xi_1/dr}{\sqrt{(x-\xi_1)^2-B^2r^2}}\right\}=$$

$$B^2r\int_0^{x-Br}\frac{[f(\xi)-f(x-Br)]d\xi}{[(x-\xi)^2-B^2r^2]^{3/2}}-\frac{(x/r)f(x-Br)}{\sqrt{x^2-B^2r^2}} \quad (8)$$

That this is a valid mathematical procedure is easily shown by direct substitution into Eq. (4). Of course, Eqs. (7) and (8) could be obtained by differentiating Eq. (5) to get ϕ_x and ϕ_r and then integrating these by parts to get Eqs. (7) and (8), respectively.

Now if $f(x)$ is a continuous function,

$$f(\xi)-f(x-Br)=\sum_{n=1}^{\infty}\frac{(\xi-x)^{(n)}-(-Br)^n}{n!}f^{(n)}(x)$$

and Eqs. (7) and (8) become

$$-4\pi\phi_z = \left\{\left[\log\left(\frac{Br}{x-\sqrt{x^2-B^2r^2}}\right) - \frac{x-Br}{\sqrt{x^2-B^2r^2}}\right]f'(x) - \left[\sqrt{x^2-B^2r^2}\right]\frac{f''(x)}{2} + \left[\frac{3B^2r^2}{2}\log\left(\frac{Br}{x-\sqrt{x^2-B^2r^2}}\right) - \frac{B^2r^2(x-Br)}{\sqrt{x^2-B^2r^2}} + \frac{x}{2}\sqrt{x^2-B^2r^2}\right]\frac{f'''(x)}{6} - \left[\frac{1}{3}(x^2-B^2r^2)^{3/2} + 2B^2r^2\sqrt{x^2-B^2r^2}\right]\frac{f^{(4)}(x)}{24} + \left[\frac{15}{8}B^4r^4\log\left(\frac{Br}{x-\sqrt{x^2-B^2r^2}}\right) + \frac{2x^5+5x^3B^2r^2-15xB^4r^4+8B^5r^5}{8\sqrt{x^2-B^2r^2}}\right]\times \frac{f^{(5)}(x)}{120} + \cdots + \frac{f(x-Br)}{x}\left(1-\frac{B^2r^2}{x^2}\right)^{-1/2}\right\} \quad (9)$$

$$-4\pi\phi_r = \left\{B^2r\left[\frac{1}{\sqrt{x^2-B^2r^2}} - \frac{x}{Br\sqrt{x^2-B^2r^2}}\right]f'(x) + B^2r\left[\log\left(\frac{Br}{x-\sqrt{x^2-B^2r^2}}\right)\right]\frac{f''(x)}{2} - B^2r\left[\sqrt{x^2-B^2r^2} + \frac{Br(x-Br)}{\sqrt{x^2-B^2r^2}}\right]\frac{f'''(x)}{6} + B^2r\left[\frac{3}{2}B^2r^2\log\left(\frac{Br}{x-\sqrt{x^2-B^2r^2}}\right) + \frac{x}{2}\sqrt{x^2-B^2r^2}\right]\frac{f^{(4)}(x)}{24} - B^2r\left[\frac{1}{3}(x^2-B^2r^2)^{3/2} + 2B^2r^2\sqrt{x^2-B^2r^2} - \frac{B^3r^3(x-Br)}{\sqrt{x^2-B^2r^2}}\right]\frac{f^{(5)}(x)}{120} + \cdots - \frac{f(x-Br)}{r}\left(1-\frac{B^2r^2}{x^2}\right)^{-1/2}\right\} \quad (10)$$

Then, expanding in powers of r,

$$\phi_z = -\frac{1}{4\pi}\left[-\left(1+\log\frac{Br}{2x}\right)f'(x) - \frac{x}{2}f''(x) + \frac{x^2}{12}f'''(x) - \frac{x^3}{72}f^{(4)}(x) + \frac{x^4}{480}f^{(5)}(x) + \cdots + \frac{f(x)}{x} + \cdots + 0(B^3rf)\right] \quad (11)$$

$$\phi r = \frac{1}{4\pi}\left[\frac{f(x)}{r} + \left(\frac{B^2r}{2}\log\frac{Br}{x}\right)f''(x) + \cdots + 0(B^2rf)\right] \quad (12)$$

The boundary condition for the meridian line is $\phi_r = u_\infty r' + \phi_z r'$; therefore, to the first order,

$$f(x) = 4\pi u_\infty rr' = 2u_\infty S' \quad (13)$$

where

$$S = \pi r^2 \quad (14)$$

Then, for the second order,

$$f(x) = 4\pi rr'(u_\infty + \phi_z) - \left(\frac{B^2r^2}{2}\log\frac{Br}{x}\right)f''(x) + 0(B^2r^2f) = 2u_\infty S'\left[1 - \left(\log\frac{Br}{x}\right)\left(\frac{3B^2rr''}{2} + \frac{B^2r^2r'''}{2r'} - rr'' - r'^2\right) + 0(r^2)\right] \quad (15)$$

Therefore, to the order $r^4\log r = 0$, Eqs. (5) and (6) become

$$\frac{\Delta u}{u_\infty} = -\frac{1}{2\pi}\left[\int_0^{\cosh^{-1}x/Br} S''(x - Br\cosh z)dz + \frac{S'(0)}{\sqrt{x^2-B^2r^2}}\right] = -\frac{1}{2\pi}\left[\int_0^{x-Br}\frac{S''(\xi)d\xi}{\sqrt{(x-\xi)^2-B^2r^2}} + \frac{S'(0)}{\sqrt{x^2-B^2r^2}}\right] = -\frac{1}{2\pi}\left\{\int_0^{x-Br}\frac{[S'(\xi)-S'(x-Br)]}{[(x-\xi)^2-B^2r^2]^{3/2}}(\xi-x)d\xi + \frac{S'(x-Br)}{\sqrt{x^2-B^2r^2}}\right\} \quad (16)$$

$$\frac{\Delta v}{u_\infty} = \frac{1}{2\pi}\left[B\int_a^{\cosh^{-1}x/Br} S''(x - Br\cosh z)\cosh z dz + \frac{(x/r)S'(0)}{\sqrt{x^2-B^2r^2}}\right] = -\frac{1}{2\pi}\left[\frac{1}{r}\int_0^{x-Br}\frac{S''(\xi)(\xi-x)d\xi}{\sqrt{(x-\xi)^2-B^2r^2}} - \frac{(x/r)S'(0)}{\sqrt{x^2-B^2r^2}}\right] = -\frac{1}{2\pi}\left\{B^2r\int_0^{x-Br}\frac{[S'(\xi)-S'(x-Br)]d\xi}{[(x-\xi)^2-B^2r^2]^{3/2}} - \frac{(x/r)S'(x-Br)}{\sqrt{x^2-B^2r^2}}\right\} \quad (17)$$

Similarly Eqs. (11) and (12) become

$$\frac{\Delta u}{u_\infty} = -\frac{1}{2\pi}\left[\frac{S'}{x} - \left(1+\log\frac{Br}{2x}\right)S'' - \frac{x}{2}S''' + \frac{x^2}{12}S^{(4)} - \frac{x^3}{72}S^{(5)} + \frac{x^4}{480}S^{(6)} + \cdots + 0(r^3)\right] \quad (18)$$

$$\frac{\Delta v}{u_\infty} = r'(x) + 0(r^3 \log r) \tag{19}$$

The pressure coefficient for compressible flow is given by

$$C_p = -2\left(\frac{\Delta u}{u_\infty}\right) - \left(\frac{\Delta v}{u_\infty}\right)^2 + \left(\frac{\Delta u}{u_\infty}\right)^2 (M^2 - 1) + 0(\Delta u^3, \Delta v^4)$$

which, in view of Eqs. (18) and (19), becomes

$$C_p = -2\,(\Delta u/u_\infty) - (r')^2 + 0(r^4 \log r)$$

or

$$C_p = \left\{\frac{1}{\pi}\left[\frac{S'}{x} - \left(1 + \log\frac{Br}{x} - \log 2\right)S'' - \frac{x}{2}S''' + \frac{x^2}{12}S^{(4)} - \frac{x^3}{72}S^{(5)} + \frac{x^4}{480}S^{(6)} + \ldots\right] - (r')^2 + 0(r^3)\right\} \tag{20}$$

Fig. 2 shows that Eq. (20) gives a solution almost identical to the one obtained by Kármán-Moore.[1] However, the terms of order r^2 contain the Mach Number and cannot be retained at high Mach Numbers unless there is an additional justification for using terms of an order neglected in obtaining Eq. (4). A comparison with the experimental data for an infinite cone shows that at high Mach Numbers only the first order term may be retained. Eqs. (5) and (15) yield

$$\frac{\phi}{u_\infty} = -\frac{1}{2\pi}\int_0^{\cosh^{-1}x/Br} S'(x - Br\cosh z)\,dz + 0(r^4 \log r) \tag{21}$$

Then, for an infinite cone with a semiwedge angle of θ,

$$\theta = r/x, \qquad S = \pi\theta^2 x^2$$

Eq. (21) becomes

$$\frac{\phi}{u_\infty} = -\theta^2\left(x\cosh^{-1}\frac{x}{Br} - \sqrt{x^2 - B^2r^2}\right) + 0(\theta^4 \log \theta) \tag{22}$$

Substituting Eq. (22) into Eq. (4) shows that it is satisfied if terms of the order θ^4 are neglected. This is in agreement with the approximation for $f(x)$ in Eq. (15) and with the work of Lighthill.[4] However, Eq. (3) is satisfied by Eq. (22) only if terms of the order θ^2 are neglected; consequently, the linearized solution for the infinite cone is valid only to the order $\theta^2 = 0$. Therefore, for an infinite cone, Eq. (20) must be reduced from

$$C_p = -2\theta^2 \log (B\theta/2) - \theta^2 + 0(\theta^4 \log \theta)$$

to

$$C_p = -2\theta^2 \log \theta + 0(\theta^2)$$

The neglected term $-2\theta^2 \log (B/2)$ is of order θ^2 but is also a function of the Mach Number in such a manner that as M increases this neglected second order term can become numerically larger than the first order term for a finite θ. Therefore, without further justification, only the first order term $S''/\pi \log (r/x)$ is a valid representation of the surface pressures. By direct substitution into Eq. (3), the exact potential equation for compressible flow, it may be shown that $S''/\pi \log (Br/x)$ is also a valid solution as the Mach Number approaches unity. It is found, however, that the additional term $\log B$ cannot be retained in a first order approximation as the Mach Number approaches and exceeds $\sqrt{2}$, not even if the Mach number approaches infinity. The rigorous linearized first order solution for the surface pressures on an extremely slender sharp nose body of revolution in supersonic flow is therefore given by

$$\left.\begin{aligned} C_p &\approx -\frac{S''}{\pi}\log\frac{Br}{x}, \qquad 1 < M < \sqrt{2} \\ C_p &\approx -\frac{S''}{\pi}\log\frac{r}{x}, \qquad M > \sqrt{2} \end{aligned}\right\} \tag{20a}$$

In Fig. 2, Eq. (20a) is compared with Eq. (20) and the experimental data from reference 1. Fig. 3 compares Eqs. (20) and (20a) with the Kármán-Moore[1] solution and the more exact Taylor-Maccoll[5] solution for an infinite cone. It is seen that, at least for the cone, Eq. (20a) is the best of the linearized solutions. For the infinite cone the Kármán-Moore[1] solution shown in

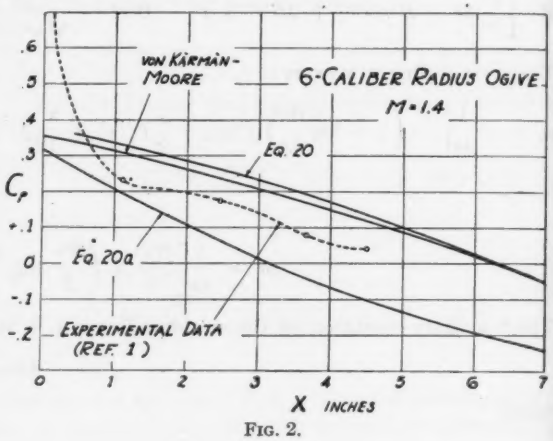

FIG. 2.

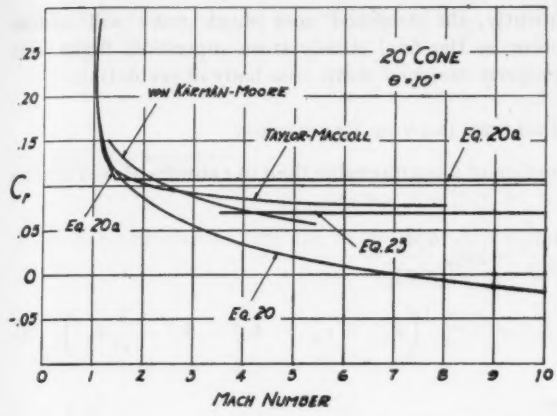

FIG. 3.

Fig. 3 is that given by reference 6 as

$$C_p = \frac{2\theta^2 \cosh^{-1}(1/B\theta)}{\sqrt{1 - B^2\theta^2} + \theta^2 \cosh^{-1}(1/B\theta)}$$

It should be noticed that this expression fails to give a solution when $B \to 1/\theta$ as indicated in Fig. 3. Also shown in Fig. 3 is the limiting asymptotic value of the pressure coefficient due to the conical adiabatic shock wave of a very slender conical nose when the Mach Number increases without limit as given by the author in reference 7:

$$C_p \to (\gamma + 1)\theta^2 = (12/5)\theta^2 \tag{23}$$

It is seen that the rate of decrease of pressure coefficient as given by the Kármán-Moore[1] solution is undoubtedly excessive.

The wave drag is given very simply by Eq. (20a) as

$$\left.\begin{aligned} C_D = \frac{\text{drag force}}{qA} &= \frac{1}{qA}\int_0^L \Delta P S'(x)dx \\ &\approx -\frac{1}{\pi A}\int_0^L S'(x)S''(x)\log\frac{Br}{x}dx, \qquad 1 < M < \sqrt{2} \\ &\approx -\frac{1}{\pi A}\int_0^L S'(x)S''(x)\log\frac{r}{x}dx, \qquad M > \sqrt{2} \end{aligned}\right\} \tag{24}$$

This gives less wave drag than the relation given by von Kármán,[6]

$$C_D = \frac{1}{2\pi A}\int_0^L\int_0^L S''(x)S''(\xi)\log\left|\frac{1}{x-\xi}\right| dxd\xi \tag{25}$$

However, if Eq. (20) is substituted into

$$C_D = (1/A)\int_0^L C_p S'(x)dx \tag{25a}$$

the wave drag coefficient will be found to be in agreement with that given by Eq. (25) for bodies of revolution whose cross-sectional area S is a uniformly continuous function, at least for Mach Numbers near $\sqrt{2}$ or at any Mach Number for sharp nose bodies that have either $r(L)$ or $r'(L)$ equal zero. This is so because Eqs. (20) and (25a) show that the wave drag coefficient given by Eq. (20) is also independent of Mach Number if $S'(L)$ is equal to $S'(O)$. For a sharp nose body $S'(O)$ is zero; therefore, according to Eq. (20), $S'(L)$ must also be zero for the wave drag coefficient to be independent of Mach Number.

Although the rigorous mathematical analysis can justify only the first order solution given by Eq. (20a), it still may be possible to justify the use of Eq. (20) at least for values of B not too much greater than unity, since the terms of order r^2 only contain the Mach Number effect in the form log B, which does not increase extremely rapidly with Mach Number. It is easily shown by comparison that, for any body of revolution whose cross-sectional area is defined by a continuous function of x, Eq. (20) will give the same surface pressures as given by the von Kármán[1, 6] method for $B = 1$. The von Kármán solution, however, will overestimate the effect of an increasing Mach Number, since the terms of order r^2 which are retained in it are all of the form B^2rS'' [see Eq. (11)]. The addition of the terms of order M^2r^2 greatly overestimate the effect of Mach Number as B exceeds unity. This may easily be shown by comparison with experimental data or the solution obtained by the characteristic method of Sauer.[3]

Lighthill[4] showed that Eqs. (16) and (19) could give a solution of Eq. (3) to the order $r^4 \log r = 0$ in the following form:

$$C_p = \frac{1}{\pi}\int_0^{x-Br} \frac{S''(\xi)d\xi}{\sqrt{(x-\xi)^2 - B^2r^2}} - [r'(x)]^2 \tag{20b}$$

However, the present development proves that Eq. (20b) still contains terms of the form M^2r^2 which greatly overestimate the effect of Mach Number so that Lighthill's[4] results are also applicable only for $M \leqq \sqrt{2}$.

If in the supersonic flow linearized solution terms of the order r^2 may be retained, at least for bodies other than an infinite cone, then Eq. (20) may be used for the surface pressures if the free-stream Mach Number is greater than $M_{min.}$ for a detached shock wave and if $S(x)$ is continuous. If there are discontinuities in the derivatives of the cross-sectional area, the von Kármán[1] solution may be used with $B = 1$ ($M = \sqrt{2}$). Eqs. (16) and (17) may be used to find the velocities anywhere in the flow field behind the Mach cone produced by the sharp leading edge of a body of revolution. For example, it will be shown later than an integration of Eq. (16) indicates that directly behind the body there exists a wake with a positive pressure increment similar to that existing in subsonic flow. In a similar manner, Eq. (16) may be used to determine the wind-tunnel wall and other interference corrections where the values of r are extremely large.

It is important to note that all of these supersonic flow solutions are applicable only if the flow is everywhere supersonic. These solutions will not apply if there is a

detached nose shock wave. However, the minimum Mach Number for a detached shock wave in front of a conical nose with a vertex angle of 20° is 1.04;[5] consequently, the detached nose shock wave will seldom occur in the final steady state supersonic flight of a properly designed sharp nose body of revolution.

The Supersonic Flow About an Inclined Body of Revolution

Without axial symmetry the potential equation for the motion of a compressible fluid in cylindrical coordinates (Fig. 1) is[3]

$$\Phi_{xx}\left(1-\frac{\Phi_x^2}{a^2}\right)+\Phi_{rr}\left(1-\frac{\Phi_r^2}{a^2}\right)+\frac{\Phi_{\omega\omega}}{r^2}\left(1-\frac{\Phi_\omega^2}{r^2a^2}\right)-2\Phi_{rx}\frac{\Phi_r\Phi_x}{a^2}-2\Phi_{x\omega}\frac{\Phi_x\Phi_\omega}{r^2a^2}-$$

$$2\Phi_{xr}\frac{\Phi_x\Phi_r}{a^2}+\frac{\Phi_r}{r}\left(1+\frac{\Phi_\omega^2}{r^2a^2}\right)=0,\quad a^2=a_\infty^2+\frac{\gamma-1}{2}\left(u_\infty^2+v_\infty^2-\Phi_x^2-\Phi_r^2-\frac{1}{r^2}\Phi_\omega^2\right) \tag{26}$$

Then, for the linearized mathematical procedure, Φ is taken:

$$\Phi=(u_\infty x+v_\infty r\cos\omega)+\phi(x,r,\omega)=u_\infty(x+r\alpha\cos\omega)+\phi+0(r\alpha^3)$$

where ϕ is a small perturbation potential superimposed on a constant uniform slightly inclined flow field. Eq. (26) then is generally written as

$$\phi_{rr}+(\phi_r/r)+(\phi_{\omega\omega}/r^2)-(M^2-1)\phi_{xx}=0+0(\phi^2) \tag{27}$$

where for supersonic flow $M^2-1=B^2>0$.

If $\phi(x,r)$ is a solution of Eq. (27), then Lamb[3] has shown that

$$\phi(x,r,\omega)=\cos\omega[\partial\phi(x,r)/\partial r] \tag{28}$$

is also a solution of Eq. (27). Now Eq. (6) is a solution of Eqs. (4) or (27), and by comparison with Eqs. (8) and (28) a solution of Eq. (27) may be written

$$\phi(x,r,\omega)=-\frac{\cos\omega}{4\pi}\left\{B^2r\int_0^{x-Br}\frac{[f_2(\xi)-f_2(x-Br)]d\xi}{[(x-\xi)^2-B^2r^2]^{3/2}}-\frac{(x/r)f_2(x-Br)}{\sqrt{x^2-B^2r^2}}\right\} \tag{29}$$

This is the desired solution corresponding to a supersonic "doublet" distribution and may be used to represent the effect of the transverse flow component of the inclined uniform flow. The boundary condition to be satisfied by the transverse flow alone is

$$\phi_r(x,r,\omega)+v_\infty\cos\omega+r'\phi_x(x,r,\omega)=0 \tag{30}$$

The effect of the transverse flow ($v_\infty=\alpha u_\infty$) and "doublet" distribution alone may be found and then superimposed on the previously found axial flow solution, since Eqs. (4) and (27) are linear. However, without additional justification it does not seem logical to consider any Mach Number effect due to the combined flow, since the Mach Number for the axial flow is u_∞/a while that for the transverse flow is essentially $\alpha u_\infty/a$ in this type of a superposition.

Eq. (12) shows that Eq. (29) may be written as

$$\phi(x,r,\omega)=\frac{\cos\omega}{4\pi}\left[\frac{f_2(x)}{r}+\frac{B^2r}{2}\left(\log\frac{r}{x}\right)f_2''(x)+0(B^2rf_2)\right] \tag{31}$$

and therefore

$$\phi_x(x,r,\omega)=\frac{\cos\omega}{4\pi}\left[\frac{f_2'(x)}{r}+\frac{B^2r}{2}\left(\log\frac{r}{x}\right)f_2'''(x)+0(B^2rf_2)\right] \tag{32}$$

$$\phi_r(x,r,\omega)=\frac{\cos\omega}{4\pi}\left[-\frac{f_2(x)}{r^2}+\frac{B^2}{2}\left(\log\frac{r}{x}\right)f_2''(x)+0(B^2f_2)\right] \tag{33}$$

Substituting Eqs. (32) and (33) into Eq. (30) shows that

$$f_2(x)=4\pi\alpha u_\infty r^2\left[1+B^2\left(\log\frac{r}{x}\right)(rr''+r'^2)+0(r^2)\right]=4\alpha u_\infty S\left[1+B^2\left(\log\frac{r}{x}\right)\frac{S''}{2\pi}\right]+0(r^4) \tag{34}$$

Then Eq. (32) becomes

$$\frac{\Delta u_2}{u_\infty} = \frac{\phi_x(x, r, \omega)}{u_\infty \cos\omega} = 2\alpha r'\left[1 + \frac{B^2}{\pi}\left(\log\frac{r}{x}\right)\left(\frac{SS'''}{S'} + \frac{S''}{2}\right)\right] =$$

$$2\alpha r'\left[1 + B^2\left(\log\frac{r}{x}\right)\left(r'^2 + 4rr'' + \frac{r^2r'''}{r'}\right)\right] + 0(r^3) \quad (35)$$

and Eq. (33) becomes

$$\Delta v_2/u_\infty = \phi_r(x, r, \omega)/u_\infty \cos\omega = -\alpha + 0(r^2 \log r) \quad (36)$$

The velocity components due to the axial flow alone are given by Eqs. (18) and (19) as

$$\Delta u/u_\infty = (r'^2 + rr'') \log (r/x) + 0(r^2) \quad (37)$$

$$\Delta v/u_\infty = r' + 0(r^3 \log r) \quad (38)$$

The static pressure is given by Eq. (26) as

$$\frac{p}{p_\infty} = \left(\frac{a^2}{a_\infty{}^2}\right)^{\gamma/\gamma-1} = \left[1 + \frac{\gamma - 1}{2a_\infty{}^2}\left(u_\infty{}^2 + v_\infty{}^2 - \Phi_x{}^2 - \Phi_r{}^2 - \frac{1}{r^2}\Phi_\omega{}^2\right)\right]^{\gamma/\gamma-1} =$$

$$\left\{1 + \frac{\gamma - 1}{2}M^2\left[1 + \alpha^2 - \left(1 + \frac{\Delta u}{u_\infty} + \frac{\Delta u_2}{u_\infty}\cos\omega\right)^2 - \left(\alpha\cos\omega + \frac{\Delta v}{u_\infty} + \frac{\Delta v_2}{u_\infty}\cos\omega\right)^2 - \left(-\alpha\sin\omega + \frac{\phi_\omega}{r}\right)^2\right]\right\}^{\gamma/(\gamma-1)} \quad (39)$$

Then

$$C_p = \frac{2}{\gamma M^2}\left(\frac{p}{p_\infty} - 1\right) = -\left\{\left[2\left(\frac{\Delta u}{u_\infty}\right) + \left(\frac{\Delta v}{u_\infty}\right)^2 + (1 - M^2)\left(\frac{\Delta u}{u_\infty}\right)^2 + \frac{\phi_\omega{}^2}{r^2}\right] + 2\left[\left(1 + \frac{\Delta u}{u_\infty}\right)\frac{\Delta u_2}{u_\infty} + \left(\alpha + \frac{\Delta v_2}{u_\infty}\right)\frac{\Delta v}{u_\infty}\right]\cos\omega + \left[(1 - M^2)\left(\frac{\Delta u_2}{u_\infty}\right)^2 + \left(\frac{\Delta v_2}{u_\infty}\right)^2 + 2\alpha\frac{\Delta v_2}{u_\infty}\right]\cos^2\omega - 2\alpha\frac{\phi_\omega}{r}\sin\omega\right\} +$$

$$0(\alpha^2, \Delta u^3, \Delta v^4) = 4\alpha r'\cos\omega - 2(\Delta u/u_\infty) - (r')^2 + 0(r_3, \alpha^2) \quad (40)$$

The resultant transverse force per unit axial length is given by

$$F_x = -\int_0^\pi qC_p r\cos\omega\, d\omega = 2\pi rq\left[\left(1 + \frac{\Delta u}{u_\infty}\right)\frac{\Delta u_2}{u_\infty} + \left(\alpha + \frac{\Delta v_2}{u_\infty}\right)\frac{\Delta v}{u_\infty}\right] \quad (41)$$

Then, substituting Eqs. (35) to (38) into Eq. (41) yields

$$\frac{F_x}{q} = 2\pi r\left(1 + \frac{\Delta u}{u_\infty}\right)\left(\frac{\Delta u_2}{u_\infty}\right) + 0(r^4) = 4\pi\alpha rr'\left\{1 + \log\left(\frac{r}{x}\right)\left[(B^2 + 1)r'^2 + (4B^2 + 1)rr'' + \frac{B^2r^2r'''}{r'}\right]\right\} \quad (42)$$

The lift and moment can then be computed from

$$\left.\begin{aligned} C_L &= (1/qA)\int_0^L F_x\, dx \\ C_m &= (1/qAL)\int_0^L F_x x\, dx \end{aligned}\right\} \quad (43)$$

Eq. (42) shows that if the cross product term $\Delta u \times \Delta u_2$ is neglected then the lift and moment must be obtained only by

$$F_x/q = 4\pi\alpha rr' + 0(r^4 \log r) = 2\alpha S' + 0(r^4 \log r) \quad (44)$$

which is the expression originally obtained by Munk[9] for the incompressible potential flow about a very slender body of revolution. This also proves that the expressions given by Tsien[2] are incorrect, since they entirely neglect $\Delta u \times \Delta u_2$ while extending the order of approximation of Δu_2 alone.

Lighthill[4] has proposed that only Eq. (44) is permissible in these linearized supersonic flow solutions. It will now be shown that this is true, at least for the flow about an infinite cone.

Ferrari[10] has shown that, for an infinite cone of semivertex angle θ, the solution of Eqs. (11) and (30) is

$$\phi(x, r, \omega) = \frac{B\alpha u_\infty \cos\omega\left[x\sqrt{(x^2/B^2r^2) - 1} - Br\cosh^{-1}(x/Br)\right]}{(B/\tan\theta)\sqrt{(1/B^2\tan^2\theta) - 1} + B^2\cosh^{-1}(1/B\tan\theta) + 2\sqrt{1 - B^2\tan^2\theta}} \quad (45)$$

where $r = \theta x$. If, instead of Eq. (30), the first order boundary condition

$$\phi_r(x, r, \omega) = -\alpha u_\infty \cos\omega \quad (46)$$

is used, the resulting expression for the potential is in agreement with Eq. (45) only if the order of the solution is restricted to $\theta^3 = 0$. To this order Eq. (45) becomes

$$\left.\begin{aligned} \phi(x, r, \omega) &= (\alpha u_\infty \cos\omega)x\theta(1 + 2\theta^2B^2 \log\theta) + 0(\theta^3) \\ \phi_x(x, r, \omega) &= (2\alpha u_\infty \cos\omega)\theta(1 + \theta^2B^2 \log\theta) + 0(\theta^3) \\ -\phi_r(x, r, \omega) &= \alpha u_\infty \cos\omega + 0(\theta^3) \end{aligned}\right\} \tag{45a}$$

However, these expressions are the same as given by Eqs. (31) to (36), indicating that, in general, if the first order boundary condition Eq. (46) has been used then only Eqs. (35), (36), and (42) should be used. If Eq. (45) is substituted into Eq. (26), however, it is satisfied only to the order $\theta^2 = 0$, showing that, at least for the infinite cone, only Eq. (44) is valid for the transverse force distribution. As a matter of fact, Eq. (44) should be the only rigorous linearized solution of this type for any body, since it is not logical to superimpose an axial and a transverse flow unless the Mach Number effect is analogous in both cases.

If the reference area A is the cross-sectional area of the base of the sharp nose body of revolution, then Eqs. (43) and (44) yield the following simple relations:

$$\frac{dC_L}{d\alpha} = 2, \qquad \frac{dC_m}{d\alpha} = 2\left(1 - \frac{\int_0^L S\,dx}{AL}\right) = 2\left(1 - \frac{\text{volume}}{AL}\right) \tag{47}$$

Fig. 4 compares Eq. (47) with the experimental data from Göttingen[11] for two bodies of revolution at an angle of attack of 3°.

The pitching moment and resultant lateral force due to a pitching velocity may also be obtained in a similar manner. If the pitching velocity is $\dot{}$, then Eqs. (32) and (33) may again be used with the new boundary condition

$$\phi_r(x, r, \omega) + \dot{\alpha}\,(x - x_{ac})\cos\omega + r'\phi_x(x, r, \omega) = 0 \tag{48}$$

This results in a transverse force distribution of

$$\frac{F_z}{q} = -\,[4\pi rr'(x_{ac} - x) - 2\pi r^2]\frac{\dot{\alpha}}{u_\infty} + 0(r^4 \log r) = -2[(x_{ac} - x)S' - S]\frac{\dot{\alpha}}{u_\infty} + 0(r^4 \log r) \tag{49}$$

which agrees with that given by Munk[9] for incompressible flow.

In a circular flight path or with an instantaneous pitching velocity ($\dot{\alpha}$), the body of revolution with a reference base area of A will experience, in addition to the lift and moment given by Eq. (47), the additional lift and moment given by Eqs. (43) and (49) as

$$\left.\begin{aligned} \frac{dC_L}{d\dot{\alpha}} &= \frac{2L}{u_\infty}[1 - (x_{ac}/L)] \\ \frac{dC_m}{d\alpha} &= \frac{2L}{u_\infty}\left\{\left[1 - \int_0^L \left(\frac{S}{A}\right)\left(\frac{x}{L}\right)d\left(\frac{x}{L}\right)\right] - \frac{x_{ac}}{L}\left[1 - \int_0^L \left(\frac{S}{A}\right)d\left(\frac{x}{L}\right)\right]\right\}\dot{} = \\ &\qquad \frac{2L}{u_\infty}\left\{\left[1 - \frac{\text{moment of volume}}{AL^2}\right] - \frac{x_{ac}}{L}\left[1 - \frac{\text{volume}}{AL}\right]\right\} \end{aligned}\right\} \tag{50}$$

where

$$x_{ac}/L = \sum C_m/\sum C_L.$$

The boundary condition, Eq. (48), is dependent on the location of the aerodynamic center, x_{ac} from Eq. (50), since the resultant transverse force vector must pass through the instantaneous center about which the body is rotating and the moments acting on the body must be in equilibrium about the point in the body where this resultant force vector intersects the body axis.

Eqs. (49) and (50) are independent of the Mach Number. The Mach Number would not enter these equations unless terms of the order $r^4 \log r$ are considered in combining Eqs. (32), (33), and (48). However, by analogy with the development of Eq. (44), it does not seem possible to obtain any Mach Number effect on the transverse force from the linearized theory. The higher order additional terms, which are implicitly contained in Tsien's solution, contain B^2 and therefore excessively decrease the lift and pitching moment coefficients with an increase in Mach Number beyond $\sqrt{2}$. However, by considering the development of Eq. (20a), it is seem that Eqs. (44), (47), (49), and (50) should only be applied for $M \geqq \sqrt{2}$.

The Subsonic Axial Flow About a Body of Revolution

Proceeding in an analogous manner, the author has shown in reference 12 that the axial subsonic flow about a sharp-nose slender body of revolution is represented, for the same body shape in either subsonic or incompressible

flow, by

$$\left.\begin{aligned}\frac{\Delta u}{u_\infty} &= -\frac{1}{4\pi}\int_0^L \frac{S'(\xi)(\xi - x)d\xi}{[(x-\xi)^2 + \beta^2 r^2]^{3/2}} + 0(r^4 \log r)\\ \frac{\Delta v}{u_\infty} &= \frac{\beta^2 r}{4\pi}\int_0^L \frac{S'(\xi)d\xi}{[(x-\xi)^2 + \beta^2 r^2]^{3/2}} + 0(r^4 \log r)\end{aligned}\right\} \tag{51}$$

where $\beta = \sqrt{1 - M^2} \leqq 1$.

Eq. (51) may be used as a first order approximation for the subsonic flow on or about a slender sharp nose body of revolution or as a solution, exact to the order $r^4 \log r = 0$, for the incompressible flow ($\beta = 1$) about any body of revolution. For example, Eq. (51) shows that the wind-tunnel wall interference correction would be given through the use of

$$\Delta u/u_\infty = (1/4\pi\beta^2 r^2)\int_0^L S'(\xi)(x - \xi)d\xi$$

so that the wind-tunnel wall compressibility correction would vary with $1/(1 - M^2)^{3/2}$.

In reference 12 it is shown that Eq. (51) may also be written on the surface of the body of revolution as

$$\left.\begin{aligned}\frac{\Delta u}{u_\infty} &= -\frac{1}{2\pi}\left\{\left[\frac{1 - (2x/L)}{1 - (x/L)}\right]\frac{S'}{2x} - \left(1 + \log\frac{\beta r}{L} - \log 2\sqrt{\frac{x}{L}\left(1 - \frac{x}{L}\right)}\right)S'' + \frac{L}{4}\left(1 - \frac{2x}{L}\right)S''' + \right.\\ &\qquad \left.\frac{L^2}{24}\left(1 - \frac{2x}{L} + \frac{2x^2}{L^2}\right)S^{(4)} + \ldots\right\} + 0(r^3)\\ \Delta v/u_\infty &= r' + 0(r^3 \log r)\end{aligned}\right\} \tag{52}$$

where the surface pressure coefficient is again given as in Eq. (20) by

$$C_p = \left\{\frac{1}{\pi}\left[\left(\frac{1 - \frac{2x}{L}}{1 - \frac{x}{L}}\right)\frac{S'}{2x} - \left(1 + \log\frac{\beta r}{2L\sqrt{\frac{x}{L}\left(1 - \frac{x}{L}\right)}}\right)S'' + \frac{L}{4}\left(1 - \frac{2x}{L}\right)S''' + \frac{L^2}{24}\left(1 - \frac{2x}{L} + \frac{2x^2}{L^2}\right)S^{(4)} + \ldots\right] - (r')^2\right\} + 0(r^3) \tag{53}$$

It is obvious that for the case of subsonic flow all of the terms in Eq. (53) may be justified as an approximation for the surface pressures on a body of revolution in compressible flow. This is true because, when $\beta = 1$, Eq. (53) is a solution of the exact potential equation for incompressible flow to the order $r^2 = 0$. For $\beta < 1$, the Mach Number effect is included as $\log \beta$ in the terms of order r^2 and therefore may be retained for $\beta \gg 0$ to give a valid approximation for the effect of Mach Number. In the supersonic case the terms of order r^2 contain $\log B$, which can only be retained for B values not much greater than unity, otherwise these terms will become numerically greater than the lower order terms as the Mach Number increases.

Eq. (53) provides the surface pressure distribution on a slender symmetrical body of revolution in either incompressible or subsonic potential flow. The first order compressibility effect is only valid for a slender sharp-nose body of revolution, but for incompressible potential flow Eq. (53) is a valid approximation even for a rounded nose symmetrical body of revolution, as shown in Fig. 5 where Eq. (53) is compared with the exact solution for a prolate spheroid of 10 per cent thickness ratio.

Eq. (53) shows that, unlike the simple first order compressibility correction of $1/\beta$ for two-dimensional subsonic flow, the first order Mach Number correction for a slender body of revolution varies with $\log \beta$, and the magnitude of the correction is affected by the body shape, as well as the actual location on a given body. Fig. 5 shows that for a prolate spheroid the correction varies only slightly with the location on the body until the stagnation points are approached. Of course, the compressibility correction given in Eq. (53) is not applicable near the stagnation point or for large values of r'; however, it may be applied as a general first order ratio correction. For example, the compressibility correction for the maximum negative surface pressure coefficient for any symmetrical body of revolution would be obtained from Eq. (53) by taking $x = L/2$ so that

$$\left(\frac{C_p}{C_{p_{M=0}}}\right)_{max.} = 1 + \left\{\log\beta \Big/ \left[1 + \log\frac{r}{L} - \left(\frac{L^2}{48}\frac{S^{(4)}}{S''} + \ldots\right)\right]\right\} \tag{54}$$

Fig. 6 compares Eq. (53) with the incompressible potential flow solution of a 10 per cent thickness ratio body of revolution generated by a parabolic arc. Also shown in Fig. 6 are the supersonic surface pressure coefficients ob-

tained from Eqs. (20) and (20a). The effect of the wave drag is seen as the unsymmetrical shift in the pressure distribution. Eq. (20a) would, of course, predict less total wave drag and predict more flow compression at the aft portion than would Eq. (20). The values given by Eq. (20) for this type of a body are in close agreement with the results of von Kármán[1, 6] and Lighthill[4] for Mach Numbers near $\sqrt{2}$.

The Subsonic Flow About an Inclined Body of Revolution

For the inclined subsonic flow the doublet distribution analogous to Eq. (29) is easily found from Eq. (28) and reference 12 as

$$\phi(x, r, \omega) = -(\beta r \cos\omega/4\pi) \int_0^L f_2(\xi)d\xi/[(x-\xi)^2 + \beta^2 r^2]^{3/2}$$

Following reference 12, this may be written as

$$\phi(x, r, \omega) = \frac{\beta r \cos\omega}{4\pi}\left[\frac{2f_2(x)}{\beta r} - \beta r \log\left(\frac{r}{L}\right) f_2''(x)\right] + 0(\beta r f_2) \tag{55}$$

The boundary conditions are again given by Eq. (30), and, combining this with Eq. (55),

$$\left.\begin{aligned} f_2(x) &= 2\alpha u_\infty \beta S[1 - \beta^2 \log(r/L)(S''/2\pi)] + 0(r^4) \\ \frac{\Delta u_2}{u_\infty} &= 2\alpha r'\left[1 - \beta^2 \log\left(\frac{r}{L}\right)\left(r'^2 + 4rr'' + \frac{r^2 r'''}{r'}\right)\right] + 0(r^3) \\ \Delta v_2/u_\infty &= -\alpha + 0(r^3 \log r) \end{aligned}\right\} \tag{56}$$

From Eq. (52) the first order terms for the axial subsonic flow components are given by

$$\left.\begin{aligned} \Delta u/u_\infty &= (S''/2\pi)\log(r/L) + 0(r^2) \\ \Delta v/u_\infty &= r' + 0(r^3 \log r) \end{aligned}\right\} \tag{57}$$

Substituting Eqs. (56) and (57) into Eq. (41) yields a resultant transverse force distribution of

$$\frac{F_x}{q} = 4\pi\alpha r r'\left\{1 - \log\left(\frac{r}{L}\right)\left[(\beta^2 - 1)r'^2 + (4\beta^2 - 1)rr'' + \frac{\beta^2 r^2 r'''}{r'}\right]\right\} \tag{58}$$

The first order approximation is again given by the simple Eq. (44), showing that Munk's[9] expression for the transverse force distribution is a valid first order approximation for supersonic, subsonic, or incompressible flow. Eq. (58) is valid only for sharp nose bodies of revolution of such small fineness ratio that Eq. (57) gives a suitable approximation to the axial flow surface pressures. Eq. (52) is valid even for a rounded nose body of revolution, but the same cannot be said of Eqs. (57) and (58), which give erroneous results for these cases. However, it may easily be shown that the exact expression for the incompressible potential flow about a prolate spheroid is given by

$$F_x/q = 4\pi\alpha\, rr'/(1 + r'^2) \tag{59}$$

In reference 13 it is shown that Eq. (59) is in excellent agreement with the transverse force distribution on arbitrary rounded nose bodies of revolution even at rather large angles of attack.

Fig. 7 compares the transverse force distributions given by Eqs. (44), (58), and (59) with the experimental values, also used in reference 13, for a typical dirigible shape at an angle of attack of 10° and a β value of approximately unity. It is seen that Eq. (59) gives a good approximation for the transverse force distribution as long as there is potential flow with no separation. Eq. (59) should be used for all subsonic flow computations, and perhaps the effects of compressibility could be estimated by using Eq. (58) as a ratio correction, although Eq. (58) is rigorously valid only for incompressible flow ($\beta = 1$) since the axial and transverse flows have different Mach Numbers for $\beta < 1$. In a real viscous fluid the flow will separate and not follow a closed trailing-edge contour; therefore, if the wake shape is known, a much better approximation may be obtained by using this wake shape as the aft portion of the body contour. If Eq. (59) is applied to the wake shape shown in Fig. 7, it will give values that are in close agreement with the experimental data.

For supersonic flow, however, as previously mentioned, only Eq. (44) should be used as a rigorously valid approximation. Eq. (44) shows that a body of revolution with a closed trailing edge ($A = 0$) will have no lift but still have an unstable pitching moment. Of course, the actual wake existing in a real viscous fluid will tend to produce a lift increment. If the cross-sectional area of the wake is taken as A, Eq. (47) should give results agreeing with the experimental data.

It is easily shown that Eqs. (49) and (50) also apply for a slender sharp nose body of revolution having a pitching velocity in subsonic flow, at least for β values considerably greater than zero. Munk[9] has shown how Eq. (49) may be modified by the apparent mass

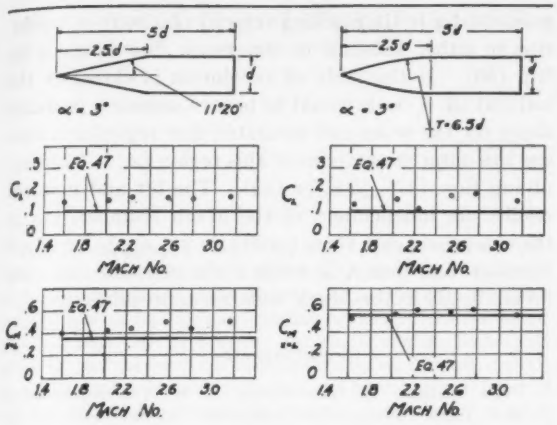

FIG. 4.

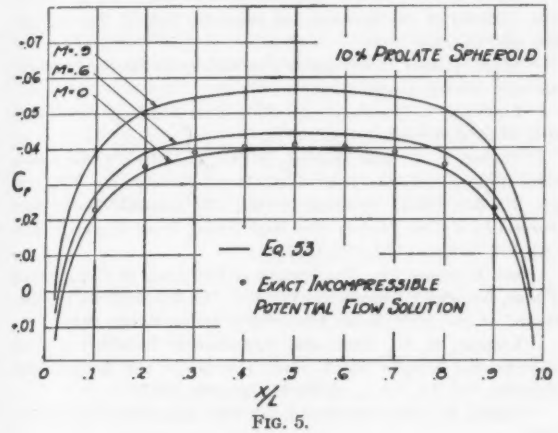

FIG. 5.

moment of inertia in order to approximate the transverse force distribution for a rounded nose body of revolution. However, for a body of revolution that is closed—that is, rounded or pointed at both ends—the resulting lift and moment of Eq. (49) will always vanish so that all the terms of Eq. (50) are zero for this case. However, the actual wake existing in a real viscous fluid will again modify these results, and an agreement with the experimental data should be made possible by taking A as the cross-sectional area of the wake at the trailing edge.

DISCUSSION

It is interesting to note that only in the two-dimensional supersonic flow solution is the wake behind the closed body eliminated; that is, in a theoretical nonviscous, compressible fluid the flow behind the trailing edge of a two-dimensional airfoil immediately resumes the free stream direction and static pressure (if it is assumed that the shock waves are so weak that the change in entropy may be neglected, as would be true for a slender sharp nose airfoil at small angles of attack[7]). Jones[14] has shown that a body of revolution in supersonic flow has a wake similar to that which it has in subsonic flow. This may be shown by writing Eqs. (16) and (51) for $r = 0$ as

$$\left.\begin{aligned} C_p &= -\frac{2\Delta u}{u_\infty} = \frac{1}{\pi}\int_0^L \frac{S'(\xi)d\xi}{(x-\xi)^2} (\text{for } M>1,\ x>L) \\ &= \frac{1}{2\pi}\int_0^L \frac{S'(\xi)d\xi}{(x-\xi)^2} (\text{for } M<1,\ x>L \text{ or } x<0) \end{aligned}\right\} \quad (60)$$

This shows that the supersonic wake is identical to the subsonic wake and has exactly twice the pressure difference, and both the subsonic and supersonic wake pressure coefficients are independent of the Mach Number to the first order. The integration of Eq. (60) along the axis either ahead of, or behind, the body is, of course, rigorously valid for the case of incompressible flow ($\beta = 1$). By analytical continuity the subsonic case should also be valid, at least for $M << 1$. Although there may be some doubt as to the validity of applying this procedure to supersonic flow, still

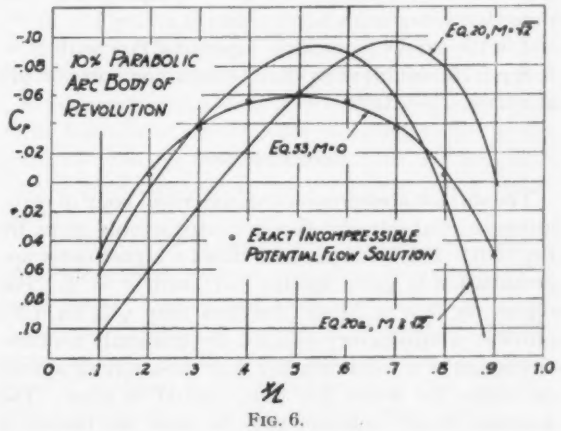

FIG. 6.

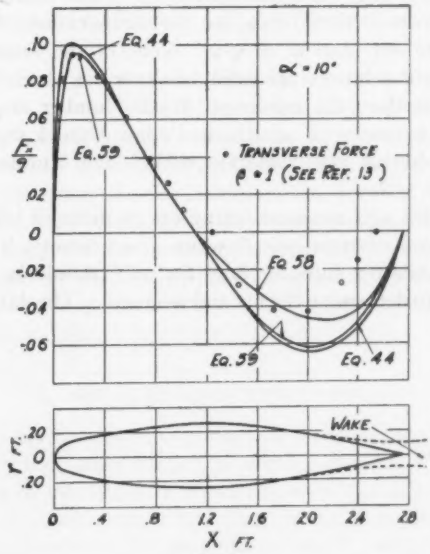

FIG. 7.

from physical considerations the integral of Eq. (60) seems to be valid. The two-dimensional supersonic flow, of course, has no wake if the flow is isentropic throughout, because, as shown in reference 7, the pressure depends only on the angle between the slope of the local velocity vector relative to the free stream direction.

It should also be noted that theoretically an ordinary stagnation point occurs at a sharp trailing edge in each case except that of the two-dimensional supersonic flow. Of course, the equations presented give an infinite negative velocity increment at the trailing edge, but this only occurs because the points (0, 0) and (L, 0) are singular points that should only be approached, never actually reached. For example, if a symmetrical parabolic arc is taken as the body profile, it will be found that, in the two-dimensional subsonic flow with $\beta \approx 1$, the equation in reference 3 or 15 for the source distribution representing the parabolic arc gives a stagnation point at $x/c \approx 1 - 10^{-4}$; in the axially symmetric subsonic flow with $\beta \approx 1$, Eqs. (51) or (53) show that a stagnation point occurs at $x/L \approx 1 - 10^{-11}$; and in the axially symmetric supersonic flow with $B \approx 1$, Eqs. (16) or (20) show that a stagnation point occurs at $x/L \approx 1 - 10^{-6}$.

Conclusions

The surface pressures on a symmetrical body of revolution in axial subsonic flow are satisfactorily given by Eq. (53). For incompressible flow, a higher order approximation is given by Eq. (51) with $\beta = 1$. For supersonic flow at Mach Numbers near $\sqrt{2}$, Eq. (20) provides a satisfactory solution for uniformly continuous bodies of revolution other than those having a conical shape, for which Eq. (20a) should be used. The Kármán-Moore[1] solution may be used for bodies of revolution that have discontinuities in the derivatives of the cross-sectional area, but the computations should be made only for $M \approx \sqrt{2}$. None of the linearized supersonic solutions are valid, however, for Mach Numbers less than the minimum Mach Number required for the existence of an attached conical shock wave or for predicting any variation with Mach Number for $M >> \sqrt{2}$.

The lift and moment acting on an inclined body of revolution in supersonic flow are given directly by Eq. (47), while for subsonic flow Eq. (59) should be integrated to determine the lift and moment. The damping moment due to the pitching velocity of a body of revolution in either subsonic or supersonic flow is given by Eq. (50). If the body of revolution is closed at the tail end ($A = 0$), it would be best to assume a probable shape for the wake and separated flow region and then use the outer streamlines of this region ($A > 0$) in applying Eqs. (47), (50), or (59). The lift and moment results are independent of the Mach Number, but in the supersonic case these results do not apply for Mach Numbers less than $\sqrt{2}$, while in the subsonic case they do not apply as the Mach Number approaches unity.

References

[1] von Kármán, Th., and Moore, N. B., *The Resistance of Slender Bodies Moving with Supersonic Velocities with Special Reference to Projectiles*, Trans. A.S.M.E., Vol. 54, pp. 303–310, 1932.

[2] Tsien, H., *Supersonic Flow over an Inclined Body of Revolution*, Journal of the Aeronautical Sciences, Vol. 5, No. 12, pp 480–484, October, 1938.

[3] Sauer, Robert, *Theoretische Einführung in die Gasdynamik*; Springer-Verlag, Berlin, 1943.

[4] Lighthill, M. J., *Supersonic Flow Past Bodies of Revolution*, R & M 2003, British A.R.C., 1945.

[5] Taylor, G. I., and Maccoll, J. W., *The Air Pressure on a Cone Moving at High Speeds*, Proc. Royal Society (A), Vol. 139, pp. 278–298, 1933. Maccoll, J. W., *The Conical Shock Wave Formed by a Cone Moving at a High Speed*, Proc. Royal Society (A), Vol. 149, pp. 459–472, 1937.

[6] von Kármán, Th., *The Problem of Resistance in Compressible Fluids*, Atti dei V Convegno "Volta": "Le alte velocita in aviazione," p. 267, 1936, Reale Academia D'Italia, Rome, 1936.

[7] Laitone, E. V., *Exact and Approximate Solutions of Two-Dimensional Oblique Shock Flow*, Journal of the Aeronautical Sciences, Vol. 14, No. 1, pp. 25–41, January, 1947.

[8] Lamb, H., *Hydrodynamics*, 6th Ed., page 524; Cambridge, 1932.

[9] Munk, Max M., *The Aerodynamic Forces on Airship Hulls*, N.A.C.A. T.R. No. 184, 1923.

[10] Ferrari, C., *Campi di Corrente Ipersonora Attorno a Solidi di Revolusione*, L'Aerotecnica, Vol. 17, pp. 507–518, 1937.

[11] Ferri, Antonio, *Supersonic-Tunnel Tests of Projectiles in Germany and Italy*, N.A.C.A., L5H08, October, 1945.

[12] Laitone, E. V., *The Subsonic Axial Flow About a Body of Revolution*, Quarterly of Applied Mathematics, Vol. 5, No. 2, pp. 227–231, July, 1947.

[13] Upson, R. H., and Klikoff, W. A., *Application of Practical Hydrodynamics to Airship Design*, N.A.C.A. T.R. No. 405, 1931.

[14] Jones, R. T., and Margolis, Kenneth, *Flow Over a Slender Body of Revolution at Supersonic Velocities*, N.A.C.A. T.N. No. 1081, 1946.

[15] Laitone, E. V., *The Subsonic and Supersonic Flow Fields of Slender Bodies*, paper presented at the 6th International Congress for Applied Mechanics at Paris, September, 1946.

The Dynamics of a Swept Wing

H. R. LAWRENCE*
Northrop Aircraft, Inc.

SUMMARY

It is assumed that a swept wing may be represented dynamically by a plane curved rod of variable cross section with finite stiffness in torsion and in bending normal to its plane. The equations of motion for this configuration are exhibited with the restriction that the curvature of the elastic axis be finite. By allowing the curvature to become infinite at a point, certain auxiliary conditions are obtained at the bend. The validity of this limiting process is examined from the physical point of view. A wing with an elastic axis consisting of a plane broken line of $(n+1)$ segments is denoted as an "n bend wing." A method is developed for calculating the natural frequencies and modes of a single bend wing. Formulas for the natural frequencies and modes of a free-free symmetric single bend uniform rod are obtained. A generalized type of orthogonality condition between the modes of a single bend wing is proved. Based on these results, formulas are developed for the dynamic response of a single bend wing to a general system of forces. A method of generalizing the above results for a single bend wing to the n bend wing is indicated. The use of an n bend wing as an approximate representation of a wing of continuous curvature is discussed.

NOTATION

$2b$ = length of rod measured along elastic axis
B = bending stiffness of wing
C = torsional stiffness of wing
e = r-coordinate of section center of gravity
f = external running shear load
F = external concentrated shear load applied at $s = a$
g = external running torque
G = external concentrated torque applied at $s = a$
J_0 = mass moment of inertia per unit span about section center of gravity
J = same about section elastic axis
m = mass per unit span
M = internal bending moment
$\bar{M}$ = external concentrated bending moment applied at $s = a$
O = see Eq. (16)
r = distance measured normal to elastic axis
s = distance measured along elastic axis
t = time variable
S = internal shear
T = internal torque
$\bar{T}$ = kinetic energy
u = vertical displacement at any point
v = vertical displacement at the elastic axis
V = potential energy
x, y, z = Cartesian coordinates
α = angle of sweep
β = angle of twist
μ = (B/C) at a bend in the elastic axis

The subscripts m, n denote integers in the following symbols:

$A_{mn} = B_{mn}$ = see Eq. (32)
C_n = see Eq. (29)
H_n = see Eq. (39)
k_n^4 = mw_n^2/B for uniform beam
l_n^2 = Jw_n^2/C for uniform beam
P_n = bending displacement of uniform beam in nth mode
Q_n = angle of twist of uniform beam in nth mode
w_n = natural frequency of nth mode of uniform beam
φ_n = bending displacement of nonuniform beam in nth mode
ψ_n = angle of twist of nonuniform beam in nth mode
λ_n = natural frequency of nth mode of nonuniform beam
Γ_{mn} = see Eqs. (35) and (41)
σ_n = see Eq. (48)
ξ_n = see Eq. (47)

NOTE: The subscripts s and t are used to denote partial differentiation.

Presented at the Structures Session, Fifteenth Annual Meeting, I.A.S., New York, January 28–30, 1947. Revised and received April 24, 1947.

* Staff Assistant to Chief of Aerodynamics.

INTRODUCTION

THE USE OF WINGS with large sweep has in the past been restricted to airplanes of the flying-wing type. With the advent of airplanes designed to fly in the transonic and supersonic régimes, the highly swept wing appears destined to become of increasing importance.

The problem of calculating the dynamic response of an airplane with a swept wing may be considered in three parts. First, a simplified model of the structure is chosen. Second, a method of calculating the dynamic response of the simplified model is developed. Finally, evidence is assembled to show that the simplified model represents the airplane dynamically.

In the case of an unswept wing, the two most frequently used models are: (1) a set of spring-connected masses and (2) a rod of variable cross section.

A generalization of the second dynamic model noted above to a swept wing is the subject of this paper.

It is assumed that a swept wing may be represented dynamically by a rod of variable density and cross section possessing an elastic axis in the form of a plane curve. Only loads and moments normal to the plane containing the elastic axis are considered. The fuselage and nacelles are considered as affecting the mass and stiffness characteristics of the wing without introducing additional degrees of freedom.

I. GENERAL EQUATIONS OF MOTION

It is convenient to consider first a rod whose greatest diameter of cross section is small compared with the radius of curvature of its elastic axis. It is assumed that the dimensions of the wing normal to a plane containing its elastic axis are small so that the wing may be

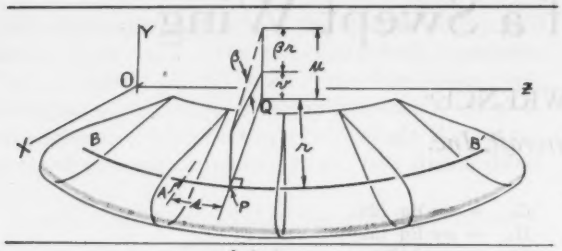

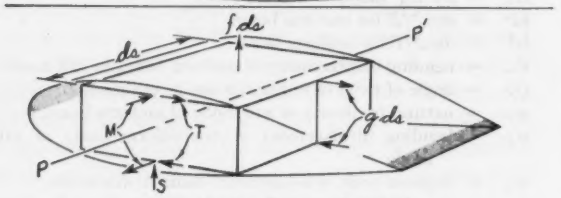

FIG. 1a (top). FIG. 1b (bottom).

treated geometrically as a plane figure containing an elastic axis. The elastic axis BAPB′ is shown in Fig. 1a lying in the plane OXZ.

It is evident from the figure that any point on the undistorted wing may be specified uniquely in terms of the coordinates s and r. Let u represent the displacement of a point Q in the $\overrightarrow{OY}$ direction. If v represents the displacement of the point P in the direction $\overrightarrow{OY}$ and β represents the rotation of the line PQ about the elastic axis at the point P, then $u = v + r\beta$.

Consider a typical slice of the wing taken normal to the elastic axis as illustrated in Fig. 1b. The line PP′ is the elastic axis where BP < BP′. The external loads are represented by a load per unit span f and a torque per unit span g. The internal elastic forces are represented by a shear S, torque T, and bending moment M.

The equations expressing the internal elastic moments in terms of the deformations of the structure may be written[1] as follows:

$$\left.\begin{aligned} M &= B(v_{ss} - \beta/\rho) \\ T &= C(\beta_s + v_s/\rho) \\ S &= -M_s \end{aligned}\right\} \qquad (1)$$

where B and C represent the bending and torsional stiffness, ρ represents the radius of curvature of the elastic axis in its plane, and subscripts are employed to denote partial differentiation.

The equations of motion will be deduced from Hamilton's Variational Principle. By using this procedure the proper end conditions are obtained in a purely mechanical fashion. The kinetic energy T and the potential energy V must be expressed in terms of the mass, stiffness, and geometric parameters.

It is evident that the kinetic energy of a slice of the beam, made by planes normal to the elastic axis and a distance ds apart measured along the elastic axis, is given by the expression

$$d\bar{T} = {}^1/_2[m(v_t + e\beta_t)^2 + J_0\beta_t^2]ds$$

where m is the mass per unit span, e is the r-coordinate of the center of gravity of the slice, and J_0 represents the mass moment of inertia per unit span of the slice about its center of gravity. Upon integrating over the span and defining J as the mass moment of inertia per unit span about the elastic axis, the kinetic energy may be written as

$$\bar{T} = {}^1/_2\int_l^{l'} [mv_t^2 + 2mev_t\beta_t + J\beta_t^2]ds \qquad (2)$$

The potential energy V may be written as the sum of two parts. Let V_1 represent the elastic energy and V_2 represent the potential energy of the external forces. The internal potential energy may be written in the familiar form of

$$V_1 = {}^1/_2\int_l^{l'} [(M^2/B) + (T^2/C)]ds \qquad (3)$$

where M and T are expressed in terms of displacements by means of Eq. (1).

The potential energy of the external forces may be expressed in the form

$$V_2 = -\int_l^{l'}(vf + \beta g)ds \qquad (4)$$

Hamilton's principle states that the integral A between arbitrary fixed limits t_0, t_1 where

$$A = \int_{t_0}^{t_1} (\bar{T} - V)dt$$

is an extremum for the motion or $\delta A = 0$.

Upon performing the variational process and collecting terms, the following equations are obtained:

$$\left.\begin{aligned} mv_{tt} + me\beta_{tt} &= -M_{ss} + (T/\rho)_s + f, \quad l < s < l' \\ mev_{tt} + J\beta_{tt} &= T_s + (M/\rho) + g, \quad l < s < l' \end{aligned}\right\} \qquad (5)$$

$$\left.\begin{aligned} M\delta v_s &= 0 \\ [S + (T/\rho)]\delta v &= 0 \\ [T - (M/\rho)\delta\beta &= 0 \end{aligned}\right\} \quad \text{at each end of the beam} \qquad (6)$$

II. The Effects of a Bend

The equations of motion obtained in Part I are valid only when the radius of curvature of the elastic axis is large compared with the largest diameter of the beam cross section. The effects of a vanishing radius of curvature are investigated first from the purely formal point of view. The general validity of the results so obtained will be considered later. A bend in the rod axis is considered as the limiting case of a circular arc. Fig. 2 represents the geometry of the elastic axis in the neighborhood of a point of large curvature.

The segments B′A′ and AB are straight lines whereas the segment A′OA′ represents a circular arc of radius a. The equations of motion valid over B′OB may be written from Eq. (5) as follows:

$$\left.\begin{aligned} mv_{tt} + me\beta_{tt} &= S_s + (T/\rho)_s + f \\ mev_{tt} + J\beta_{tt} &= T_s + (M/\rho) + g \end{aligned}\right\} \qquad (7)$$

The first equation is multiplied by ds and integrated from B′ to B; thus,

$$[S + (T/\rho)]\,\Big|_{B'}^{B} = \int_{B'}^{B} (mv_{tt} + me\beta_{tt} - f)ds$$

or noting that $\rho = \infty$ at B and B′ and defining S_1 and S_0 as the shear at B and B′, respectively,

$$S_1 - S_0 = \int_{B'}^{B} (mv_{tt} + me\beta_{tt} - f)ds$$

If the points B $\rightarrow$ A and B′ $\rightarrow$ A′ while $a \rightarrow 0$, the length of the path of integration approaches zero. Since the integrand is assumed to be finite

$$S_1 = S_0 \tag{8}$$

Consider the equations of motion on the arc A′OA. The integration of the first of Eqs. (7) may be written as

$$-M_s + (T/\rho) = \int_0^s (mv_{tt} + me\beta_{tt} - f)ds + \text{const.}$$

or in polar coordinates

$$-M_\theta + T = a^2 \int_0^\theta (mv_{tt} + me\beta_{tt} - f)d\theta + (a) \times (\text{const.})$$

Since both the constant and the integrand are assumed to be finite, the limit of the above equation as $a \rightarrow 0$ is

$$-M_\theta + T = 0 \tag{9}$$

In the same way the second equation may be written as $a \rightarrow 0$ in the form:

$$T_\theta + M = 0 \tag{10}$$

if $(mev_{tt} + J\beta_{tt})$ is finite.

Let M_0, T_0, and M_1, T_1 represent, respectively, the values of M and T at $\theta = -\alpha$ and $\theta = \alpha$. Eqs. (9) and (10) may be integrated to obtain M and T in terms of two arbitrary constants; thus,

$$\left.\begin{aligned} T &= -A_1 \sin\theta + A_2 \cos\theta \\ M &= A_1 \cos\theta + A_2 \sin\theta \end{aligned}\right\} \tag{11}$$

Upon substituting the values of T and M at $\theta = -\alpha$ and $\theta = \alpha$ in Eqs. (11), four equations are obtained. Upon eliminating the two arbitrary constants A_1 and A_2, the following boundary conditions at a bend are found:

$$\left.\begin{aligned} (T_1 + T_0)\sin\alpha - (M_1 - M_0)\cos\alpha &= 0 \\ (T_1 - T_0)\cos\alpha + (M_1 + M_0)\sin\alpha &= 0 \end{aligned}\right\} \tag{12}$$

Eqs. (1) may be used to obtain two additional boundary conditions at a bend as follows. On the arc A′OA, Eqs. (1) may be written in polar coordinates as follows:

$$\left.\begin{aligned} -(dv_s/d\theta) + \beta &= -(aM/B) \\ (d\beta/d\theta) + v_s &= a(T/C) \end{aligned}\right\} \tag{13}$$

As $a \rightarrow 0$, the right-hand members of the above equations approach zero, since M/B and T/C are assumed to be finite. Let v_s and β be, respectively, v_{s_0}, β_0 and v_{s_1}, β_1 at $\theta = -\alpha$ and $\theta = +\alpha$.

Then Eqs. (13), with the right-hand sides equal to zero and the special values at $\theta = \pm\alpha$, are identical with Eqs. (9) and (10) under the substitutions $v_s \rightarrow M$ and $\beta \rightarrow T$. Hence, the following boundary conditions are obtained:

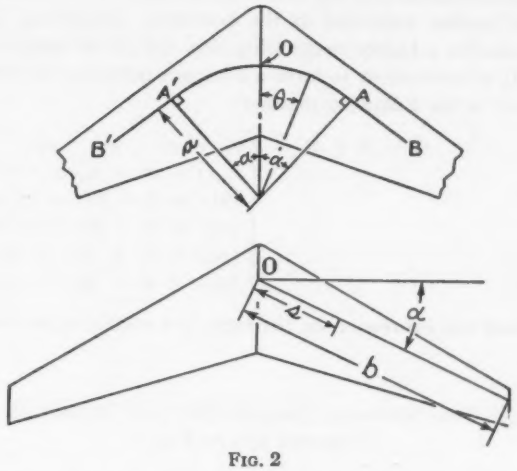

FIG. 2

$$\left.\begin{aligned} (\beta_1 + \beta_0)\sin\alpha - (v_{s_1} - v_{s_0})\cos\alpha &= 0 \\ (\beta_1 - \beta_0)\cos\alpha + (v_{s_1} + v_{s_0})\sin\alpha &= 0 \end{aligned}\right\} \tag{14}$$

The second Eqs. (13) may be transformed into the form:

$$dv/d\theta = a^2(T/c) - a(d\beta/d\theta)$$

Upon integrating with respect to θ, allowing a to approach zero, and defining v_1 and v_0 as the values of v at $= -\theta$ and θ, respectively, there results

$$v_1 = v_0 \tag{15}$$

providing T/C and $\beta_1 - \beta_0$ are not infinite.

Thus, the Eqs. (8), (12), (14), and (15) give six conditions connecting the loads and deformations on the opposite sides of a bend in the elastic axis. The equations fall into two sets of three. One set is independent of the elastic properties of the system. This set, Eqs. (14) and (15), may be interpreted simply as conditions of continuity of the beam elastic axis. The second set, Eqs. (8) and (12), represent the equilibrium between the shears and moments acting on the sides of the bend. In order to evaluate Eq. (12) in terms of the deformations of the beam, it is necessary to know the ratio $B/C = \mu$ at the bend. The theory of elasticity as employed herein is not adequate to produce this ratio, since its assumptions have been violated. On the other hand, it is evident physically that this ratio exists, since one can imagine an experiment that would yield it. Although the author is unable to prove that the only effect of allowing an infinite curvature of the elastic axis is to produce an undetermined elastic constant, results of calculations seem to support such a view.

It is evident that any wing elastic axis may be approximated by a set of straight-line segments meeting at bends. The simplification results from the fact that a differential equation with variable coefficients such as Eqs. (5) is replaced by an equation with con-

stant coefficients at the cost of more involved boundary conditions. The complicated coupling between bending and torsion exhibited in the boundary conditions, Eqs. (12) and (14), indicates that the use of uncoupled modes for a highly swept wing may not prove satisfactory.

It is convenient to have a compact notation for the boundary conditions at a bend. The operator O is defined in the following manner:

$$O(v, \beta, s, \mu) = \begin{bmatrix} v(s+o) - v(s-o) \\ v_{sss}(s+o) - v_{sss}(s-o) \\ [\beta(s+o) + \beta(s-o)] \sin\alpha - [v_s(s+o) - v_s(s-o)] \cos\alpha \\ [\beta(s+o) - \beta(s-o)] \cos\alpha + [v_s(s+o) + v_s(s-o)] \sin\alpha \\ [\beta_s(s+o) + \beta_s(s-o)] \sin\alpha - [\mu(s)][v_{ss}(s+o) - v_{ss}(s-o)] \cos\alpha \\ [\beta_s(s+o) - \beta_s(s-o)] \cos\alpha + [\mu(s)][v_{ss}(s+o) + v_{ss}(s-o)] \sin\alpha \end{bmatrix} \tag{16}$$

where the expression on the right is a matrix of six rows and one column.

III. The Natural Frequencies and Modes of a Uniform Swept Rod

An analytic solution is obtained for the natural frequencies and modes of a uniform free-free rod with a bend at the centerline. This solution exhibits the form of the results obtained by use of the bend boundary conditions. It is also useful in the calculation of the modes and natural frequencies of a free-free swept wing.

The geometry of the configuration under consideration is illustrated in Fig. 3. The differential equations and boundary conditions may be written

$$\left.\begin{aligned} &mv_{tt} + Bv_{ssss} = 0, \qquad (-b < s < b) \\ &J\beta_{tt} - C\beta_{ss} = 0, \qquad (-b < s < b) \\ &v_{ss} = v_{sss} = \beta_s = 0 \text{ at } s = \pm b \\ &O(v, \beta, 0, \mu) = 0 \end{aligned}\right\} \tag{17}$$

Upon performing the substitutions for v and β,

$$\left.\begin{aligned} v &= Pe^{iwt} \\ \beta &= Qe^{iwt} \end{aligned}\right\} \tag{18}$$

in Eqs. (17), there results

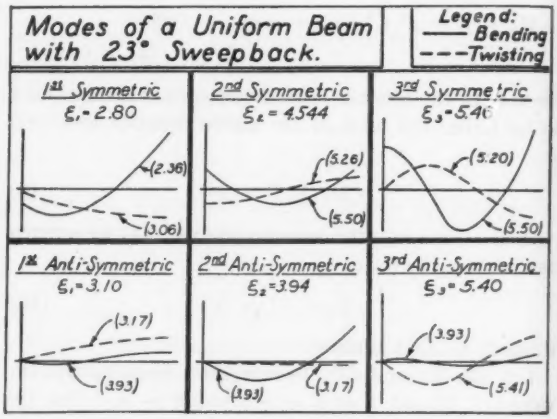

Fig. 3.

$$\left.\begin{aligned} &P_{ssss} - k^4 P = 0, \qquad (-b < s < b) \\ &Q_{ss} + l^2 Q = 0, \qquad (-b < s < b) \\ &P_{sss} = P_{ss} = Q_s = 0 \text{ at } s = \pm b \\ &O(P, Q, 0, \mu) = 0 \end{aligned}\right\} \tag{19}$$

where $k^4 = mw^2/B$ and $l^2 = Jw^2/C$.

For certain discrete values of $w = w_n$, the above equations have solutions P_n, Q_n. The values of w_n are the coupled natural frequencies of the system, whereas the functions P_n, Q_n together form a coupled mode of vibration. The displacement u of any point on the wing in the nth mode is given in r,s-coordinates by the expression $u = P_n(s) + rQ_n(s)$.

The solution of Eqs. (19) shows that the symmetric and antisymmetric modes may be considered independently. With k_n and l_n corresponding to the frequency w_n, the solutions may be written as follows:

Symmetric Modes

Case I.—$w_{-1} = w_0 = 0$.

$$P_{-1} = 1, \qquad Q_{-1} = 0 \tag{20}$$

$$\left.\begin{aligned} P_0 &= s, \qquad Q_0 = \cot\alpha, \qquad s > 0 \\ P_0' &= -s, \qquad Q_0' = \cot\alpha, \qquad s < 0 \end{aligned}\right\} \tag{21}$$

Case II.—$w_n \neq 0$, then w_n may be evaluated from the frequency equation:

$$\frac{k_n(1 - \cos k_n b \cosh k_n b)}{\sin k_n b \cosh k_n b + \cos k_n b \sinh k_n b} + \mu \cot^2\alpha \times l_n \tan l_n b = 0 \tag{22}$$

and the mode P_n, Q_n is given by the formulas:

$$\left.\begin{aligned} P_n &= \frac{(1 - \cos k_n b \cosh k_n b)(\cosh k_n s + \cos k_n x) - \sin k_n b \sinh k_n b(\cosh k_n x - \cos k_n x)}{\sin k_n b \cosh k_n b + \cos k_n b \sinh k_n b} + \\ &\qquad \sin k_n x + \sinh k_n x \\ Q_n &= 2k_n(\cot \alpha/\cos l_n b) \cos l_n(b - s) \end{aligned}\right\} \tag{23}$$

Antisymmetric Modes

Case I.—$w_0 = 0$.

$$\left.\begin{aligned} P_0 &= s, \quad Q_0 = -\tan \alpha \\ &= s, \quad Q_0 = \tan \alpha \end{aligned}\right\} \quad \begin{aligned} s &> 0 \\ s &< 0 \end{aligned} \tag{24}$$

Case II.—$w_n \neq 0$. The frequency equation is:

$$\frac{k_n(\sin k_n b \cosh k_n b + \cos k_n b \sinh k_n b)}{1 + \cos k_n b \cosh k_n b} + \mu \tan^2 \alpha \times l_n \tan l_n b = 0 \tag{25}$$

and the modes are:

$$\left.\begin{aligned} P_n &= \frac{\sin k_n b \cosh k_n b\,(\cosh k_n s - \cos k_n s) - \cos k_n b \sinh k_n b\,(\cosh k_n s + \cos k_n s)}{1 + \cos k_n b \cosh k_n b} + \\ &\qquad \frac{(1 + \cos k_n b \cosh k_n b)(\sinh k_n s + \sin k_n s) - \sin k_n b \sinh k_n b\,(\sinh k_n s - \sin k_n s)}{1 + \cos k_n b \cosh k_n b} \\ Q_n &= -2k_n(\tan \alpha/\cos l_n n) \cos l_n(b - s) \end{aligned}\right\} \tag{26}$$

A plot of the first three modes for particular values of the stiffness parameters is given in Fig. 4.

It is evident that an analytic expression for the natural frequencies and modes of a uniform swept rod with any set of homogeneous end conditions may be obtained.

IV. The Natural Frequencies and Modes of a Swept Wing

A method is developed for calculating the natural frequencies and modes of a free-free swept wing. It will be noted that the same procedure is applicable to other end conditions with only minor modifications.

The configuration geometry is again illustrated by Fig. 3. The differential equation and boundary conditions may be written as follows:

$$\left.\begin{aligned} mv_{tt} + me\beta_{tt} &= -(Bv_{ss})_{ss}, \qquad (-b < s < b) \\ mev_{tt} + J\beta_{tt} &= (C\beta_s)_s, \qquad (-b < s < b) \end{aligned}\right\} \tag{27}$$

$$(Bv_{ss})_s = (Bv_{ss}) = C\beta_s = 0 \text{ at } s = \pm b$$

$$O(v, \beta, 0, \mu) = 0$$

or with

$$v = e^{\mu t} \varphi(s)$$
$$\beta = e^{\mu t} \psi(s)$$

$$\left.\begin{aligned} (B\varphi_{ss})_s &= \lambda^2(m\varphi + me\psi), \qquad (-b < s < b) \\ (C\psi_s)_s &= -\lambda^2(me\varphi + J\psi), \qquad (-b < s < b) \\ (B\varphi_{ss})_s &= B\varphi_{ss} = C\beta_s = 0 \text{ at } s = \pm b \\ O(\varphi, \psi, 0, \mu) &= 0 \end{aligned}\right\} \tag{28}$$

Eqs. (28) are of the generalized Sturm-Liouville type. The following results concerning such systems may be borrowed from the mathematical literature:[2]

(1) There exists a denumerably infinite set of eigenvalues or natural frequencies λ_n such that $\lambda_n \leqq \lambda_{n+1}$ for all n.

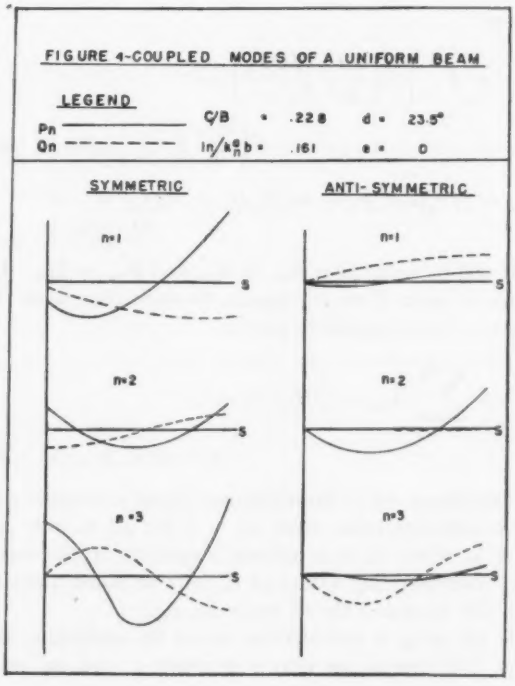

(2) Corresponding to each value λ_n there exists an eigenfunction or mode (φ_n, ψ_n).

(3) The eigenfunctions or modes form a complete set of functions.

Upon applying the above theorems to Eqs. (19) and noting that (P_n, Q_n) and (φ, ψ) satisfy the same boundary conditions, the following result may be stated. The function φ and ψ may be represented in the form:

$$\left.\begin{aligned}\varphi(s) &= \sum_{n=0}^{N} C_n P_n(s)\\ \psi(s) &= \sum_{n=0}^{N} C_n Q_n(s)\end{aligned}\right\} \tag{29}$$

where the C_n are independent of s. By choosing N sufficiently large, the above representations of φ and ψ may be made as accurate as required, providing all the modes of frequency less than λ_N are used.

Although the functions (P_n, Q_n) are seen to be a satisfactory means of representing (φ, ψ) from the mathematical standpoint, they are by no means unique in this respect. An additional argument for their use lies in the fact that (P_n, Q_n) and (φ, ψ) satisfy twelve boundary conditions in common.

The differential equations of Eqs. (28) may be shown to be equivalent to the problem of determining an extremum of the expression

$$L = {}^1/_2 \int_{-b}^{b}(B\varphi_{ss}^2 + C\psi_s^2)ds - {}^1/_2\lambda^2 \int_{-b}^{b}(m\varphi^2 + 2me\varphi\psi + J\psi^2)\,ds \tag{30}$$

Upon substituting the expressions for φ and ψ from Eqs. (29) and (30), the following result is obtained:

$$L = {}^1/_2 \sum_{n=0}^{N}\sum_{m=0}^{N}(A_{mn} - \lambda^2 B_{mn})C_n C_m \tag{31}$$

where

$$\left.\begin{aligned}A_{mn} &= \int_{-b}^{b}\left[B\left(\frac{\partial^2 P_m}{\partial s^2}\right)\left(\frac{\partial^2 P_n}{\partial s^2}\right) + C\left(\frac{\partial Q_m}{\partial s}\right)\left(\frac{\partial Q_n}{\partial s}\right)\right]ds\\ B_{mn} &= \int_{-b}^{b}[mP_mP_n + me(P_mQ_n + P_nQ_m) + JQ_mQ_n]ds\end{aligned}\right\} \tag{32}$$

It will be noted that $A_{mn} = A_{nm}$ and $B_{mn} = B_{nm}$. In order to make L an extremum, its derivative with respect to C_n is equated to zero or

$$\frac{\partial L}{\partial C_m} = \sum_{n=0}^{N}(A_{mn} - \lambda^2 B_{mn})C_n = 0, \qquad m = 0, 1, 2 \ldots N \tag{33}$$

The above set of homogeneous linear equations will have solutions other than $C_n = 0$ for all n, only for $\lambda = \lambda_r$ where λ_r is a natural frequency of the wing. The corresponding values of C_n may be substituted in Eq. (29) to obtain the r^{th} mode (φ_r, ψ_r).

If the wing is symmetrical about its centerline, the Eqs. (33) break up into a symmetric and an antisymmetric set. In each case the range of integration of Eqs. (32) may be taken from zero to b. In considering the symmetric (antisymmetric) modes of the wing, only the symmetric (antisymmetric) modes of the uniform beam need be employed.

In the case of the antisymmetric modes, the A_{mn} and B_{mn} are calculated from the modes given by Eqs. (24) and (26). Since the terms $A_{m0} = 0$, the Eqs. (33) take the form:

$$\left.\begin{aligned}-\lambda^2\left(B_{00}C_0 + \sum_{n=1}^{N} B_{0n}C_n\right) &= 0\\ -\lambda^2 B_{m0}C_0 + \sum_{n=1}^{N}(A_{mn} - 2\,B_{mn})C_n &= 0\\ m &= 1, 2, \ldots N\end{aligned}\right\} \tag{34}$$

If $\lambda = 0$, there is a solution corresponding to the rigid body motion $C_0 = 1$ $C_n = 0$, $n \geq 1$.

If $\lambda \neq 0$, C_0 may be eliminated from Eqs. (34) and the equations may be written as

$$C_0 = -\sum_{n=1}^{N} B_{0n}C_n/B_{00} \tag{35}$$

$$\sum_{n=1}^{N}(A_{mn} - \lambda^2\,\Gamma_{mn})C_n = 0; \qquad m = 1, 2, \ldots N \tag{36}$$

$$\Gamma_{mn} = \frac{1}{B_{00}}\begin{vmatrix}B_{00} & B_{m0}\\ B_{0n} & B_{mn}\end{vmatrix} \tag{35.1}$$

Since the matrices $[A_{mn}]$ and $[\Gamma_{mn}]$ are nonsingular, Eqs. (36) may be solved by matrix iteration methods and C_0 may be determined by Eq. (35).

In the symmetric case, the A_{mn} and B_{mn} are calculated from Eqs. (20), (21), and (23). Since Eqs. (20) and (21) represent rigid body motions with zero frequency, $A_{-1,\,n} = 0$ and $A_{0,\,n} = 0$ for all n. Hence, the Eqs. (33) acquire the form:

$$-\lambda^2\left(B_{-1,\,-1}C_{-1} + B_{-1,\,0}C_0 + \sum_{n=1}^{N} B_{-1,\,n}C_n\right) = 0 \tag{37}$$

$$-\lambda^2\left(B_{0,\,-1}C_{-1} + B_{0,\,0}C_0 + \sum_{n=1}^{N} B_{0,\,n}C_n\right) = 0 \tag{38}$$

$$-\lambda^2\,(B_{m,\,-1}C_{-1} + B_{m0}C_0) + \sum_{n=1}(A_{mn} - \lambda^2 B_{mn})C_n = 0, \qquad m = 2, 3 \ldots \tag{39}$$

When $\lambda = 0$, there are two solutions corresponding to rigid body motions $C_{-1} = 1$, $C_0 = C_n = 0$ for all n, and $C_{-1} = 0$, $C_0 = 1$, $C_n = 0$ for all n.

When $\lambda \neq 0$, Eqs. (37) and (38) may be solved for C_{-1} and C_0:

$$\left.\begin{aligned}C_{-1} &= -\frac{\sum_{n=1}^{N}\begin{vmatrix}B_{00} & B_{-1,\,0}\\ B_{-1,\,n} & B_{0n}\end{vmatrix}}{\begin{vmatrix}B_{-1,\,-1} & B_{-1,\,0}\\ B_{0,\,-1} & B_{0,\,0}\end{vmatrix}}\\ C_0 &= -\frac{\sum_{n=1}^{N}\begin{vmatrix}B_{-1,\,-1} & B_{0,\,-1}\\ B_{-1,\,n} & B_{0n}\end{vmatrix}}{\begin{vmatrix}B_{-1,\,-1} & B_{0,\,-1}\\ B_{-1,\,0} & B_{00}\end{vmatrix}}\end{aligned}\right\} \tag{40}$$

Upon substituting the values of C_0 and C_1 from Eqs. (40) in Eqs. (39), the following result is obtained:

$$\left.\begin{aligned}\sum_{n=1}^{N}(A_{mn}-\lambda^2\Gamma_{mn})C_n &= 0\\ \Gamma_{mn} &= \frac{\begin{vmatrix} B_{-1,-1} & B_{-1,0} & B_{-1,n}\\ B_{0,-1} & B_{0,0} & B_{0,m}\\ B_{m,-1} & B_{m,0} & B_{m,n}\end{vmatrix}}{\begin{vmatrix} B_{-1,-1} & B_{-1,0}\\ B_{0,-1} & B_{00}\end{vmatrix}}\end{aligned}\right\} \tag{41}$$

Since the matrices $[A_{mn}]$ and $[\Gamma_{mn}]$ are nonsingular, Eqs. (41) may be solved by matrix iteration and the results may be substituted in Eqs. (40) to find C_0 and C_{-1}.

V. Dynamics of a Swept Wing

A method of calculating the response of a swept free-free wing to a system of time varying loads is developed in terms of coupled natural frequencies and modes. The procedure may be employed with only minor modification for most of the common end conditions. The geometry is illustrated in Fig. 3. The differential equations and boundary conditions may be written as follows:

$$\left.\begin{aligned} &mv_{tt}+me\beta_{tt}=-(Bv_{ss})_{ss}+f, \quad (-b<s<b)\\ &mev_{tt}+J\beta_{tt}=(C\beta_s)_s+g, \quad (-b<s<b)\\ &(Bv_{ss})_s=Bv_{ss}=C\beta_s=0 \quad \text{at } s=\pm b\\ &O(v,\beta,0,\mu)=0\end{aligned}\right\} \tag{42}$$

It is assumed that the natural frequencies and modes of the dynamical system are known. The differential equations satisfied by the modes may be written in matrix form as follows:

$$\begin{bmatrix}\{B(\varphi_n)_{ss}\}_{ss}\\ -\{C(\psi_n)_s\}_s\end{bmatrix}=\lambda_n^2\begin{bmatrix}m & me\\ me & J\end{bmatrix}\begin{bmatrix}\varphi_n\\ \psi_n\end{bmatrix} \tag{43}$$

Eq. (43) will be rewritten for the rth mode as follows:

$$\begin{bmatrix}\{B(\varphi_r)_{ss}\}_{ss}\\ \{-C(\psi_n)_s\}_s\end{bmatrix}=\lambda_r^2\begin{bmatrix}m & me\\ me & J\end{bmatrix}\begin{bmatrix}\varphi_r\\ \psi_r\end{bmatrix} \tag{44}$$

Upon multiplying Eq. (43) on the left by the matrix $[\varphi_r, \psi_r]$, multiplying Eq. (44) on the left by the matrix $[\varphi_n, \psi_n]$, and subtracting and integrating from $-b$ to b with respect to s, there results

$$\int_{-b}^{b}\left\{[\varphi_r,\psi_r]\begin{bmatrix}\{B(\varphi_n)_{ss}\}_{ss}\\ -\{C(\psi_n)_s\}_s\end{bmatrix}-[\varphi_n,\psi_n]\begin{bmatrix}\{B(\varphi_r)_{ss}\}_{ss}\\ -\{C(\psi_r)_s\}_s\end{bmatrix}\right\}ds=\lambda m^2\int_{-b}^{b}[\varphi_r,\psi_r]\begin{bmatrix}m & me\\ me & J\end{bmatrix}\begin{bmatrix}\varphi_n\\ \psi_n\end{bmatrix}ds-\lambda_r^2\int_{-b}^{b}[\varphi_n,\psi_n]\begin{bmatrix}m & me\\ me & J\end{bmatrix}\begin{bmatrix}\varphi_r\\ \psi_r\end{bmatrix}ds \tag{45}$$

By integrating by parts, the left member of the above equation may be shown to vanish if the following conditions hold:

$$\left.\begin{aligned}\varphi_r\times\{B(\varphi_n)_{ss}\}_s&=0 \quad \text{at } s=\pm b\\ B(\varphi_r)_s\times(\varphi_n)_{ss}&=0 \quad \text{at } s=\pm b\\ C\psi_r(\psi_n)_s&=0 \quad \text{at } s=\pm b\end{aligned}\right\}\text{for all } n \text{ and } r \text{ where } n\neq r$$

The above conditions are satisfied for most of the common end conditions. In the case of a free-free beam

$$(\varphi_n)_{ss}=[B(\varphi_n)_{ss}]_s=(\psi_n)_s=0$$

at $s=\pm b$; hence, the left-hand member of Eq. (45) vanishes; thus,

$$(\lambda_n^2-\lambda_r^2)\int_{-b}^{b}[\varphi_r,\psi_r]\begin{bmatrix}m & me\\ me & J\end{bmatrix}\begin{bmatrix}\varphi_n\\ \psi_n\end{bmatrix}ds=0 \tag{46}$$

If $\lambda_n\neq\lambda_r$, the integral of Eq. (43) must vanish or the modes (φ_n, ψ_n) must satisfy the orthogonality condition.

$$\int_{-b}^{b}[\varphi_r,\psi_r]\begin{bmatrix}m & me\\ me & J\end{bmatrix}\begin{bmatrix}\varphi_n\\ \psi_n\end{bmatrix}ds=\begin{cases}0, & (n\neq r)\\ \zeta_n, & (n=r)\end{cases} \tag{47}$$

From the results of the Sturm-Liouville type analysis discussed previously, the deformations v and β may be expressed in the form

$$\left.\begin{aligned}v(s)&=\sum_{n=0}^{N}\sigma_n(t)\varphi_n(s)\\ \beta(s)&=\sum_{n=}^{N}\sigma_n(t)\psi_n(s)\end{aligned}\right\} \tag{48}$$

Upon substituting Eqs. (48) for v and β in Eqs. (42) and making use of matrix notation, the result may be written:

$$\sum_{n=0}^{N} \ddot{\sigma}_n \begin{bmatrix} m & me \\ me & J \end{bmatrix} \begin{bmatrix} \varphi_n \\ \psi_n \end{bmatrix} = \sum_{n=0}^{N} \sigma_n \left[\begin{Bmatrix} -B(\varphi_n)_{ss} \}_{ss} \\ C(\psi_n)_s \}_s \end{Bmatrix} + \begin{bmatrix} f \\ g \end{bmatrix} \tag{49}$$

Multiplying Eq. (49) on the left by the matrix $[\varphi_r, \psi_r]$ and making use of the orthogonality condition [Eq. (46)] and Eq. (43), there is obtained:

$$\ddot{\sigma}_n \int_{-b}^{b} [\varphi_n, \psi_n] \begin{bmatrix} m & me \\ me & J \end{bmatrix} \begin{bmatrix} \varphi_n \\ \psi_n \end{bmatrix} = -\lambda_n^2 \sigma_n \int_{-b}^{b} [\varphi_n, \psi_n] \begin{bmatrix} m & me \\ me & J \end{bmatrix} \begin{bmatrix} \varphi_n \\ \psi_n \end{bmatrix} ds + \int_{-b}^{b} [\varphi_n, \psi_n] \begin{bmatrix} f \\ g \end{bmatrix} ds$$

or upon making use of the orthogonality condition [Eq. (47)],

$$\ddot{\sigma}_n + \lambda_n^2 \sigma_n = (1/\zeta n) \int_{-b}^{b} (\varphi_n f + \psi_n g) ds$$

Let

$$H_n(t) = (1/\zeta n) \int_{-b}^{b} (\varphi_n \times f + \psi_n g) ds \tag{50}$$

Then the above equation may be written:

$$\ddot{\sigma}_n + \lambda_n^2 \sigma_n = H_n(t) \tag{51}$$

If there is a small amount of damping in the system, it may be taken into account approximately at this point by replacing Eq. (51) by

$$\ddot{\sigma}_n + 2\gamma\lambda_n \dot{\sigma}_n + \lambda_n^2 \sigma_n = H_n(t) \tag{52}$$

where γ represents the fraction of critical damping. A solution of Eq. (52) such that $\sigma_n(0) = \dot{\sigma}_n(0) = 0$ is given approximately for small γ by the expression

$$\sigma_n(t) = \frac{1}{\lambda_n} \int_0^t H_n(\tau) e^{-\lambda_n \gamma (t-\tau)} \sin \lambda_n (t - \tau) d\tau \tag{53}$$

Upon substituting the value of σ_n from Eq. (53) in Eq. (48), the dynamic response of the wing to distributed torque and running shear may be calculated. In the case of a concentrated load $F(t)$ applied at a point $s = a$ on the span, the value of $H_n(t)$ is given by a limiting process as

$$H_n(t) = \varphi_n(a) F(t)/\zeta_n$$

Similarly, for a concentrated torque $G(t)$ applied at $s = a$,

$$H_n(t) = \psi_n(a) G(t)/\zeta_n$$

The case of a concentrated moment $M(t)$ applied at $s = a$ may be obtained by taking equal and opposite forces $\pm M(t)/2\epsilon$ applied at $a \pm \epsilon$ and going to the limit. The value of $H_n(t)$ becomes

$$H_n(t) = [M(t)/\zeta_n][d\varphi_n(a)/ds]$$

Conclusion

A method has been developed for calculating the natural frequencies, coupled modes of vibration, and the response of an airplane to an arbitrary time dependent set of loads. This method may be used directly to compute the dynamic loads due to landing[3] when the external forces are known. The flutter characteristics of an airplane may be investigated by an extension of the procedure.[4] The derivatives used in dynamic stability of airplane may be modified for wing flexibility by another extension.

The utility of the results obtained in this paper depend on the assumption that an airplane with a swept wing may be represented dynamically by a rod of varying cross section. The statement that a rod of variable cross section represents an airplane with a swept wing may be put more precisely in the following manner:

(1) The kinetic energy of the airplane may be represented by Eq. (2) by proper choice of mass parameters m, e. J.

(2) The strain energy of the airplane may be represented by Eq. (3) by proper choice of an elastic axis and stiffness coefficients B, C.

It is the opinion of the author that both of the above statements are true for many airplanes in an engineering sense. However, methods of calculating the position of the elastic axis and the coefficients B and C are not completely satisfactory.

References

[1] Love, A. E. H., *Mathematical Theory of Elasticity*, p. 381; Dover, 1944.

[2] Courant, R., and Hilbert, D., *Methods of Mathematical Physics*, Vol. I.

[3] Unpublished paper by Dr. A. Zahorski.

[4] Unpublished paper by Dr. W. Cox.

Fluid Dynamic Aspects of Axial-Flow Compressors and Turbines

JOHN R. WESKE*

Rensselaer Polytechnic Institute

SUMMARY

Pertinent facts of the two-dimensional theory of flow through blade grids are used to establish relationships for the three-dimensional flow through axial-flow blade rows. Certain aspects of flow in boundary layers and wakes encountered in blade rows are investigated qualitatively, particularly with regard to their effect upon operating characteristics. A criterion of stability of flow is proposed and defined mathematically.

SYMBOLS

D = diameter, ft.
Q = volume rate of flow, ft.^{3} per sec.
h = total head, ft.
h_s = static head, ft.
E = rate of total energy, ft.lbs. per sec.
c = absolute velocity, ft. per sec.
c_l = lift coefficient
l = chord, ft.
t = pitch, ft.
n = rotative speed, 1 per sec.
p = static pressure, lb. per sq.ft.
u = blade velocity, ft. per sec.
z = number of blades
γ = adiabatic exponent
Γ = circulation, sq.ft. per sec.
ω = angular velocity, 1 per sec.
ρ = mass density, lb. sec.^{2} per ft.^{4}
Δ = difference between conditions in plane 2 and plane 1
φ = $[Q/(\pi D^2/4)u]$ flow coefficient
ψ = $\Delta h/(u^2/2g)$ pressure coefficient
κ = h_s'/h coefficient of reaction

Subscripts: u is component parallel to u; 1 and 2 refer to conditions upstream and downstream, respectively; and T refers to tip diameter.

Superscripts $'$ and $''$ refer to the moving and fixed rows, respectively.

INTRODUCTION

ESTIMATES OF THE CAPACITY and efficiency of turbine and axial-flow compressor stages on the basis of the present two-dimensional blade grid theory lead to extremely high values. While corresponding test results have been improved greatly over earlier results, chiefly through the application of the two-dimensional theory, there still exists a large discrepancy between experimental and theoretical values which cannot be explained without consideration of factors relating to the three-dimensional nature of the flow, inherently neglected in the two-dimensional theory. It is expected that a better understanding of these three-dimensional effects will improve the correlation of theory and test and possibly lead to an extension of the present limits of capacity and attainable efficiency. To this end an attempt is made to analyze the flow through axial-flow blade rows of turbines and compressors, with particular consideration of three-dimensional effects.

Received May, 1947.

* Now with General Electric Company.

ENERGY TRANSFER

The problems to be considered center around the process of conversion of kinetic energy into shaft work, or vice versa. This process, although but one link in the chain of various states of energy, is next to the question of thermodynamic availability of energy the controlling factor influencing stage characteristics. It is primarily a flow process subject to the laws of fluid dynamics. Basic relations may be stated as follows: If the flow through a stage is assumed to be rotationally symmetrical, an element of this stage, bounded by two neighboring coaxial stream surfaces, may be considered, for which the rate of energy transfer is given by Euler's equation:

$$E = \rho Q \omega \Delta(r c_u) \tag{1}$$

or, when introducing the circulation about the blade section

$$\Gamma = 2\pi \Delta(r c_u) = (\Gamma_2 - \Gamma_1)/z \tag{2}$$

in Eq. (1)

$$E = Q\rho(\omega/2\pi) z \Gamma$$

Eqs. (1) and (2) apply to any coaxial stream surface. For pure axial flow, Eq. (1) reduces to

$$E = Q\rho(u \Delta c_u) \tag{1a}$$

The equations may be applied to an entire stage only if the circulation about the blade sections in all stream surfaces is the same.

Eq. (2) states that the rate of energy transfer depends upon the action of a rotating system of vortices upon a streaming working fluid. In view of this dependence of energy transfer upon the action of vortices (vortex = "turbo"), it seems appropriate to refer to turbines and compressors collectively as "turbomachines." The form of the expression for the rate of energy transfer, Eq. (2), is analogous to the equation defining energy

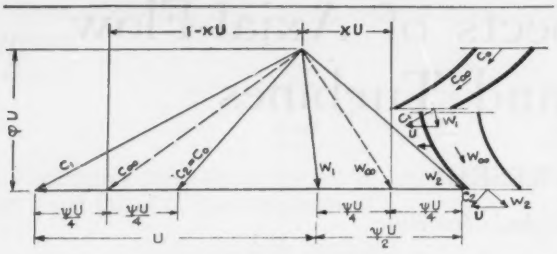

FIG. 1.

conversion in electrical machinery. It is customary to express the rate of energy transfer in terms of nondimensional quantities—namely, the flow coefficient

$$\varphi = \frac{Q}{(\pi D^2/4)u} = \frac{4Q}{\pi^2 D^3 n} \tag{3a}$$

and the pressure coefficient

$$\psi = \frac{\Delta h}{u^2/2g} = \frac{2\Delta c_u}{u} = \frac{2\Delta c_u}{\pi n D} \tag{3b}$$

These nondimensional quantities relate the primary performance quantities—namely, the volume rate of flow, Q, the difference of total head, Δh, and the rotative speed, n—to the dimensions of the stage, tenuously given by D.

Substitution of φ and ψ into Eq. (1a) leads to:

$$E = \rho(\pi^4/8)D^5 n^3 \varphi\psi \tag{4}$$

More positive relations between the significant physical features of the stage and its operating characteristics can be established for a restricted family of stages designated "normal stages," for which the conditions of flow, whether compressible or uncompressible, are identical at inlet and outlet as to direction and velocity of flow, except for a difference in head.

For normal stages, one additional quantity is needed to establish the rational relations desired, since it is necessary to account for the percentage of variation of static head in the fixed and in the moving row which otherwise would remain arbitrary. A suitable nondimensional quantity relating to this degree of freedom of normal stages is the degree of reaction, defined as the ratio of the difference of static head of the moving row to that of the stage, $\kappa = \Delta h_s'/\Delta h$.

Relations Between Nondimensional Parameters and the Velocity Diagram

It is significant that the quantities φ, ψ, and κ appear explicitly in the velocity diagram of normal stages, see the lengths φu, $\psi u/2$, κu, in Fig. 1. In fact, these three quantities define the velocity diagram completely. As shown previously by Traupel,[1] they may be used as parameters to establish the direction of flow at inlet and outlet of both the fixed and moving rows of the

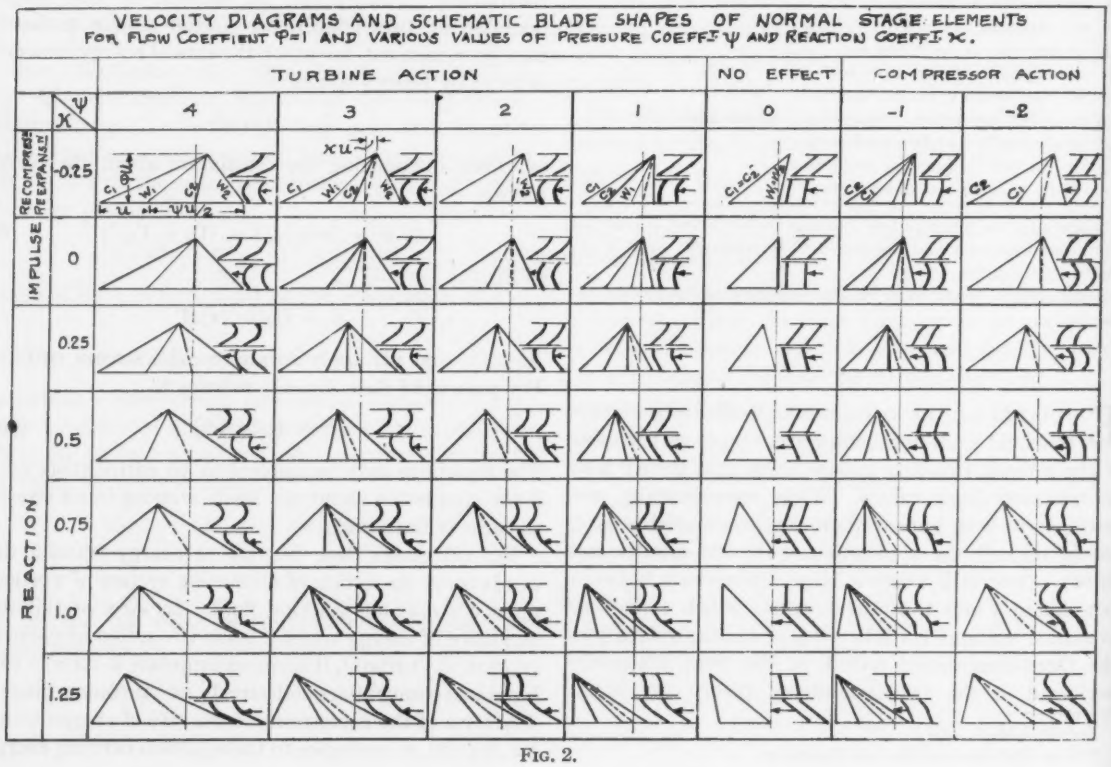

FIG. 2.

normal stage, hence, the ideal blade angles for any given operating condition of a blade element.

A tabulation of the velocity diagrams and of the shape of blade of the fixed and moving rows, in schematic presentation, is given in Fig. 2 for various values of the pressure coefficient and the degree of reaction and for a constant value of the flow coefficient, since the latter is of secondary importance. The range of variation of both ψ and κ is believed to cover the entire field of normal operation of "normal stages" of both compressors and turbines. The blade combinations derived for two-dimensional flow, and shown schematically in Fig. 2, constitute the elements for a functional design of blade rows. This figure will be used to illustrate certain three-dimensional aspects of flow in blade rows.

Variation of Conditions of Flow and of Shape of Blades Along the Radius

Since the blade velocity of a moving axial-flow blade row and also, in general, the circumferential velocity component of the working fluid varies with radius, there will be corresponding changes in the fundamental parameters of the stage element necessitating changes in the velocity diagram and changes in the shape of the blading along the radius. A properly designed blade for an axial-flow stage therefore will represent a combination of various blade elements, each selected to meet precisely the functional requirements.

Let us consider a condition of operation of a stage for which the axial velocity and the energy transfer are constant along the radius and, furthermore, for which the total energy upstream of the grid is constant. Then it follows that the total energy downstream is likewise constant and the flow is irrotational throughout. In that case the fundamental parameters vary with the radius as follows:

$$\psi = \psi_T(r_T/r)^2$$
$$\varphi = \varphi_T(r_T/r)$$
$$1 - \kappa = (1 - \kappa_T)(r_T/r)^2$$

Fig. 3 shows the variation of the two parameters ψ and κ with radius and likewise the change of shape of blades from tip to root in schematic presentation. Of interest is the pronounced change of both the pressure and reaction coefficient. The above applies to what is commonly known as a vortex type of stage.

Let us consider further a stage of constant axial velocity which produces a constant increase of energy along the radius but for which the degree of reaction is arbitrarily prescribed. We choose $\kappa = 1/2$ constant along the radius. This condition is represented by Fig. 4. It is seen that in this case the total energy h varies with the radius. In fact, the flow corresponding to conditions halfway through a row is identical with a solid body rotation $c_u = u/2 = \text{const.} \times r$, the fluid rotating at half the angular velocity of the moving row.

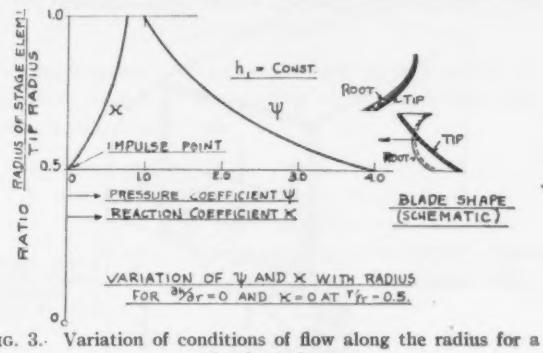

FIG. 3. Variation of conditions of flow along the radius for a vortex type stage.

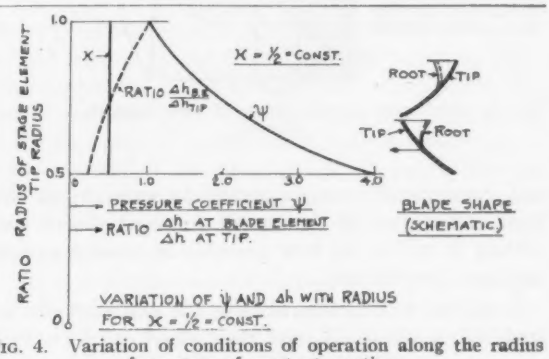

FIG. 4. Variation of conditions of operation along the radius for a stage of constant reaction.

It is possible to design stages for other variations of the coefficient of reaction along the radius which may have practical advantage, for instance, with regard to tip and root leakage of the moving and fixed blades, respectively, if the condition of radial stability is satisfied, a point to which reference will be made later.

Calculation of the variation of lift coefficient of the moving and fixed blade sections along the radius,

$$c_l' = t/l(\psi/\sqrt{\varphi^2 + \kappa^2})$$

and

$$c_l'' = (t/l)[\psi/\sqrt{\varphi^2 + (1 - \kappa)^2}]$$

respectively, for the conditions of Figs. 3 and 4 shows that, in general—e.g., for constant chord, l = const.—the maximum lift coefficient occurs at the root radius. Attempts to relate the stalling limit of the root sections of a blade row to a corresponding factor limiting the operating range of the stage have not been successful, and it is evident that in this respect, as in others, account must be taken of the properties of the real fluid.

Boundary-Layer Effects in Blade Rows

Disregarding various other factors of importance, such as compressibility, attention will be given to those effects resulting from the viscosity of the working fluid which cause radial displacements of portions of the working fluid with respect to the main body of the fluid

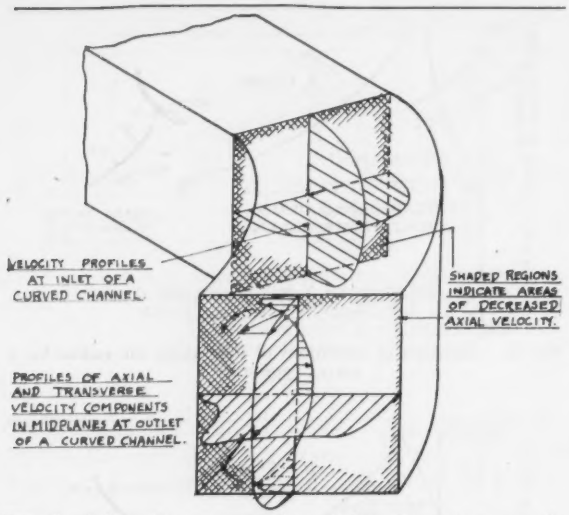
VELOCITY PROFILES AT INLET OF A CURVED CHANNEL
SHADED REGIONS INDICATE AREAS OF DECREASED AXIAL VELOCITY
PROFILES OF AXIAL AND TRANSVERSE VELOCITY COMPONENTS IN MIDPLANES AT OUTLET OF A CURVED CHANNEL.

FIG. 5. Schematic representation of flow through a curved channel.

and, consequently, render invalid to some degree the basic assumption of the two-dimensional theory, according to which the flow proceeds on coaxial stream surfaces of revolution.

A number of characteristics of the real fluid can be analyzed qualitatively, and their effect can be traced upon the performance of axial-flow blade rows. A quantitative theory for these effects, however, does not exist as yet. At this stage, application of the results of investigations of curved ducts to the flow through blade rows appears most profitable. It is, therefore, proposed to consider the flow through a blade grid as a flow through individual channels.

For purposes of comparison, the incompressible flow through an elbow of rectangular cross section will be analyzed (Fig. 5). It is assumed that the flow approaches the elbow through a straight duct of length sufficient to establish appreciable boundary layers. At the inlet of the curved channel, centrifugal acceleration produces a displacement of the main body of the fluid toward the outer wall (front of the blade) and a displacement of the surrounding fluid in the boundary layer, having a lower kinetic energy, toward the inside wall (back of the blade). An increase of the boundary-layer thickness along the back of the blade is observed. The displacements of fluid give rise to velocity components in the plane normal to the axis of the channel, which are directed toward the back of the blade along the walls and toward the front of the blade throughout the core, as shown in Fig. 5.

Another basic phenomenon, important for the flow through blade grids, requires discussion here—namely, the different behavior of boundary layers when adhering to a solid surface as contrasted with boundary layers detached from a solid surface, the latter usually referred to as wakes, indicated on Fig. 6.

Under the action of shear stresses of surface friction, a boundary layer attached to a surface tends to grow in thickness, which growth may be intensified by deceleration or counteracted by acceleration under the effect of pressure gradients. In detached boundary layers, the shear stress resulting from skin friction is no longer active, and, therefore, the boundary layer thickness does not continue to grow unless subjected to a field of positive pressure gradients. On the other hand, the action of turbulence causes an exchange of momentum which tends to dissipate the wake. The rate of decay of a wake after its detachment from a solid surface is of intense interest in the design of turbomachines, since on it depends the distance allowed between successive blade rows. It is also a factor that influences the noisiness of turbomachines. In the following, use will be made of the fact that detached boundary layers decay rapidly, while boundary layers adhering to a solid surface persist or continue to grow. The decay of wakes is a process involving relatively high losses of kinetic energy, the magnitude of which is affected favorably by acceleration of the entire fluid stream and distinctly adversely by retardation. Retardation of the fluid stream as a result of the decay of wakes, and consequent positive pressure gradients, are likely to occur downstream of a blade row unless compensated by changes of flow area. Typical variations of pressures downstream of a grid are indicated in Fig. 6.

A third factor of major influence upon the three-dimensional character of flow in moving blade grids is the effect of centrifugal acceleration upon the fluid introducing radial motion and corresponding radial momentum components and affecting the boundary layers of the moving rows in particular. As a consequence, boundary layers of backwardly sloping blades are displaced radially outward; of forwardly sloping surfaces, inward. This action is equivalent to bound-

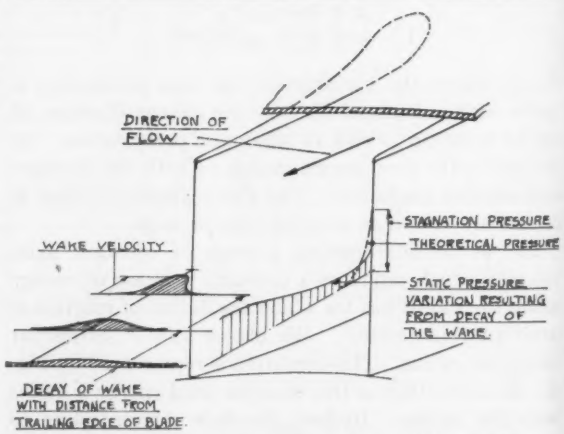
DIRECTION OF FLOW
STAGNATION PRESSURE
THEORETICAL PRESSURE
WAKE VELOCITY
STATIC PRESSURE VARIATION RESULTING FROM DECAY OF THE WAKE.
DECAY OF WAKE WITH DISTANCE FROM TRAILING EDGE OF BLADE.

DECAY OF DETACHED BOUNDARY LAYERS (WAKE) AND STATIC PRESSURE VARIATION DOWNSTREAM OF A GRID.

FIG. 6.

ary-layer removal on some portion of the blades, resulting in accumulation on others.

A Criterion of Radial Stability

The occurrence of displacements of flow referred to invalidates the assumption of flow on coaxial surfaces, and it appears desirable to establish a criterion for its existence or nonexistence. The following formulation is offered:

A stable flow on coaxial surfaces exists if a particle of fluid, when displaced radially and thereby undergoing a change of state of constant energy, corresponding to the variation of pressure of the surrounding fluid along the path of displacement (however, not affecting the meridional components of acceleration), is subjected to a resultant force tending to return it to its original position.

Indifferent equilibrium of flow on coaxial surfaces exists if the resultant force is zero; instability prevails if the resultant force acts in the direction of further displacement.

This criterion is applicable also to boundary layers along the casing and the hub.[2]

It may be expressed in differential form for compressible and incompressible flow,

$$\frac{\partial^2 p}{\partial r^2} \gtreqless \frac{\partial}{\partial r}\left(\rho \frac{c_u^2}{r}\right)_{\text{particle}} \tag{5}$$

with the additional condition $\partial h/\partial r = 0$ applied to the displacement motion of the particle. The $>$ sign in Eq. (5) applies to stable condition, the $=$ sign to indifferent equilibrium, and the $<$ sign to instability.

Development of Eq. (5) leads to the following expressions for the condition of stability of flow on coaxial surfaces of revolution, for incompressible flow:

$$\partial^2 p/\partial r^2 \gtrless -(3/r)(\partial p/\partial r) \tag{6}$$

or, in terms of total head h

$$(\partial h/\partial r)_{\text{field}} \gtrless 0 \tag{7}$$

and for compressible flow:

$$\frac{\partial^2 p}{\partial r^2} \gtreqless \frac{1}{\gamma p}\left(\frac{\partial p}{\partial r}\right)^2 - \frac{3}{r}\frac{\partial p}{\partial r} \tag{8}$$

or, again in terms of total energy h

$$\frac{\partial h}{\partial r} - RT\left[\frac{1}{\gamma - 1}\frac{\partial}{\partial r}(\log_e T) - \frac{\partial}{\partial r}(\log_e \rho)\right] \gtrless 0 \tag{9}$$

In all instances, the upper sign applies to stability and the lower to instability. It is noted that stability of compressible flow depends not only upon the radial distribution of total energy, as is the case for incompressible flow, but also upon the temperature distribution.

Eqs. (8) and (9) are reducible to the form of Eqs. (6) and (7) upon introducing the condition of incompressibility.

Specific Examples of Boundary-Layer Displacement

Consideration will be given now to the action of boundary layers in the blading of turbomachines for the following conditions:

(1) Fixed grids with zero circulation at outlet.
(2) Fixed grids with circulation at outlet.
(3) Rotating grids with zero circulation at outlet.
(4) Rotating grids with circulation at outlet.
(5) Unsymmetrical boundary layers upstream of the grid.
(6) Flow through blade grids operating in a rotational field of flow.

The type of boundary-layer flow occurring in the above grids is illustrated in Figs. 7 to 10. Fig. 7 shows a fixed grid with axial discharge. The boundary layer originally at the casing and the hub only is partly displaced to the back of the blade. Upon detachment from the blade a part of the boundary layer originally adhering to the wall of the casing and to the hub is inserted into the fluid and thereby subjected to rapid decay. This is a feature that commends the design for axial discharge from a stage.

Fig. 8, a schematic presentation of the flow through a fixed grid with circulation at outlet, shows a displacement of the boundary layer from the casing to the back of the blade which is more accentuated than the corresponding displacement of the boundary layer of the

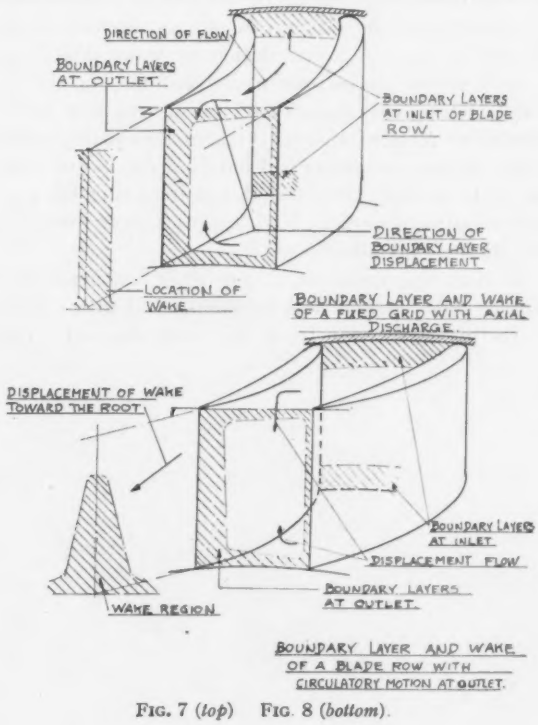
DIRECTION OF FLOW
BOUNDARY LAYERS AT OUTLET
BOUNDARY LAYERS AT INLET OF BLADE ROW
DIRECTION OF BOUNDARY LAYER DISPLACEMENT
LOCATION OF WAKE
BOUNDARY LAYER AND WAKE OF A FIXED GRID WITH AXIAL DISCHARGE
DISPLACEMENT OF WAKE TOWARD THE ROOT
BOUNDARY LAYERS AT INLET
DISPLACEMENT FLOW
BOUNDARY LAYERS AT OUTLET
WAKE REGION
BOUNDARY LAYER AND WAKE OF A BLADE ROW WITH CIRCULATORY MOTION AT OUTLET

Fig. 7 (*top*) Fig. 8 (*bottom*).

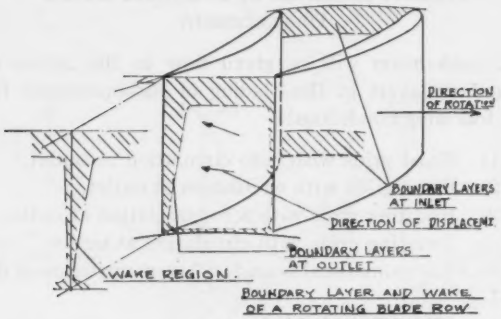

BOUNDARY LAYER AND WAKE OF A ROTATING BLADE ROW WITH AXIAL DISCHARGE.

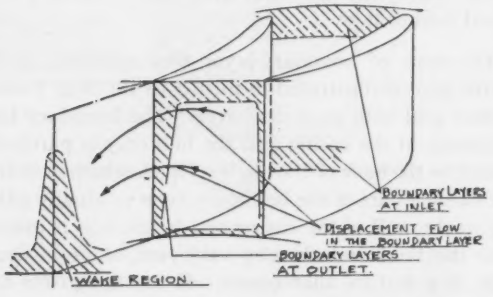

BOUNDARY LAYERS AND WAKE OF A ROTATING BLADE ROW WITH CIRCULATORY MOTION AT OUTLET

FIG. 9 (*top*). FIG. 10 (*bottom*).

hub. A pressure gradient downstream of the grid further tends to displace the wake toward the hub.

Boundary layers along backwardly sloping moving blades, Fig. 9, and along the rotating hub are displaced toward the region of the tip by centrifugal acceleration, as stated before, and, in the case of axial discharge from the blade row, an accumulation of wake fluid "attached" to the downstream casing wall may be the result. If the fluid at outlet of the moving row has a circulatory motion, however (Fig. 10), the existing radial static pressure gradients will induce a displacement of the wake radially inward and, counteracting the preceding outward motion, tend toward a more even distribution of wake fluid.

In discussing condition 2, (Fig. 8), it was noted that the secondary motion was unsymmetrical with respect to the plane of symmetry of the blade channel. This phenomenon, which is equivalent to a twisting motion in the boundary layer, may originate also from causes other than a field of pressure gradients—e.g., from unsymmetry of the flow at inlet of the curved channel in respect to the thickness of the lateral boundary layers. If twisting motion is imparted not only to the boundary layers but to the main body of the fluid as well, relatively large amounts of kinetic energy may be involved, and direct and indirect losses are apt to be large.

Considering now the action of a blade grid in a field of incompressible flow in which the total energy increases with the radius, it may be shown that in this case displacement of fluid normal to the coaxial stream surfaces is effectively opposed by stabilizing forces, and, consequently, secondary flows may be expected to be small.

In conclusion, it should be stated that, whereas for single-stage units, the boundary layers generally are relatively thin and the effects discussed therefore minute and probably negligible, evidence from tests of multistage compressors, particularly, seems to indicate that the three-dimensional effects in question have practical significance.

The analysis of boundary-layer displacements seems to offer an explanation of the observation that, particularly for blades of short span, it is the tip section of the moving row rather than the root section, as might be assumed from two-dimensional theory, which proves to be critical in respect to stalling.

While secondary motion introduces several factors responsible for losses in the stage, the action of blade rows by which attached boundary layers are detached and thereby exposed to rapid decay—a process to which the term "metabolism" might be applied with some justification—deserves the attention of the designer, since it might very well be applied consciously to the improvement of the characteristics of multistage units in particular.

REFERENCES

[1] Traupel, W., *Neue Allgemeine Theorie der Mehrstufigen Axialen Turbomaschinen*, Leemann & Co., Zürich, 1942.

[2] Taylor, G. I., *Stability or Rotating Flow*, summarized in Goldstein, *Modern Developments of Fluid Dynamics*, Vol. 1, p. 196; Oxford Press, 1938.